Dissertation zur Erlangung des Doktorgrades
der Fakultät für Chemie und Pharmazie
der Ludwig-Maximilians-Universität München

# A physical link between mRNA translation and degradation: Structures of the Ski complex and eIF-5A bound to the ribosome


Christian Schmidt
aus
Ulm, Deutschland

2017

Dissertation zur Erlangung des Doktorgrades
der Fakultät für Chemie und Pharmazie
der Ludwig-Maximilians-Universität München

# A physical link between mRNA translation and degradation: Structures of the Ski complex and eIF-5A bound to the ribosome

Christian Schmidt
aus
Ulm, Deutschland

2017

## Erklärung

Diese Dissertation wurde im Sinne von § 7 der Promotionsordnung vom 28. November 2011 von Herrn Prof. Dr. Roland Beckmann betreut.

## Eidesstattliche Versicherung

Diese Dissertation wurde eigenständig und ohne unerlaubte Hilfe erarbeitet.

München,

_____

Christian Schmidt

Dissertation eingereicht am: 09.05.2017

1. Gutachter: Prof. Dr. Roland Beckmann

2. Gutachter: Prof. Dr. Daniel N. Wilson

Mündliche Prüfung am: 25.07.2017

**Parts of this thesis have been published or submitted to scientific journals:**

"The cryo-EM structure of a ribosome–Ski2-Ski3-Ski8 helicase complex"

**Christian Schmidt**, Eva Kowalinski, Vivekanandan Shanmuganathan, Quentin Defenouillère, Katharina Braunger, André Heuer, Markus Pech, Abdelkader Namane, Otto Berninghausen, Micheline Fromont-Racine, Alain Jacquier, Elena Conti**, Thomas Becker** and Roland Beckmann**

** Corresponding Author

Published in Science 354 (6318), 1431-1433. 2016 Dec 16.

"Structure of the hypusinylated eukaryotic translation factor eIF-5A bound to the ribosome"

**Christian Schmidt***, Thomas Becker*, André Heuer, Katharina Braunger, Vivekanandan Shanmuganathan. Markus Pech, Otto Berninghausen, Daniel N. Wilson** and Roland Beckmann**

* These authors contributed equally to the work
** Corresponding Author

Published in Nucleic Acids Research 44 (4), 1944-1951. 2016 Feb 29.

**Parts of this thesis have been presented at international conferences:**

Oral presentation at the Protein Synthesis and Translational Control Meeting, Heidelberg, 2015

"The Ski complex binds 80S ribosomes for 3' to 5' decay of mRNA in NSD"

**Christian Schmidt**, Eva Kowalinski, Vivekanandan Shanmuganathan, Quentin Defenouillère, Katharina Braunger, Markus Pech, Otto Berninghausen, Micheline Fromont-Racine, Alain Jacquier, Elena Conti, Thomas Becker and Roland Beckmann

Poster presented at the RNA Society Meeting in Kyoto, Japan, 2016

"Cryo-EM structure of a ribosome-Ski complex reveals interactions between the translation and 3'-5' mRNA degradation machineries"

**Christian Schmidt**, Eva Kowalinski, Vivekanandan Shanmuganathan, Quentin Defenouillère, Katharina Braunger, André Heuer, Markus Pech, Otto Berninghausen, Micheline Fromont-Racine, Alain Jacquier, Elena Conti, Thomas Becker and Roland Beckmann

# Summary

mRNA translation and degradation are mutually interdependent processes in the cell. The best characterized examples of the interplay between these two processes are the mRNA quality control pathways taking care of aberrant mRNAs that cause translation stalling in most cases. It was shown for these pathways that mRNA degradation is initiated in a ribosome-dependent manner directly on the stalled intermediate. Aberrant transcripts are either degraded in 5'-to-3' direction by Xrn1 or in 3'-to-5' direction by the cytosolic exosome together with the Ski proteins. However, no structural insights exist on how translation and degradation are coupled for general mRNA turnover and quality control.

Beside ribosome stalling on aberrant transcripts, poly-basic or poly-proline stretches have been shown to cause translation arrests in the cell. Yet, these stretches are commonly found in proteins. To that end, eukaryotic initiation factor 5A (eIF-5A) was identified to rescue ribosomes stalled on poly-proline, allowing translation to continue. Moreover, eIF-5A was shown to alleviate many poly-basic stalling events and promoting translation elongation in general. It is, however, unknown how eIF-5A functions on a molecular level.

The first part of this thesis focuses on the interactions of the Ski proteins with ribosomes in the exosome-dependent 3'-to-5' mRNA degradation pathway. We show that in contrast to most proposed models, the Ski complex and not Ski7 associates stably with ribosomes *in vitro* and *in vivo*. A high resolution cryo-EM structure of a native ribosome-Ski complex reveals how the Ski complex interacts with the 40S subunit of the ribosome, facilitating the threading of mRNA into the Ski2 helicase. Furthermore, we show by ribosomal profiling analysis that this interaction is probably not limited to mRNA quality control, but might rather represent a general mRNA turnover intermediate. Collectively, these results are the first structural insights into how translation and degradation of mRNAs are coupled on a molecular level.

The second part of this thesis focuses on the surprising discovery that eIF-5A binds to Ski complex-associated ribosomes. We show that eIF-5A targets ribosomes

with a vacant E-site, thus recognizing translation-arrested intermediates by scanning for tRNA occupancy. A cryo-EM structure reveals that eIF-5A reaches deep into the peptidyl transferase center and interacts with A76 of the P-site tRNA via its unique hypusine residue. Our structural data supports a model where this interaction leads to the stabilization and orientation of the P-tRNA CCA-end to assist in peptide-bond formation, explaining eIF-5A's function as a general rescuing factor.

# Contents

# List of Figures

# List of Tables

# 1 Introduction

According to the central dogma of molecular biology (Crick, 1970), the genetic information stored in form of complementary deoxyribonucleic acid (DNA) strands inside the cell is transformed into functional proteins in three distinct steps: First, this information has to propagate from one generation to the next, thus DNA is replicated to be passed on. Second, specific DNA sequences called genes are transcribed into RNA molecules by RNA polymerases during transcription. These RNAs can fulfil different functions in the cell, for example as transfer RNA (tRNA), ribosomal RNA (rRNA), small non-coding RNA (snRNA) or act as templates for protein synthesis in form of messenger RNA (mRNA). The third and final step is the translation of mRNAs into proteins, a process catalysed by ribosomes. Proteins are large biomolecules that perform a wide range of tasks in our cells from catalysing metabolic reactions to giving the cell its shape. Each protein has a specific three-dimensional architecture (called native state) that often dictates its molecular function. To reach its native state, proteins are often bound by molecular chaperones that help the protein accommodating its final fold. Because of the importance of proteins to the viability of the cell, transcription and translation are tightly regulated and monitored throughout each step.

## 1.1 Overview of the ribosome

The ribosome is a large macromolecular complex consisting of numerous ribosomal proteins (r-proteins) and rRNAs. It is universally conserved and responsible for protein biosynthesis. Because of its central function in the cell, it has been studied thoroughly by various structural biology techniques (i.e. reviewed in Schmeing and Ramakrishnan, 2009; Steitz, 2008; Voorhees and Ramakrishnan, 2013) like X-ray crystallography or cryo-electron microscopy (cryo-EM). It is composed of a large and a small subunit (LSU and SSU, respectively), each harbouring different functional sites. The SSU and LSU can move with respect to each other, referred to as subunit rotation (Frank and Agrawal, 2000). In eukaryotes, the 40S subunit shows further

flexibility through a rotation along its long axis referred to as subunit rolling (Budkevich et al., 2014). In the SSU, the mRNA binding tunnel and the decoding center (DC) are found. Here, mRNA codons consisting of triplets of nucleotides are decoded by the accommodation of a complementary tRNA that carries a specific amino acid (Berg and Offengand, 1958; Crick et al., 1961; Ogle et al., 2001). The LSU contains the peptidyl transferase center (PTC) and the peptide exit tunnel. In the PTC, peptide-bond formation occurs where amino acids are linked with each other to form a nascent polypeptide chain (NC) that is built from N- to C-terminus (Dintzis, 1961; Leung et al., 2011). The peptide exit tunnel is a large cavity spanning from the PTC to the solvent-facing surface of the LSU accommodating the NC (Frank et al., 1995). Through this tunnel, the NC is funnelled to the outside of the ribosome where it can be immediately contacted by chaperones or other protein factors. Finally, the intersubunit space between both subunits harbours three different binding sites for tRNAs: the aminoacyl (A-), peptidyl (P-) and exit (E-) sites. The A-site usually contains the aminoacyl-tRNA carrying the next amino acid that should be incorporated into the peptide chain. In the P-site, a peptidyl-tRNA is bound that has the NC attached after peptide bond formation. The E-site contains a deacylated tRNA that is ready to dissociate from the ribosome. Thus, throughout the translation cycle, tRNAs move from A- to P- to E-site.

Even though their function is conserved, ribosomes show large differences between the three different kingdoms of life with the most apparent difference in size as elucidated by many structural studies (Fig. 1.1). Generally, prokaryotic and archaeal ribosomes are smaller than their eukaryotic counterparts, differing in about 1.2-2.0 MDa in mass (Anger et al., 2013; Melnikov et al., 2012). Consistently, the ribosomes also show different sedimentation coefficients (given in Svedberg units) with 70S for prokaryotic and archaeal ribosomes and 80S for those of eukaryotes. The most conserved part in all ribosomes is the core containing the PTC, the DC and the tRNA binding sites. Apart from that, eukaryotic ribosomes show a larger and more complex variety of r-proteins and rRNA, giving rise to protein-RNA and RNA-RNA layers around the ribosomal core that are not present in prokaryotic ribosomes (Anger et al., 2013). For example, the *E. coli* SSU (30S) and LSU (50S) contain much less proteins and rRNA than the SSU and LSU of *S. cerevisiae* (40S and 60S, respectively). These additional layers are believed to reflect the higher complexity of eukaryotic organisms compared to prokaryotic cells and this difference can even be seen when comparing lower eukaryotic ribosomes with that of higher eukaryotes.

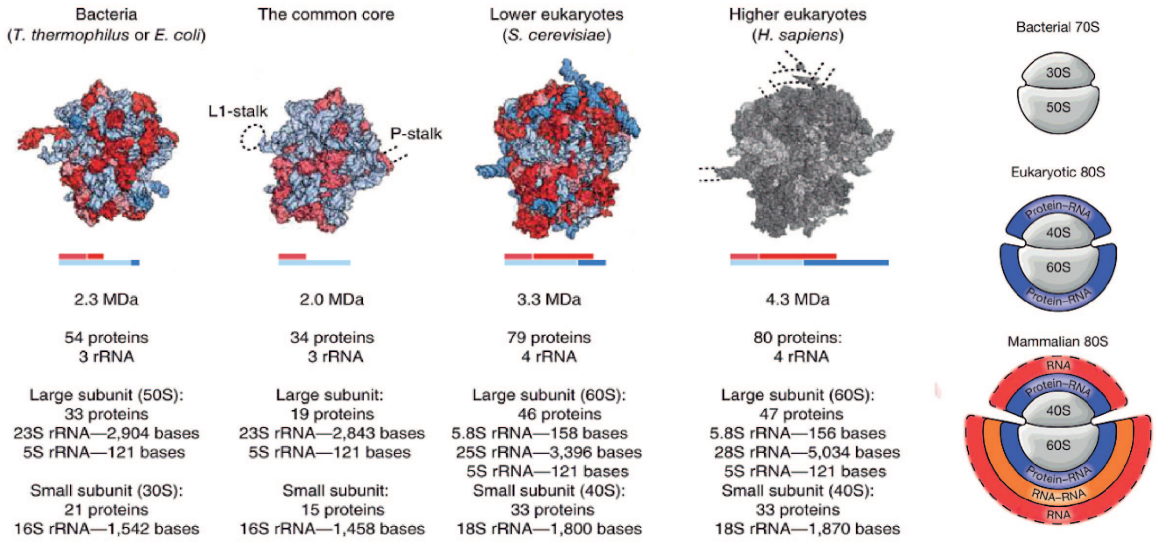


FIGURE 1.1: **Comparison of prokaryotic and eukaryotic ribosomes.** Ribosomes have a highly conserved inner core that contains the PTC, DC and the tRNA binding sites (right panel; schematically shown in grey). Eukaryotic ribosomes show larger amounts of r-proteins and rRNA giving rise to additional layers (blue, orange, red) that have developed during evolution and are thought to reflect the higher complexity of eukaryotic cells. Comparing lower (*S. cerevisiae*) with higher (*H. sapiens*) eukaryotes reveals that these differences even exist within one of the kingdoms of life. Adapted from Anger et al., 2013 and Melnikov et al., 2012.

Whereas r-proteins generally differ in number and sometimes in structure , most differences in the rRNA are found in the so-called expansion segments (ES), which are essentially not present in prokaryotic ribosomes (Melnikov et al., 2012; Wilson and Cate, 2012). Even though these ES are long known to be specific and often essential for eukaryotic ribosomes (Armache et al., 2010; Beckmann et al., 2001; Bradatsch et al., 2012; Leidig et al., 2012; Leidig et al., 2014), their function still remains largely unknown.

Since the beginning of structural biology, ribosomes posed a popular target for various structural techniques. The first atomic models were obtained for archaeal and bacterial subunits and ribosomes via X-ray crystallography (Ban et al., 2000; Rabl et al., 2011; Schluenzen et al., 2000; Selmer et al., 2006; Wimberly et al., 2000). Most importantly, these structures could show that the PTC contains no r-proteins and only rRNA, making the ribosome a ribozyme relying on RNA for its enzymatic activity (Cech, 2000; Nissen et al., 2000). Eukaryotic ribosomes turned out to be much more complicated to crystallize and where almost exclusively studied by cryo-EM in the beginning (Beckmann et al., 2001; Spahn et al., 2001). These first structural studies

built the foundation for many research papers regarding the translation cycle. In 2010, the first crystal structure of an entire 80S ribosome was solved and allowed to visualize atomic interactions in detail (Ben-Shem et al., 2010; Ben-Shem et al., 2011). Since then, many aspects could be visualized and solved to gain a better understanding of the translation cycle (Schmeing and Ramakrishnan, 2009; Steitz, 2008; Voorhees and Ramakrishnan, 2013). With the development of direct electron detectors, near-atomic resolution can nowadays also be achieved by cryo-EM, which lead to the so-called "resolution revolution" and a vast majority of papers have been published allowing an even deeper understanding of canonical translation (reviewed for example in Bai et al., 2015; Cheng, 2015; Kühlbrandt, 2014; Nogales, 2015), but also of many processes that are happening co-translationally or are in any way connected to ribosomes.

## 1.2 Translation cycle

The translation cycle displays the same underlying principles in all organisms and can be divided into four different steps: initiation, elongation, termination and recycling. Generally, mRNA nucleotide triplets are organized into codons where each codon represents one of the 20 specific amino acids (Crick et al., 1961). Since there are four different nucleotides (adenosine, cytosine, guanine and thymine), there are $4^3=64$ different codons, leading to degeneration of the genetic code. Thus, most amino acids are coded by several codons (Lagerkvist, 1978). Additionally, there are three codons not coding for any amino acid called stop codons (UAA, UAG, UGA). These codons signal to terminate translation and to release the polypeptide chain from the ribosome. Similar to stop codons, AUG is signalling the start of translation, thus referred to as start codon. A significant difference, however, is that AUG also codes for methionine, hence it acts as a start codon only under certain circumstances. After translation is initiated, each codon is read by a complementary tRNA that delivers a specific amino acid which is attached to it. Through this decoding of an mRNA by tRNAs, the mRNA is translated into a specific amino acid sequence that is synthesized by the ribosome. Even though the principles are the same, each of the four translation steps is differently regulated and carried out when comparing pro- and eukaryotic translation, with elongation being the most conserved process.

**Initiation.** Initiation differs vastly in pro- and eukaryotes (Sonenberg and Hinnebusch, 2009). In prokaryotic cells, three different initiation factors (IF1, IF2 and

IF3) mediate translation initiation together with the Shine-Dalgarno (SD) sequence (Shine and Dalgarno, 1974). The SD sequence ensures the correct positioning of the start codon in the ribosomal A-site by base-pairing with the 3' end (anti-SD) of the 16S rRNA in the SSU (Kaminishi et al., 2007; Korostelev et al., 2007). Subsequently, IF1, IF2 and IF3 act in concert to promote binding of the initiator fMet-tRNA$_i^{fMet}$ and the mRNA and monitor subunit joining to form an initiation complex.

In comparison, eukaryotic initiation is much more complex. It involves at least twelve initiation factors that work in concert to generate an elongation-competent ribosome containing the AUG start codon in the P-site (Hinnebusch and Lorsch, 2012; Jackson et al., 2010). First, a ternary complex (TC) is formed by GTP-bound eIF2 (consisting of three subunits $\alpha$, $\beta$ and $\gamma$) together with the initiator tRNA$_i^{Met}$. eIF1, 1A, 3 and 5 promote 40S binding with the TC to form the 43S pre-initiation complex. Additionally, the 5' cap of the mRNA is bound by the eIF4F complex consisting of eIF4A, B, G and E. eIF4E recognizes the cap and eIF4G binds to poly-A binding protein (Pab1) at the poly-A tail, leading to the circularization of the mRNA. Subsequently, eIF4G can interact directly with the 43S pre-initiation complex which consequently leads to the formation of the 48S complex. This complex moves over the mRNA in 5'-to-3' direction to recognize the first AUG start codon, a process referred to as scanning. After reaching the start codon, eIF5 and eIF5B promote GTP hydrolysis of eIF2 which leads to subunit joining and transition into the elongation phase (Jackson et al., 2010). At this point, the initiator tRNA is accommodated in the P-site, leaving an empty A-site to bind the next aminoacyl-tRNA.

**Elongation.** After transition into the elongation phase, the mRNA is translated continually from 5'-to-3'. Aminoacyl-tRNAs are delivered to the A-site in a GTP-bound ternary complex by EF-Tu (prokaryotes) or eEF1$\alpha$ (eukaryotes) (Agirrezabala and Frank, 2009; Dever and Green, 2012; Noble and Song, 2008). Only if a cognate tRNA is bound to the codon in the A-site, GTP hydrolysis by EF-Tu or eEF1$\alpha$ is triggered, leading to dissociation of the elongation factor, accommodation of the A-site tRNA, and formation of the peptide bond. Subsequently, a deacylated tRNA is bound to the P-site and both bound tRNAs and the mRNA must be translocated to the next binding site on the ribosome. This translocation is a highly dynamic process (Blanchard et al., 2004), where the tRNAs move with respect to the LSU resulting in so-called A/P and P/E hybrid states (where the last letter indicates the respective position of the tRNA on the LSU). In unison, the SSU rotates relative to the LSU, leading to a rotated state ribosome (Frank and Agrawal, 2000). At this stage, the

rotated and non-rotated form are in an equilibrium, where the ribosome switches between these two states. Translocation is catalysed by the elongation factors EF-G (prokaryotes) or eEF-2 (eukaryotes). EF-G and eEF-2 are translational GTPase with high affinity to rotated-state ribosomes (Dever and Green, 2012) bearing hybrid-state tRNAs. During translocation, EF-G and eEF-2 undergo a conformational change upon GTP hydrolysis, which is thought to drive translocation (Dever and Green, 2012; Noller et al., 2002). As a result, the deacylated tRNA will be repositioned into the E-site and the peptidyl-tRNA into the P-site, leaving the A-site empty again to bind a new aminoacyl-tRNA. This elongation cycle is repeated until translation is terminated by a stop codon, releasing the deacylated tRNA from the E-site with each step.

**Termination.** Upon reaching a stop codon on the mRNA, no new elongation cycle is started. Instead, the stop codon in the A-site is recognized by termination factors to terminate translation and release the NC from the ribosome (Brown et al., 2015; Dever and Green, 2012; Korostelev et al., 2008; Matheisl et al., 2015; Preis et al., 2014; Weixlbaumer et al., 2008; Zhou et al., 2012). In prokaryotes, two different class-I termination factors are needed. RF1 recognizes UAA and UAG whereas RF2 recognizes UAA and UGA. In eukaroytes, eRF1 is able to recognize all three stop codons. Recent reports have shown that eRF1 actually recognizes a quadruplet codon (Matheisl et al., 2015). Here, all four bases contribute to the formation of a UNR-type U-turn that is recognized by the N-terminal domain of eRF1. Even though RF1 and RF2 are not structurally related to eRF1 (Song et al., 2000), all factors contain a universally conserved GGQ motif that positions a water molecule in the PTC, leading to a subsequent nucleophilic attack on the peptidyl-tRNA ester bond and allowing the release of the NC (Kisselev et al., 2003; Korostelev, 2011; Song et al., 2000). Alongside class-I termination factors, the class-II termination factors RF3 (prokaryotes) or eRF3 (eukaryotes) are needed for termination, though having different functions during this process. RF3 releases RF1 or RF2 from the ribosome (Zavialov et al., 2002), whereas eRF3 delivers eRF1 and stimulates its action (Preis et al., 2014; Shao et al., 2016).

**Recycling.** Due to the different functions of RF3 and eRF3 during termination, the post-termination complexes differ in pro- and eukaryotes. This difference is also reflected in the different mechanisms of the recycling step, where the mRNA is released and the ribosome gets split into its subunits which allows it to enter a new

translation cycle. In prokaryotes, the post-termination complex consists of a ribosome with deacylated P-site tRNA and an empty A- and E-site. Here, splitting is performed by EF-G in concert with the dedicated splitting factor RRF (Zavialov et al., 2005). After splitting, the tRNA and mRNA are released from the 30S subunit with the help of IF3 which also inhibits reassociation of the subunits (Peske et al., 2005). However, it is still not entirely clear how the process of mRNA and tRNA dissociation occurs on a molecular level.

In eukaryotic cells, the post-termination complex still contains eRF1 and eRF3, alongside a deacylated tRNA in the P/E-site. After eRF3 is released from the ribosome, the ribosome splitting ATPase ABCE1 can bind to the ribosome-eRF1 complex, which stimulates peptide release and triggers ribosome recycling (Becker et al., 2012; Franckenberg et al., 2012; Pisarev et al., 2007). Thus, in contrast to prokaryotes, recycling and termination are coupled by a combined action of eRF1 and ABCE1. Furthermore, several initiation factors like eIF3, eIF1, eIF2 eIF2D and eIF5 show interactions with ABCE1 and bind to the SSU after recycling. These interactions also link translation initiation to recycling, which is coordinated by ABCE1 (Heuer et al., 2017; Pisarev et al., 2007). Moreover, binding of initiation factors and ABCE1 prevent subunit joining.

## 1.3 A fresh start – mRNA and protein degradation in the cell

Not only the production of proteins and RNAs but also their degradation is important to maintain cellular homeostasis. Hence, their equilibrium is regulated in a concerted fashion. Consistently, to keep steady-state levels in the cell, mRNAs and proteins are constantly degraded and re-synthesized (Amm et al., 2014; Nedelsky et al., 2008; Parker, 2012). Consequently, mRNAs and proteins are constantly monitored and checked, also allowing a quick change of their basal levels, for example in response to differences in the environment. Thus, it was not surprising that earlier studies already highlighted possible connections between translation (therefore synthesis) and protein and RNA degradation (Coller and Parker, 2005; Franks and Lykke-Andersen, 2008; Jacobson and Peltz, 1996; LaGrandeur and Parker, 1999; Muhlrad et al., 1994; Roy and Jacobson, 2013; Schwartz and Parker, 1999). Nevertheless, detailed information about the interactions between these central pathways is scarce, particularly on a structural level. Only in recent years, researchers could elucidate interactions

between both pathways in more detail and could show that these processes are indeed tightly intertwined in the cell. The following introduction will focus on protein and mRNA degradation in *S. cerevisiae*.

### 1.3.1 General pathways of protein degradation

Two main systems are responsible for basically all protein degradation in eukaryotic cells (as reviewed in Amm et al., 2014; Nedelsky et al., 2008; Fig. 1.2). The first system is the ubiquitin-proteasome system (UPS), relying on marking proteins with ubiquitin for subsequent degradation by the proteasome. A second pathway includes degradation of proteins in lysosomes, known as the autophagy-lysosomal system. Both pathways work in parallel in eukaryotic cells. Proteins showing shorter lifetimes are often targeted by the UPS whereas long-lived proteins are often degraded by the autophagy-lysosomal system (Nedelsky et al., 2008). Despite being different pathways, both share the same basic principles of marking proteins for degradation before they are transported to the degradation sites.

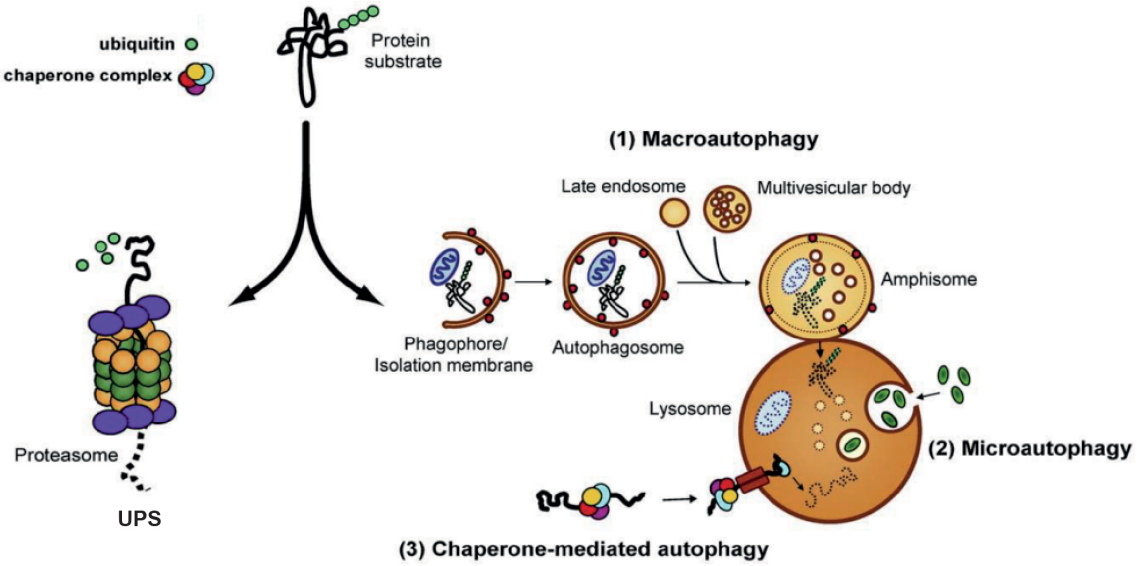


FIGURE 1.2: **General protein degradation in yeast.** Two major systems for protein degradation exist in eukaryotes. Proteins are either degraded by the ubiquitin-proteasome system (UPS) or via the autophagy-lysosomal system. For the autophagy-lysosomal system, three different pathways are known: (**1**) Macroautophagy of large parts of the cytoplasm; (**2**) Microautophagy of small volumes; and (**3**) Chaperone-mediated autophagy. A common mechanism is to mark the target protein by ubiquitin (UPS) or ubiquitin-like proteins (autophagy-lysosomal) and subsequent delivery to the degradation site. Adapted from Nedelsky et al., 2008.

For the autophagy-lysosomal system, three different events are generally distinguished: a) microautophagy, where only a very small part of the cytosol is engulfed, often including only very few target proteins (Ahlberg et al., 1982); b) chaperone-mediated autophagy, where chaperones deliver target protein to the lysosomes (Dice, 1990); and c) macroautophagy, where a very large part of the cytoplasm is engulfed into a lysosomal vesicle, sometimes even including entire organelles (Arstila and Trump, 1968). To target a protein by the autophagy-lysosomal system, Atg (autophagy-regulating gene) proteins mark their targets with ubiquitin-like proteins (UBL) very similar to the UPS (see below). After being marked, the target proteins are subjected to either of the three different pathways of the autophagy-lysosomal degradation system (Nedelsky et al., 2008).

The UPS works in a very similar manner. Target proteins are marked with ubiquitin, a 76 amino acid protein, which destines them for degradation by the proteasome (Amm et al., 2014). Ubiquitin is added during a three-step process (Amm et al., 2014; Pickart, 2001). First, so called E1 ubiquitin-activating enzymes activate ubiquitin by coupling ATP hydrolysis to binding ubiquitin via an energy-rich thioester bond and deliver the ubiquitin to its target (Schulman and Wade Harper, 2009). Afterwards, an E2 ubiquitin-conjugating enzyme transfers the activated ubiquitin onto itself by a transesterification (van Wijk and Timmers, 2010). Finally, ubiquitin is linked to its target via an E3 ubiquitin ligase. Following ubiquitination, the target protein is often actively channelled into the proteasome by ATPases (Nedelsky et al., 2008). Moreover, the UPS system is not only active in the cytoplasm but is also found in more specific protein degradation pathways like the unfolded protein response and the ER-associated degradation (Nedelsky et al., 2008).

### 1.3.2 mRNA architecture and steps preceding degradation

As mentioned, also mRNAs are constantly degraded, a process known as mRNA turnover (reviewed for example in Parker, 2012). The general design of an mRNA includes several distinct regions that are important for its stability and that ensure that it will be correctly and efficiently translated and localized. mRNAs contain two chemically distinct ends called 5' and 3', which result from chemical directionality and describe which end of the nucleotide is unlinked and free. Oftentimes, the 5' end contains a phosphate group attached to the 5' carbon of the furanose ring whereas the 3' carbon is linked to a hydroxyl group. Commonly found regions of an mRNA are the 5' untranslated region (UTR), the open reading frame (ORF) containing the sequence that is translated into a protein marked by a start codon at the beginning

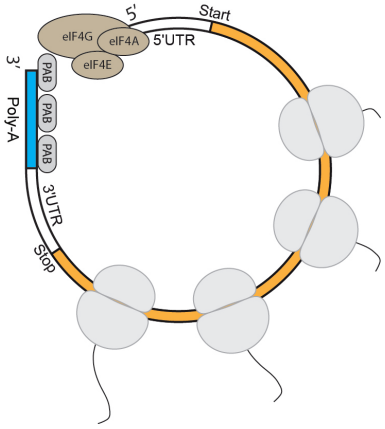


FIGURE 1.3: **Schematic view of a polysome-associated circular eukaryotic mRNA.** The 5' cap is bound by the cap-binding complex eIF4F consisting of eIF4A, E and G. eIF4G can interact with Pab1 at the 3' poly-A tail, therefore circularizing the mRNA. The open reading frame (orange) flanked by the start and stop codon is the actively translated region and often translated by multiple ribosomes.

and a stop codon at the end, a 3' UTR and, for eukaryotic mRNAs, a poly-adenosine (poly-A) tail. In yeast, the length of this tail is generally around 70-80 nucleotides (Brown and Sachs, 1998), whereas human poly-A tails are much longer with up to 200 nucleotides (Eckmann et al., 2011). Additionally, the 5' end of the mRNA is protected by a unique 7-methylguanylate cap ($m^7G$) ensuring the stability of the mRNA (Shatkin, 1976). This architecture is common to basically all healthy eukaryotic mRNAs.

In most eukaryotes, mRNAs undergo a maturation process in the nucleus that includes end modifications and splicing before they are transported to the cytoplasm. During transcription in the nucleus, the 5' cap and the poly-A tail are added to the pre-mRNA transcript. Here, the poly-A tail is not encoded on the DNA template, but rather added by specific enzymes like poly-A polymerases (PAPs). Additionally, pre-mRNAs are subjected to splicing where introns are removed and exons are ligated to form the mature mRNA.

In the cytoplasm, most translationally active mRNAs are ribonucleoproteins (RNPs) which are circularized due to the interaction of the cap binding eIF4F complex that can interact with poly-A binding protein Pab1 (Fig. 1.3). Hereby, Pab1 coats the poly-A tail of the mRNA and interacts directly with the eIF4G subunit of the cap-binding complex. These mRNAs are often associated with multiple translating ribosomes and constantly translated.

Two major mRNA exonucleolytic degradation pathways are known, utilizing the

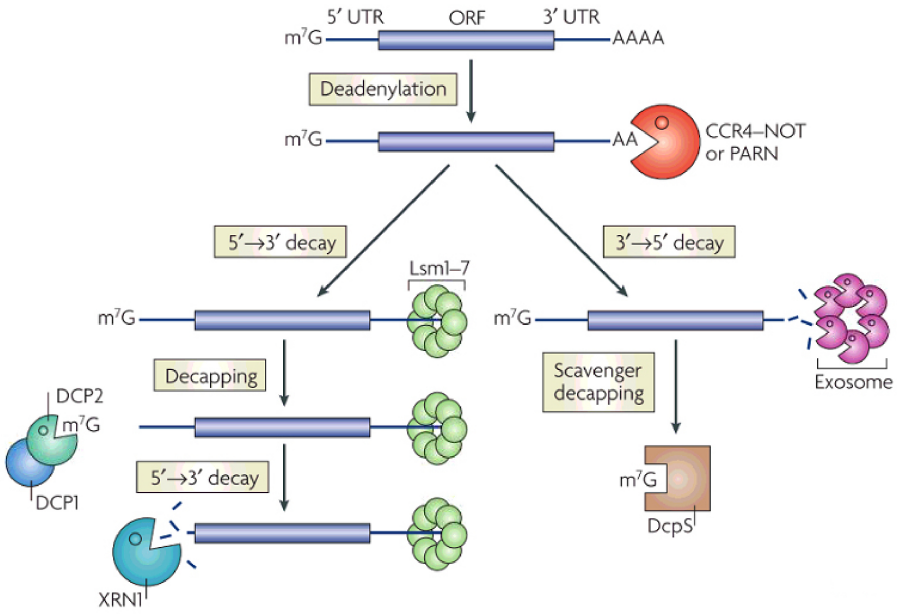


FIGURE 1.4: **General mRNA degradation in *S. cerevisiae*.** mRNAs can either be degraded by the 5'-to-3' pathway via Xrn1 or the 3'-to-5' pathway by the cytosolic exosome. For both pathways, deadenylation prior to degradation is carried out by the main deadenylase complexes Pan2/Pan3 (not shown) and Ccr4/Not. Afterwards, most mRNAs are decapped by Dcp1/Dcp2, generating a 5' monophosphate end for Xrn1-dependent degradation. Exosomal degradation can be performed without decapping. For exosomal degradation, the Ski proteins need to be recruited to the mRNA (not shown). Adapted from Garneau et al., 2007.

two different ends of an mRNA (Parker, 2012; Fig. 1.4). Hereby, mRNAs are either degraded in 5'-to-3' direction by Xrn1 (Hsu and Stevens, 1993; Muhlrad et al., 1994) or in 3'-to-5' direction by the cytosolic exosome (Anderson and Parker, 1998). Xrn1-dependent 5'-to-3' degradation is the main mRNA turnover pathway in yeast and most other eukaryotes (Parker, 2012). However, before an mRNA can be degraded, several prior steps have to be carried out. The first step involves the deadenylation of the 3' poly-A tail followed by decapping of the 5' cap structure.

**Deadenylation and decapping.** Deadenylation is tightly regulated as it vastly effects the stability of the mRNA. Regulation usually occurs through factors directly binding to the mRNA that recruit the deadenylase complexes or because of factors promoting their activity *per se*. Additionally, environmental cues can influence deadenylation positively or negatively (Parker, 2012). Initially, the Pan2/Pan3 complex deadenylates mRNAs until the poly-A tail is shortened to roughly 65 residues. This process appears to be very fast as no mRNA fragments with poly-A tails longer than

70 residues can be detected under native conditions (Brown and Sachs, 1998). Afterwards, the Ccr4/Pop2/Not complex shortens down the poly-A tail even further until reaching approximately 10 residues (Tucker et al., 2001). Interestingly, it has been shown that Pab1 bound to the poly-A tail of mRNAs strongly influences deadenylation and therefore the stability of mRNAs in yeast. Pab1 strongly promotes Pan2/Pan3 dependent deadenylation (Boeck et al., 1996), but inhibits Ccr4/Pop2/Not (Tucker et al., 2002). This lead to a model where Pab1 bound to the poly-A tail of the mRNA promotes initial shortening by Pan2/Pan3. After having less Pab1 bound because of poly-A shortening, deadenylation can switch to Ccr4/Pop2/Not. Thus, by influencing the binding of Pab1 to the poly-A tail, deadenylation can be regulated and controlled (Parker, 2012). Notably, studies have shown that the length of the poly-A tail of an mRNA can have strong effects on its stability and translational state (reviewed in Jalkanen et al., 2014). This effect could be due to less bound Pab1, therefore fast deadenylation by Ccr4/Pop2/Not. Since Pab1-mRNA interactions are also influenced by translation and Pab1 has been shown to interact with translation initiation and termination factors (Cosson et al., 2002; Funakoshi et al., 2007; Kobayashi et al., 2004), translation can be coupled directly to the stability and degradation of an mRNA.

After deadenylation, the mRNA can be directly degraded via the 3'-to-5' degradation pathway (Parker, 2012). More commonly however, the mRNA is subjected to decapping first. Reaching a shortened poly-A tail length of approximately 10 residues triggers binding of Pat1/Lsm1-7 to the short poly-A tail, replacing bound Pab1 and leading to removing the 5' cap by recruiting Dcp1/Dcp2 (Tharun and Parker, 2001). Subsequently, the mRNA is degraded by the 5'-to-3' degradation pathway via Xrn1.

### 1.3.3 5'-to-3' mRNA degradation

As mentioned above, 5'-to-3' degradation is the major pathway for mRNA turnover in yeast (Parker, 2012). mRNAs are degraded by the exonuclease Xrn1 after deadenylation and decapping (Hsu and Stevens, 1993; Muhlrad et al., 1994). In contrast to deadenylation and 3'-to-5' degradation which happens exclusively in the cytoplasm, initial reports could show that Xrn1 dependent degradation and decapping of mRNAs occurs in localized foci inside of the cell called P-bodies (Sheth et al., 2003). These P-bodies have been reported to be the major sites of mRNA decapping and 5'-to-3' degradation, leading to a proposed model where mRNAs are classified into one of two classes: a) mRNAs that are part of active translation and are associated to polysomes that are not subjected to degradation; and b) mRNAs that are part of

a nontranslating pool present in P-bodies being a target for decapping and decay (Sheth et al., 2003). Thus, the fate of an mRNA would be decided by its translation status. Early observations supported this model by showing that accumulating mRNAs on polysomes by addition of the translation inhibitor cycloheximide (CHX) leads to a harsh decrease of decapping and P-bodies inside of cells (Sheth et al., 2003; Teixeira et al., 2005) and that translation initiation rates correlate inversely with decay rates (Jacobson and Peltz, 1996). However, this view is challenged by newer studies showing that decapping and 5'-to-3' degradation can take place outside of P-bodies on mRNAs that are still associated to polysomes and thus still translationally active to some extent (Hu et al., 2009; Pelechano et al., 2015). Xrn1 was shown to degrade mRNAs following the translating ribosome in 5'-to-3' direction in these cases, arguing that P-bodies are not essential for mRNA decay (Hu et al., 2009; Pelechano et al., 2015).

### 1.3.4 3'-to-5' mRNA degradation - the exosome

Instead of decapping and 5'-to-3' degradation, the mRNA can be degraded directly after deadenylation via the 3'-to-5' pathway by the cytosolic exosome (Anderson and Parker, 1998), as mentioned above. The exosome is a large ring-like structure composed of 9 proteins forming the Exo-9 core (Liu et al., 2006; Makino et al., 2013; Fig. 1.5). Binding of Rrp44/Dis3 to Exo-9 leads to the formation of the catalytically active Exo-10 complex (Fig. 1.5A) displaying endo- and exonuclease activity. Here, Rrp44/Dis3 seems to be the only catalytically active protein and responsible for the entire nucleolytic activity of Exo-10 (Dziembowski et al., 2007; Liu et al., 2006). The mRNA substrate is channelled through the ring-like Exo-9 complex into the active site of Rrp44 reminiscent of the prokaryotic counterpart RNase PH that adopts an overall similar structure (Makino et al., 2013). Furthermore, it could be shown that an RNA duplex can be unwound by structural features of the cap proteins of Exo-9, leading to a single stranded RNA that is traversing through the exosome (Fig. 1.5B). This mode of action seems to be conserved between the cytosolic and nuclear exosome, with the only change being that Rrp44 is substituted by Rrp6 in the nucleus (Makino et al., 2013). Despite Rrp44 showing endonuclease activity, mRNA turnover solely relies on its exonucleolytic capabilities (Dziembowski et al., 2007).

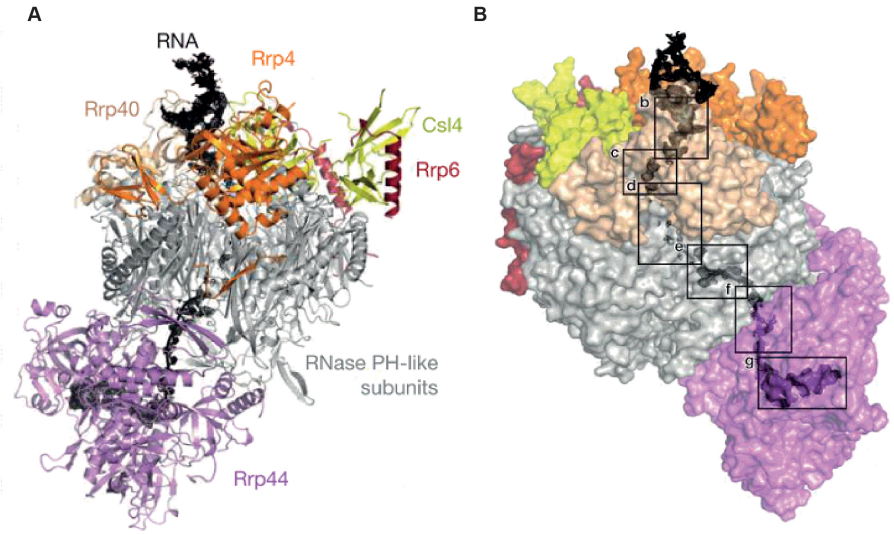


FIGURE 1.5: **Overview of the exosome from *S. cerevisiae* and the path of the RNA.** (**A**) Overview of the Exo-10 structure containing the Exo-9 ring-like core (upper part) with its RNase PH-like subunits, the catalytic subunit Rrp44 (bottom) and the RNA (black). Important cap proteins Csl4 and Rrp6 for RNA duplex unwinding are highlighted. (**B**) A slice through the exosome structure reveals the RNA path. RNA is unwound by the cap proteins of Exo-9 and funnelled into the catalytic center of Rrp44 where it is exonucleolytically degraded. Adapted from Makino et al., 2013.

### 1.3.5 3'-to-5' mRNA degradation - the Ski proteins

Even though the exosome is the responsible nuclease to degrade mRNAs *per se*, additional accessory factors are needed for 3'-to-5' degradation. Studies could show that a set of proteins known as superkiller (or Ski) proteins are essential for exosome-dependent degradation of mRNAs (Anderson and Parker, 1998; Araki et al., 2001; van Hoof et al., 2000). Particularly, four proteins could be identified to be necessary for this pathway: Ski2, Ski3, Ski7 and Ski8. All proteins were reported to interact with the exosome directly or indirectly and deletions of any of these proteins lead to complete shut-down of the 3'-to-5' pathway.

**Ski7.** Ski7 is a translational GTPase of the eEF1$\alpha$-family (Benard et al., 1999), structurally similar to other translational GTPases like EF-Tu, eRF3, the eponymous eEF1$\alpha$ and especially Hbs1, a protein involved in the recognition of stalled ribosomes on aberrant mRNA. Originally detected in viral repressor assays (Toh-E et al., 1978), it was soon clear that Ski7 is essential for 3'-to-5' mRNA degradation (Araki et al.,

2001; Benard et al., 1999; van Hoof et al., 2000). Ski7 consists of two short N-terminal domains N1 and N2 and a larger C-terminal GTPase domain (Araki et al., 2001). N1 was shown to interact with Ski3 and Ski8 whereas N2 interacts with the exosome (Araki et al., 2001). Under native conditions, Ski7 appears to be stably bound to the exosome in cells via the cap protein Csl4 (Dziembowski et al., 2007; van Hoof et al., 2000; Kowalinski et al., 2016). Moreover, it was assumed that Ski7 could interact with ribosomes because of its relation to other translational GTPases, possibly fulfilling a similar role and identifying specific targets for NSD similar to Hbs1 (van Hoof et al., 2002). However, this interaction could never be proven by biochemical or structural means. Interestingly, it was shown that the GTPase domain of Ski7 is not necessary for general 3'-to-5' degradation of mRNAs (Araki et al., 2001).

Only recently, first structural insights into the overall architecture of Ski7 were gained. A crystal structure of the GTPase domain of Ski7 revealed an overall striking similarity to the GTPase domain of Hbs1 with the typical monovalent cation bound to the active site, as expected from sequence alignments (Kowalinski et al., 2015). However, two distinct differences in the catalytic centre could be visualized arguing that Ski7 cannot be catalytically active like its GTPase family members. First, a different polar residue was found in the active site where an otherwise conserved histidine is substituted by serine. Second, another polar residue was found to be substituted near the $\gamma$-phosphate of the bound nucleotide (threonine instead of valine)(Kowalinski et al., 2015). These changes argue in favour of Ski7 being a GTP binding protein and pseudo-GTPase, without GTPase hydrolysis activity (although its activity in the presence of an unknown cofactor cannot be disregarded yet). Notably, the mammalian homologue of Ski7 was only recently identified as a splicing variant of the mammalian HBS1 gene (Kalisiak et al., 2016). Since Ski7 is the only protein known to be able to interact with both the exosome and the other Ski proteins, it was assumed that it would act as an adaptor in 3'-to-5' degradation (Araki et al., 2001; van Hoof et al., 2000; Wang et al., 2005).

**The Ski2-Ski3-Ski8 helicase complex.** In contrast to Ski7, the cytosolic proteins Ski2, Ski3 and Ski8 form a stable tetrameric complex known as the Ski complex consisting of one copy of Ski2 and Ski3 and two copies of Ski8 (Brown et al., 2000; Synowsky et al., 2009; Wang et al., 2005). The Ski complex is evolutionary conserved and is involved in essentially all cytosolic pathways including the exosome (Halbach et al., 2013). Within the Ski complex, only Ski2 harbours enzymatic activity, being an RNA helicase of the DExH family (Halbach et al., 2012, Halbach et al., 2013).

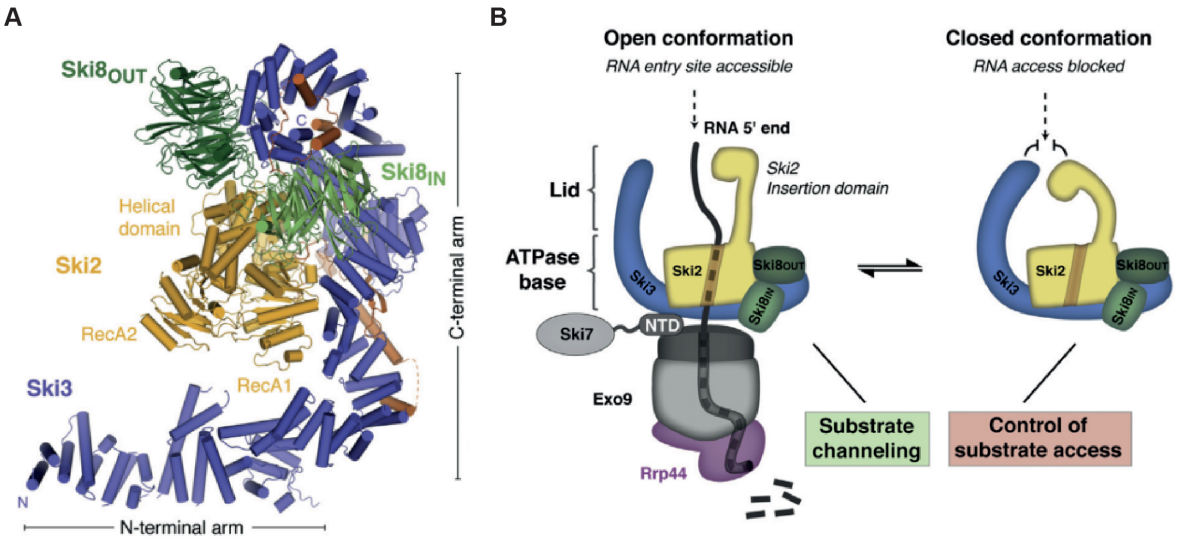


FIGURE 1.6: **Structure of the Ski complex and RNA channelling into the exosome.** (**A**) Structural overview of the Ski complex. Ski3 acts as a scaffold protein and has a long N- and C-terminal arm consisting of TPR repeats (blue). Two subunits of Ski8 (green; $Ski8_{OUT}$ and $Ski8_{IN}$ according to their position in the complex) are contacting the C-terminal arm of Ski3 and the helical domain of Ski2 (yellow). The DExH helicase Ski2 is centrally positioned. (**B**) Proposed model for RNA channelling by the Ski complex. RNA is funnelled through the Ski2 helicase into the exosome. Ski7 is proposed to act as an adaptor, bringing both complexes together. The N-terminal arm of Ski3 and the arch domain of Ski2 are believed to allosterically regulate Ski2 by allowing or preventing access to the helicase core. Adapted from Halbach et al., 2013.

Moreover, as for most complexes and proteins that are involved in RNA degradation, a nuclear pendent of the Ski complex exists where Mtr4 acts as the catalytic subunit in a multiprotein complex called the TRAMP complex (Houseley and Tollervey, 2006; Vanacova and Stef, 2007; Wyers et al., 2005).

A crystal structure of the *S. cerevisiae* Ski complex could elucidate its overall architecture and led to a possible model for its interaction with the cytosolic exosome (Halbach et al., 2013; Fig. 1.6A). Ski3 has an overall L-shape with long N- and C-terminal arms consisting of 33 tetratricopeptide repeats (TPRs). Its C-terminal arm (TPR 11-33) binds to the globular helicase domain of Ski2 as well as to both Ski8 subunits (named $Ski8_{IN}$ and $Ski8_{OUT}$ for their inner and outer position within the complex) that show the 7-bladed $\beta$-propeller structure characteristic for WD40 repeat proteins. Both Ski8 proteins recognize specific Q-R-x-x-$\phi$ sequences (x being any amino acid and $\phi$ being aromatic residues) in TPR 31 and TPR 33. In addition, the N-terminal region of Ski2 wraps around this C-terminal arm of Ski3. The N-terminal arm of Ski3 features an interruption of the regular TPR motif having a

split B helix in TPR 4-5 and large interrepeat angles in TPR 6-7. This arrangement leads to a higher flexibility of the N-terminal arm, allowing it to move into a more extended position. Ski2 is positioned centrally in the complex, sandwiched between Ski3 and both Ski8 subunits. Its globular helicase domain consisting of two RecA domains and a helical domain characteristic of DExH helicases create an RNA channel where the helical domain flanks both RecA domains. As for all DExH helicases, Ski2 contains a so-called $\beta$-hairpin loop at the helicase entrance. This characteristic loop has been shown to be important for mRNA unwinding in the related DExH helicase Hel308 (Büttner et al., 2007) and is believed to be essential for the processivity of the helicase. Furthermore, Ski2 contains a large and highly flexible arch (or insertion) domain extending from its globular core that was predicted to act as a lid to allow or prevent access to the helicase core of Ski2 (Halbach et al., 2012, Halbach et al., 2013; Fig. 1.6B). Because of its high flexibility, the arch domain could not be resolved in the crystal structure of the Ski complex and was truncated for crystallization attempts. However, it was still resolved in the crystal structure of Ski2 alone without any other subunits of the Ski complex (Halbach et al., 2012).

All components of the Ski complex show effects on the Ski2 ATPase and helicase activity (Halbach et al., 2013). Compared to single Ski2, the ATPase activity decreases 5-fold in presence of Ski3 and Ski8. Disrupting the interaction sites of $Ski8_{IN}$ and $Ski8_{OUT}$ with Ski3 results in either an insoluble sample or a complex where RNA binding is severely disrupted, respectively. These findings argue that $Ski8_{IN}$ is important for the structural integrity of the Ski complex whereas $Ski8_{OUT}$ is needed for RNA binding. RNase protection assays revealed that the Ski complex binds RNA fragments of 9-10 nucleotides. Upon removing the Ski2 arch domain and the N-terminal arm of Ski3, Ski2 shows a significant increase in ATPase and helicase activity. This lead to a model whereby the arch domain together with the N-terminal arm of Ski3 allosterically regulate the activity of Ski2, possibly by forming a lid-like structure to regulate access of RNA to the helicase core (Halbach et al., 2013). Finally, additional RNase protection assays could show an extended protection length of 43-44 nucleotides for RNA fragments by adding the exosome to the Ski complex. This extended length exactly represents the combined protection lengths of the Ski complex and the exosome, arguing in favour of the Ski complex channelling RNA into the exosome, thus resulting in a long extended RNA binding tunnel (Fig. 1.6B).

## 1.4 When translation goes awry - eukaryotic quality control pathways

Protein and mRNA degradation are not only key processes for turnover pathways. As for all cellular processes, translation and transcription are not flawless and give rise to errors. In fact, optimizing speed and reaction accuracy is one of the major points in most cellular pathways and puts conflicting demands on enzymes. Both RNA polymerase II (the main polymerase involved in mRNA transcription) and ribosomes show relatively high fidelity. RNA polymerase II incorporates mistakes with an error rate of roughly $2x10^{-4}$ to $2x10^{-6}$ (Alic et al., 2007; Kireeva et al., 2008). This error rate is magnitudes higher than that of DNA replication (Bird, 2007), but seems to be acceptable since mistakes are not taken over to next generations. Yeast ribosomes have an error rate estimated between 2x10-5 to 5x10-6, depending on the analysed codon (Stansfield et al., 1998). These error rates are the product of intrinsically precise enzymes coupled to proofreading mechanisms, i.e. kinetic proofreading for translation (Blanchard et al., 2004). Nevertheless, mistakes can happen during both processes, making it necessary that cellular checkpoints and surveillance systems exist. These security systems are generally known as quality control pathways and can either act on mRNAs (mRNA quality control) or proteins (protein quality control). Quality control systems are found in all eukaryotes and often show high conservation in their involved processes and factors (as reviewed for example in Brandman and Hegde, 2016; Inada, 2013; Shoemaker and Green, 2012). Nevertheless, most pathways were only discovered during the last decade, leaving many questions still unanswered .

### 1.4.1 Protein quality control response

Protein quality control of aberrant peptides generally involves degradation via the UPS. Aberrant proteins can be potentially dangerous since they are non-functional and often prone to aggregation which can be toxic to the cell. In cases where translation errors occurred but the mRNA template is still healthy, the aberrant protein is recognized and targeted by the UPS and subjected to degradation. If the mRNA is faulty, mRNA quality control is initiated first and the already translated aberrant peptide is targeted by an alternative protein quality control pathway called RQC (see below).

### 1.4.2 mRNA quality control response

mRNA quality control is a highly regulated and complex process, since errors in mRNAs can propagate through many translation cycles and are thus not tolerated by the cell. The most common cases of aberrant mRNAs in eukaryotic cells are either truncated or chemically damaged mRNAs, mRNAs without stop codons but still containing a poly-A tail due to premature poly-adenylation or mRNAs with premature stop codons (Shoemaker and Green, 2012). Each of these mRNAs is targeted by one of the three major mRNA quality control pathways known in eukaryotes (Fig. 1.7):

1) **Nonsense-mediated decay (NMD),** targeting mRNAs with premature stop codons

2) **No-go decay (NGD),** targeting mRNAs that contain translational road-blocks like stable secondary structure elements or damaged nucleobases

3) **Nonstop decay (NSD),** targeting mRNAs lacking a stop codon

A common feature of these mRNA quality control pathways is their co-translational initiation including the ribosome (Shoemaker and Green, 2012). Since aberrant mRNAs are often the cause for translational stalling, ribosomes tend to get stuck on these mRNAs. Since this is unusual for translating ribosomes, these stalled intermediates are recognized by the different quality control factors involved in NMD, NGD or NSD. Thus, translation is driving quality control with the starting point being the ribosome stalled on the aberrant mRNA. Quality control itself can be divided into three different steps. First, after target recognition and initiation, the mRNA has to be degraded to avoid further production of aberrant protein. In contrast to general mRNA turnover, mRNA degradation in quality control is not dependent on prior deadenylation (Doma and Parker, 2006; Frischmeyer et al., 2002; Muhlrad et al., 1994). Second, the so-far translated aberrant peptide also needs to be degraded. Third, the ribosome is rescued so that it can enter a new translation cycle. These three steps are common to all mRNA quality control pathways and are regulated and guided by different factors (Shoemaker and Green, 2012).

**NMD.** As all stop codons eventually must be recognized by the termination factor complex eRF1-eRF3, the question arises how a premature stop codon can be distinguished from an authentic one. In higher eukaryotes, the presence of a large protein complex, called exon-junction complex (EJC), seems to dictate whether NMD is initiated or not (Le Hir et al., 2000). EJCs are deposited on exon-exon boundaries during pre-mRNA splicing and are present until after the first round ("pioneer round") of

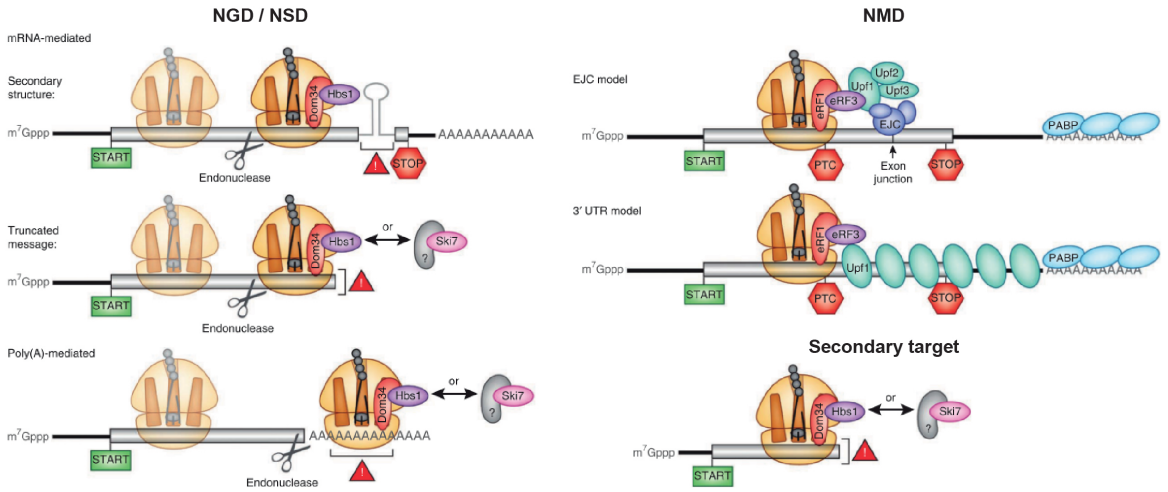


FIGURE 1.7: **Eukaryotic mRNA quality control pathways are initiated co-translationally on the ribosome.** For NMD (right panel), the premature stop codon is recognized by eRF1-eRF3 and its close proximity to the exon-junction complex (EJC) sitting on exon-exon boundaries (EJC model). The EJC and the ribosome are bridged by Upf1-Upf2-Upf3. If no splicing and EJC exist, the premature stop codon leads to an extended 3' UTR which is presumably covered by Upf1 (3' UTR model). The interaction of eRF1-eRF3 with Upf1 and the larger distance to termination promoting factors like PABP/Pab1 are thought to initiate NMD. In contrast, targets for NGD and NSD are not entirely clear and separable anymore (left panel). Both pathways can target ribosomes that are stalled on truncated mRNAs, within the poly-A tail or where secondary structure features of the mRNA forbid translation. These stalled intermediates are believed to be recognized by Dom34-Hbs1 or Ski7 (and possibly an unidentified A-site factors). How this exactly works and which targets are recognized by which complex is, however, largely unknown. A common feature is an upstream endonucleolytic cleavage, leading to a primary and secondary target. After recognition, mRNA and protein decay are initiated. Adapted from Shoemaker and Green, 2012.

translation (Maquat et al., 2010). Since the authentic stop codon is at the 3' end of an mRNA within the final exon, no EJC should be in proximity downstream of the termination codon, signalling its authenticity. Furthermore, the upstream frameshifting (Upf) proteins are the key factors to initiate the NMD pathway (Cui et al., 1995; Leeds et al., 1991, Leeds et al., 1992; Peltz et al., 1993). Upf1, a helicase with ATPase activity (Czaplinski et al., 1995; Weng et al., 1996), has been shown to interact with eRF1-eRF3 and is believed to act in premature stop codon recognition (Czaplinski et al., 1998). Together with the kinase Smg1, these proteins form the so-called SURF complex (Kashima et al., 2006). Additionally, Upf2 and Upf3 directly interact with Upf1 and with subunits of the EJC, therefore bridging the prematurely terminating

ribosome with the EJC (He et al., 1997).

In *S. cerevisiae*, where essentially no mRNA splicing takes place and EJCs are not present, NMD still exists. Here, it has been reported that a premature stop codon is recognized by its extended 3' UTR (also called faux 3' UTR)(Amrani et al., 2004; Hogg and Goff, 2010; Muhlrad and Parker, 1999). This leads to increased distance to promoting termination factors like Pab1 whereas other proteins like Upf1 might cover the extended 3' UTR to promote NMD (Kervestin et al., 2012). Numerous other factors have been identified in NMD, the exact mechanism however still needs to be elucidated (Chang et al., 2007). mRNA degradation in NMD seems to differ in yeast and higher eukaryotes. Whereby in yeast both 5'-to-3' and 3'-to-5' degradation seem to be important, higher eukaryotes mostly rely on the 5'-to-3' pathway (Mitchell and Tollervey, 2003; Muhlrad et al., 1994). In yeast, Ski7 seems to interact with Upf1 to initiate exosome-dependent degradation (Takahashi et al., 2003), whereas in higher eukaryotes Smg5-Smg7 binding to phosphorylated Upf1 initiates decapping and Xrn1-dependent degradation (Loh et al., 2013; Unterholzner and Izaurralde, 2004). If the ribosome in NMD is split by ABCE1 and how the nascent peptide is degraded and if this is a target for the RQC pathway (see below) is unclear.

**NGD and NSD.** As the name implies, NSD targets mRNAs lacking a stop codon (Frischmeyer et al., 2002; van Hoof et al., 2002). Originally, NSD was referred to as 'end-of-message stalling' since it was believed that ribosomes would translate to the very 3' end of an mRNA without a stop codon. The logical consequence would be that there are two types of mRNA targets possible for NSD: a) mRNAs that are truncated and end at some position within the ORF; and b) mRNAs that lack a stop codon but still contain a poly-A tail as the result of premature poly-adenylation, an event that is proposed to happen in up to 10% of cases in *S. cerevisiae* (Frischmeyer et al., 2002; Klauer and van Hoof, 2012). In contrast, NGD was believed to target mRNAs that generally cannot be translated anymore leading to ribosomal arrest due to any kind of translational road-block (Doma and Parker, 2006; Gandhi et al., 2008). The distinction from NSD targets would be the stalling mid-message instead of at the 3' end of the aberrant mRNA. Nevertheless, it became more and more clear over the last years that the boundaries between NSD and NGD are very fluid. For example, it has been shown that translation of as few as six lysines (coded by AAA) can already result in translation arrest (Inada and Aiba, 2005; Ito-Harashima et al., 2007; Kuroha et al., 2010). Considering that poly-A tails in yeast and human are much longer than 20 nucleotides, translation until the end of the mRNA seems to be highly unlikely.

In fact, it seems to become more apparent that NGD and NSD share some similar principles and common factors (Shoemaker and Green, 2012) and that the actual cause of stalling seems to be much more important for the downstream response than the position of the translational arrest. Because of these fluid boundaries, reports in the literature sometimes tend to be inconsistent with the definition of NSD and NGD targets.

One common fact of both NGD and NSD is an observed endonucleolytic cleavage of the aberrant mRNA upstream of the stalled ribosome leading to a so-called downstream primary and upstream secondary stalling target (Doma and Parker, 2006; Eberle et al., 2009; Gatfield and Izaurralde, 2004). Even though first reports about this cleavage were already published in 2004 and 2006, the identity of the endonuclease(s) involved is still unknown as of now. After endonucleolytic cleavage, the mRNA of the 5' secondary target in NGD has been shown to be degraded by the exosome in 3'-to-5' direction whereas the primary target is degraded by Xrn1 (Doma and Parker, 2006). In NSD, all target mRNAs seem to be exclusively degraded by the exosome (van Hoof et al., 2002; Maquat, 2002). Here, in contrast to mRNA turnover, the GTPase domain of Ski7 is essential to initiate the degradation process, leading to the beforementioned model where Ski7 recognizes the stalled ribosome on nonstop mRNA to recruit the exosome and the Ski complex (Frischmeyer et al., 2002; van Hoof et al., 2002).

Two factors originally identified as dedicated NGD factors are Pelota (Dom34 in yeast) and Hbs1, both related to translation termination factors (Doma and Parker, 2006; Inagaki et al., 2000). Dom34 shares similar central and C-terminal domains with eRF1, whereas the N-terminal domain differs (Lee et al., 2007). Where eRF1 is recognizing the stop codon in the A-site of the ribosome via a network of interactions formed between the stop-codon quadruplet and the eRF1 N-terminal domain (Brown et al., 2015; ; Matheisl et al., 2015), Dom34 was shown to recognize stalled mRNA via an Sm fold in its N-terminal domain reaching deep into the A-site decoding centre (Becker et al., 2011; Lee et al., 2007). High-resolution cryo-EM structures could validate earlier claims that the $\beta$3'- $\beta$4' loop of Dom34 takes the path of the mRNA in the A-site DC (Hilal et al., 2016; Shao et al., 2016). As mentioned above, Hbs1 is a translational GTPase of the eEF1$\alpha$-family and shows similarities to eRF3 (Inagaki et al., 2000). As for most translational GTPases, the C-terminal part with its G domain, domain II and domain III are highly conserved, whereas the N-terminal part differs (similar to the aforementioned Ski7). Together with Dom34, Hbs1 forms a heterodimer akin to eRF1-eRF3 and Dom34-Hbs1 have been proposed to work in a

similar way than the termination factors (Graille et al., 2008). Cryo-EM structures of Dom34-Hbs1 bound stalled ribosomes could show that they bind in a similar fashion to the termination factors on the ribosome (Becker et al., 2011; Hilal et al., 2016; Shao et al., 2016). Interestingly, it could be seen that the N-terminal domain of Hbs1, however, is far away from the A-site and seems to bind near the mRNA entry channel, connected by a highly flexible linker. Because of the similarities of Dom34-Hbs1 to eRF1-eRF3, a competition model has been proposed where binding of Dom34-Hbs1 is kinetically preferred over eRF1-eRF3 in case of a stalled ribosome (Becker et al., 2011; Passos et al., 2009).

Notably, Dom34 plays an important role in ribosome recycling of stalled quality control intermediates (Saito et al., 2013; Shoemaker et al., 2010; Tsuboi et al., 2012). As for canonical recycling after translation termination, ABCE1 can split the ribosome for recycling. In contrast to acting with eRF1 in canonical recycling (Pisareva et al., 2011; Shoemaker and Green, 2011), ABCE1 substitutes Hbs1 and acts together with Dom34 for ribosome splitting (Becker et al., 2012; Doma and Parker, 2006; Franckenberg et al., 2012; Saito et al., 2013). As of now, this is the only known system for ribosome splitting in eukaryotic cells. Additionally, Dom34 has been shown to be involved in rescuing ribosomes that are found in the 3' UTR of mRNAs (Guydosh and Green, 2014). Thus, Dom34 is often not anymore considered as a primarily dedicated NGD factor.

### 1.4.3 The fate of the aberrant peptide – ribosome quality control

After the initiation of mRNA quality control, the already translated aberrant peptide has to be degraded as well. The so-called ribosome quality control (RQC) system targets the aberrant NC to ubiquitinate it for proteasomal degradation via the UPS (Brandman et al., 2012; Defenouillère et al., 2013; Fig. 1.8). The RQC complex responsible for marking the NC consists of three different proteins: Rqc1, Tae2 and Ltn1 (Listerin in mammals). Ltn1 is a RING domain E3 ligase and the key factor for ubiquitination of the NC, consisting of a long elongated N-terminal HEAT repeat domain and the characteristic C-terminal zinc finger RING domain (Lyumkis et al., 2013). Recent reports could show that the RQC complex binds to the 60S subunit still attached to peptidyl-tRNA and the NC after ribosome splitting (Shao and Hegde, 2014; Shao et al., 2015; Shen et al., 2015). Hereby, Tae2 and Ltn1 recognize the peptidyl-tRNA-60S species and Ltn1 ubiquitinates the NC by reaching around the 60S, a fact that is made possible by its elongated and flexible form. Notably, it could also be shown that Tae2 recruits alanyl- and threonyl-tRNAs to the 60S species (Shen

et al., 2015). In a 40S-mRNA-independent translation event, alanine and threonine are added to the NC forming C-terminal alanine-threonine (CAT) tails. These CAT tails seem to promote degradation and even have an impact on the aggregation properties of the protein, leading to different responses by the cell (Choe et al., 2016; Defenouillère et al., 2016; Yonashiro et al., 2016). Eventually, the NC is extracted from the ribosome by the ATPase Cdc48 and delivered to the proteasome for degradation (Brandman et al., 2012; Defenouillère et al., 2013). Rqc1 is the most elusive of the RQC complex proteins and was not visible in any structures as of now. Due to this fact, its function remains to be established.

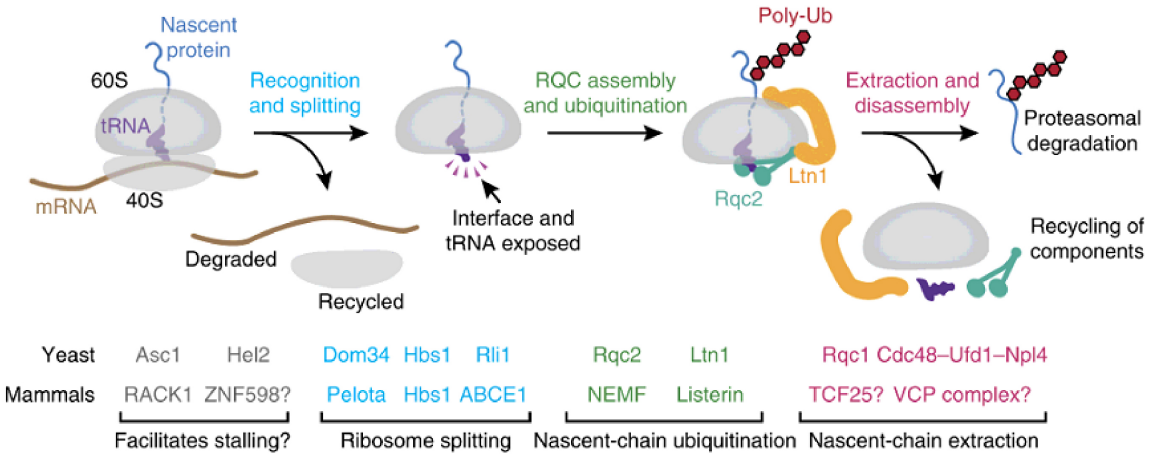


FIGURE 1.8: **Protein quality control by the RQC pathway.** Ribosome splitting of stalled intermediates is possibly mediated by Dom34-Hbs1 and ABCE1. After splitting, the RQC complex consisting of Ltn1, Rqc2/Tae2 and Rqc1 (in yeast) binds to the peptidyl-tRNA containing 60S species. Rqc2 recognizes the tRNA and the RING domain E3 ligase Ltn1 ubiquitinates the nascent peptide for proteasomal degradation. Afterwards, the ATPase Cdc48 extracts the peptide from the 60S subunit and delivers it to the proteasome. Recent reports show evidence that this system is conserved in mammalian cells, being able to identify homologues for almost every protein factor involved in the yeast RQC response. Adapted from Brandman and Hegde, 2016.

Very recent studies indicate that other factors are contributing to the RQC response, before Rqc1-Tae2-Ltn1 bind to the LSU. RACK1 (Asc1 in yeast), a non-essential protein of the 40S subunit, and the E3 ubiquitin ligase Hel2 have been identified as factors important for the RQC response, having strong impacts on initial ribosome stalling to trigger RQC (Brandman et al., 2012; Kuroha et al., 2010; Sitron et al., 2017). In particular, the ubiquitination of ribosomal proteins by Hel2 seems to regulate whether stalling occurs or not, a mechanism that seems conserved in human cells (Juszkiewicz and Hegde, 2017; Sundaramoorthy et al., 2017). Additional

factors might be implicated in guiding Hel2 to its targets, further data is needed however to completely understand the regulation of the RQC pathway by Hel2 and RACK1.

## 1.5 Ribosome stalling events outside quality control

Translational stalling is a feature not only seen during translation of aberrant mRNAs and quality control. Some specific sequences like the arginine attenuator peptide AAP or the upstream ORF of gp48 in human cytomegalovirus (CMV) can stall ribosomes very efficiently and these events are used for regulatory purposes (Bhushan et al., 2010; Matheisl et al., 2015). For example, the CMV peptide forms a compact helix in the ribosome tunnel interacting with its surface. This in turn leads to silencing of the PTC. Sometimes, stalling sequences can even be used to transform the ribosome into a nutrient sensor, making them a viable tool for different pathways (Bischoff et al., 2014). However, these specific stalling sequences are rather rare. In cells, two other reasons were identified to contribute to the majority of translation stalling events which are poly-proline and poly-basic stretches, both of which are further discussed below.

### 1.5.1 A struggle to translate – poly-proline and poly-basic stretches in protein synthesis

Proline is a common cause for translation slow-down or stalling, as indicated by several studies (Doerfel et al., 2013; Ude et al., 2013; Woolstenhulme et al., 2013, Woolstenhulme et al., 2015). Stretches of prolines were observed to be problematic for ribosomes to synthesize which was contributed to proline's unusual geometry being the only amino acid with a secondary amine, leading to its properties to disrupt secondary structure features (Johansson et al., 2011; Muto and Ito, 2008; Pavlov et al., 2009; Wohlgemuth et al., 2008).

Furthermore, one of the most common stalling events in eukaryotic cells are ribosomes stalled on poly-basic stretches, in particular stretches of lysine or arginine (Brandman et al., 2012; ; Ito-Harashima et al., 2007; Kuroha et al., 2010). Reports of such stalling events were made relatively early, but are surprising since stretches of arginine and lysine (and to some lesser extent proline) are commonly found in proteins. Additionally, as already mentioned above, poly-lysine is also to be expected if a ribosome translates into the poly-A tail of an mRNA, making it a stalling event expected in NSD. An early model suggested that poly-basic sequences, giving rise to

mostly positively charged peptides, leads to stalling by interacting with the negatively charged surface of the peptide exit tunnel (Lu and Deutsch, 2008). This event would resemble peptide-mediated stalling that had been investigated before. Nevertheless, it became clear that this model is too simplistic and cannot explain all stalling events observed. For example, experimental data could show that even two arginines coded by a CGA-CGA di-codon are enough to stop translation in its tracks, long before they can extend into the peptide exit tunnel (Gamble et al., 2016; Letzring et al., 2010). Several other codon combinations were identified which resulted in strong stalling properties, mostly combinations of arginine or lysine and proline (Gamble et al., 2016). Thus, poly-basic stalling is no longer viewed as a peptide-mediated stalling event, but rather a mixture of different stalling mechanisms.

A common feature appearing in most studies is that codon optimality has an effect on translation speed and hence ribosome stalling (Gamble et al., 2016; Pechmann and Frydman, 2013; Presnyak et al., 2015; Tuller et al., 2010). Given the redundancy of the genetic code, amino acids are coded by multiple codons that are not equal regarding translational efficiency. This lead to two classes of codons considered as optimal and non-optimal codons (Akashi, 1994; Pechmann and Frydman, 2013; dos Reis et al., 2004; Zhou et al., 2009). Non-optimal codons show much lower translation speeds than optimal ones, leading to stalled ribosomes (and even polysomes) at these positions with severely slowed down translation, also impacting mRNA half-life (Presnyak et al., 2015). Two common explanations have been given to explain this translation slow-down. First, the lower abundancy of cognate tRNAs for these non-optimal codons would result directly in slower translation. Second, non-optimal codons often contain Wobble- instead of Watson-Crick base pairs in the third position of the codon, making the actual accommodation of the cognate tRNA slower and less stable (Akashi, 1994; Gamble et al., 2016; Letzring et al., 2010; Pechmann and Frydman, 2013; dos Reis et al., 2004; Tuller et al., 2010; Zhou et al., 2009). Given the fact that codon composition has such an impact on translation, it seems unwise to generally refer to poly-basic stalling and necessary to specify exactly the cause of the translation arrest.

### 1.5.2 The rescuing factor eIF-5A

Finally, the question arises how proteins with poly-basic and -proline stretches can actually be synthesized by the ribosome. In that regard, the eukaryotic initiation factor eIF-5A (the eukaryotic homologue to EF-P in prokaryotes) has been implicated as a rescue factor. Having been proposed to act as an initiation factor that helps forming

the first peptide bond early (Glick and Ganoza, 1975), it was soon shown that EF-P (Ude et al., 2013) and eIF-5A (Gutierrez et al., 2013) help promoting translation of poly-proline, rescuing ribosomes that are stuck on these stretches. Notably, eIF-5A has a unique post-translationally modified amino acid called hypusine that is essential to its function (Dever et al., 2015; Park et al., 1981). Hypusine is generated in a two-step process by first adding the 4-aminobutyl group of spermidine to the $\epsilon$-amino group of a conserved lysine (K51 in yeast) by deoxhypusine synthetase (DHS) and subsequent conversion to hypusine via hydroxylation by deoxyhypusine hydroxylase (DOHH) (Dever et al., 2015; Park et al., 2010; Wolff et al., 1990). Whereas the dehydroxylated form of hypusine shows basically the same activity in yeast as the hydroxylated form, only the latter is active in higher eukaryotes, making DOHH an essential protein (Dever et al., 2015). Even though a crystal structure of unmodified EF-P in complex with a bacterial ribosome has been reported (Blaha et al., 2009), the molecular basis of eIF-5A's recue activity and in particular the role of the unique hypusine modification remain unknown.

## 1.6 Aims of this thesis

Throughout this thesis, it has been pointed out that the connection between mRNA translation and degradation is known, however there is rather limited knowledge on the details of this interplay. The aim of this thesis is to shed light onto this subject, with a focus on the 3'-to-5' mRNA degradation pathway.

Even though a working model for the action of Ski7 on the ribosome exists, it was so far not proven by biochemical or structural studies. Additionally, it is unclear how the Ski complex interacts with Ski7 or the ribosome in quality control (and possibly general mRNA degradation) and how the exosome is recruited to its target mRNA. Here, we investigate the function of the Ski proteins in mRNA decay *in vitro* and *in vivo*, with particular focus on their interactions with the ribosome. Our goal is to elucidate any interactions that occur in the cell between the Ski proteins and the ribosome during mRNA quality control or general turnover. Any identified intermediates should then be analysed by cryo-EM to obtain high-resolution reconstructions for structural studies. With these structures, we aim to investigate possible mechanisms and functions of Ski7 and the Ski complex to gain a better understanding of how translation interacts with the mRNA degradation system. Concomitantly, we want to elucidate how mRNAs are targeted for 3'-to-5' mRNA degradation in quality control.

# 2 Materials and Methods

## 2.1 Generation and amplification of DP120-poly-$A_{50}$ template DNA

For RNC preparations, we used the well-characterized DP120 mRNA with a 50 nucleotide long poly-A tail (DP120-poly-$A_{50}$) to stall ribosomes within the poly-A tail. The DP120-poly-$A_{50}$ reporter mRNA codes for a T7 RNA polymerase promotor, a leader sequence to promoto translation initiation, a hexahistidine ($His_6$) tag for affinitiy purification, a Hemagglutinine (HA) tag for Western Blot detection and the first 120 amino acids of dipeptidyl-aminopeptidase B followed by the poly-$A_{50}$ tail. The construct did not contain a stop codon.

The DP120-poly-$A_{50}$ DNA template was amplified by PCR using a pEX-A plasmid containing the DP120-poly-$A_{50}$ fragment as template (plasmid was synthesized by Eurofins). Used primers were a 5' T7 forward primer (5'-TAATACGACTCACTATAGGG-3') and a 3' reverse DP120-pA primer (5'-TTTTTTTTTTTTTTTTTTTTTTTTTTTTTT-TTTTTTTTTTTTTTTTTTTTATCGTAGACAGATTTAACAACGTA-3').

For PCR, the Thermo Scientific Phusion Flash High-Fidelity PCR Master Mix was used and protocols were used as recommended by Thermo Scientific. 50 $\mu$l reactions were generally prepared with 0.5 $\mu$M primers and 10 ng DNA template. The PCR program was used as follows:

TABLE 2.1: PCR program

| | Temperature | Time | Cycles |
|---|---|---|---|
| Initial Denaturation | 98 °C | 30 s | 1x |
| Denaturation | 98 °C | 10 s | |
| Annealing | 51 °C | 15 s | 30x |
| Elongation | 72 °C | 20 s | |
| Final extension | 72 °C | 300 s | 1x |

The obtained PCR product was subsequently purified using the QIAGEN PCR Purification Kit. Concentrations were measured with a NanoDrop 1000 spectrophotometer device.

## 2.2 SDS-PAGE

SDS-PAGE for separating proteins according to their molecular weights was performed using standard protocols (Laemmli, 1970). For RNC preparations and *in vitro* reconstitutions, we used 15% discontinuous polyacrylamide gels in 1x SDS running buffer (25 mM Tris, 192 mM glycine, 0.1% (w/v) SDS). For the polysomes profile analysis and the native pullout preparation, we used 4-12% NuPAGE gradient gels in 1x MOPS running buffer (50 mM MOPS, 50 mM Tris Base pH 7.7, 0.1% SDS, 1 mM EDTA). Denaturation of samples was performed at 65 °C for 10 min in case of RNC samples to preserve the peptidyl-tRNA bond. All other samples were denaturated at 95 °C for 10 min. Samples containing 1x SDS-SB (50 mM tris(hydroxymethyl)aminomethane (Tris) / HCl pH 6.8, 2% (w/v) SDS, 10% (v/v) glycerol, 0.1% (w/v) bromophenol blue, 100 mM 1,4-dithiothreitol) were loaded and electrophoresis was performed at constant voltage, using 100–175 V for polyacrylamide gels or 200V for NuPAGE gels for 90 min.

## 2.3 Simply Blue and SYPRO Orange staining

For small amounts of proteins (i.e. in case of most in vitro reconstitution assays), protein gels were stained with SYPRO Orange and subsequently visualized with a Typhoon FLA 900 scanner. Gels were stained in a 1:5000 dilution of SYPRO Orange (Invitrogen) in freshly prepared 10% acetic acid for 1h on a shaker and washed 3x with water for 5 min afterwards. In all other cases, gels were stained with Simply Blue Coomassie staining solution (Novex). Gels were 3x shortly cooked in water to remove SDS. Subsequently, gels were cooked in Simply Blue staining solution and shaken 5-10 min at RT.

## 2.4 Western Blotting

Semi-dry Western blotting was used after SDS-PAGE to transfer proteins onto a membrane. Blotting was performed at 150 mA per gel for 90 min in methanol-based blotting buffer (20% (v/v) methanol, 48 mM Tris/HCl, 39 mM glycine, 0.037% (w/v)

SDS). The membrane was stained with Amido Black (0.1% (w/v) naphthol blue black, 7.5% (v/v) acetic acid, 20% (v/v) ethanol) for 1 min under shaking conditions and destained ((40% (v/v) ethanol, 10% (v/v) acetic acid) until clear bands were visible on white background. For antibody detection with $\alpha$-PAP ($\alpha$-Protein A), the membrane was blocked 3x in 2% milk/PBS (137 mM NaCl, 2.7 mM KCl, 10 mM $Na_2HPO_4$, 1.8 mM $KH_2PO_4$) at RT for 10 min and subsequently washed with 1x PBS for 1 min. Afterwards, the membrane was incubated for 1h at RT on a shaker with 1:5000 $\alpha$-PAP (abcam) in 2% milk/PBS. Subsequently, the membrane was washed 3x with 1xPBS for 5 min.

For antibody detection with $\alpha$-CAB ($\alpha$-Calmodulin), the membrane was blocked in 5% milk / TBS (20 mM Tris HCl pH 7.6, 150 mM NaCl) at RT for 30-45 min and subsequently washed with 1x TBS for 1 min. Afterwards, the membrane was incubated over night at 4 °C on a shaker with 1:1000 $\alpha$-CAB antibody (Thermo Fisher). For the secondary antibody, the membrane was washed 2x with TBS and 1x with TBS-T (TBS with 0.1% (v/v) Tween) for 5 min, blocked in 5% milk / TBS for 10 min and incubated with 1:5000 goat anti-mouse HRP-conjugate in the blocking solution. In case of RNCs, the same procedure was used with the exception that the first antibody was HA-probe (Santa Cruz) instead of $\alpha$-CAB. Protein signals were visualized with ECl solution (AppliChem) on a Fujifilm LAS-3000 Imager.

## 2.5 *In vitro* transcription of DP120-poly-$A_{50}$ mRNA

*In vitro* transcription reactions were carried out with the Ambion T7 mMESSAGE mMACHINE Kit. The reaction was performed according to the manual.

The reaction mixes were incubated for 2 h at 37 °C and the RNA was precipitated over night at -20 °C by adding 30 $\mu$l H20 and 30 $\mu$l LiCl solution (Ambion). The precipitated RNA was separated by centrifugation (20 min, 4 °C, 14000 rpm) and the pellet was washed with 1 ml EtOH. After a second centrifugation (10 min, 4 °C, 14000 rpm), the pellet was dried at room temperature for 5 min and resuspended in 30 $\mu$l nuclease-free $H_2O$. Concentrations were measured with a NanoDrop 1000 spectrophotometer.

## 2.6 NS-RNC preparation

Ribosome nascent chain complexes (RNCs) were purified by programming ribosomes in a yeast cell-free translation system with DP120-poly-$A_{50}$ mRNA essentially as described before (Beckmann et al., 2001; Halic et al., 2004). 1.2 ml *in vitro* translation reaction mixes were used. Reactions were incubated for 75 min at 17 °C and stopped by adding 200 $\mu$g/ml cycloheximide. Subsequently, 4x300 $\mu$l of the total reaction mix were loaded onto 800 $\mu$l of 750 mM sucrose cushion in 250 buffer (50 mM Tris/HCl pH 7.0, 250 mM KOAc, 25mM, 250 mM sucrose, 10 mM $Mg(OAc)_2$, 5 mM 2-mercaptoethanol, 10 $\mu$g/ml cycloheximid, 0.1% Nikkol, 0.1% EDTA-free protease inhibitor cocktail pill (pill)/ml, 0.2 U/ml RNAsin) and ribosomes were pelleted by centrifugation in a TLA120.2 rotor (100000 rpm, 45 min, 4 °C). The ribosomal pellet was resuspended in 250 buffer over 45 min.

The resuspended ribosomes were added to 2x1 ml of Talon metal affinity resin slurry equilibrated with 250/tRNA buffer (250 buffer with 10 $\mu$g/ml tRNA) and incubated for 15 min at RT. The flowthrough was collected and the resin was washed with 8x 1.5 ml 250 buffer and 2x 2.25 ml 500 buffer (50 mM Tris/HCl pH 7.0, 500 mM KOAc, 25mM, 250 mM sucrose, 10 mM $Mg(OAc)_2$, 5 mM 2-mercaptoethanol, 10 $\mu$g/ml cycloheximid, 0.1% Nikkol, 0.1% pill/ml, 0.2 U/ml RNAsin). Elution was performed with 2x 1.5 ml 250/100 buffer (250 buffer with 100 mM imidazole) over 15 min at RT. Eluted RNCs were loaded onto 400 $\mu$l 750 mM sucrose cushion in 250 buffer and centrifuged in a TLA 110.4 rotor (100000 rpm, 45 min, 4 °C) to separate RNCs. RNCs were resuspended in 30 $\mu$l 250 buffer and concentrations were measured with UV-Vis photometer (1:70 dilution; 1 A260 = 20 pmol 80S ribosomes).

## 2.7 *In vitro* reconstitutions of ribosomal Ski complexes

*S. cerevisiae* Ski complex and Ski7 constructs were purified by Felix Halbach or Eva Kowalinski (Conti lab, Max Planck Institute of Biochemistry, Martinsried) as described before (Halbach et al., 2012, Halbach et al., 2013, Kowalinski et al., 2015).

*In vitro* reconstitution assays were performed using 2 pmol RNCs and 5-fold molar excess of purified Ski complex or 10-fold molar excess of Ski7. Reactions were incubated for 15 min at RT. To assess ligand binding to ribosomes, reactions were spun through sucrose cushions (50 mM Tris/HCl pH 7.0, 250 mM KOAc, 25mM, 250 mM sucrose, 10 mM $Mg(OAc)_2$, 750 mM sucrose, 5 mM 2-mercaptoethanol, 10

$\mu$g/ml cycloheximid, 0.1% Nikkol, 0.1% pill/ml, 0.2 U/ml RNAsin) and analyzed by SDS-PAGE. Protein gels were stained with SYPRO Orange as described.

## 2.8 Polysome profile and sucrose gradient analysis

Yeast cultures from C-terminally TAP (tandem affinity purification)-tagged Ski3 and Ski7 strains (obtained from Euroscarf) were harvested in early log phase (0.9-1.0 $OD_{600}$, resuspended in lysis buffer (20 mM HEPES pH 7.5, 100 mM KCl, 10 mM $MgCl_2$, 10 $\mu$g/ml cycloheximide, 0.5 mM PMSF) and lysed by glass bead disruption (10x 30 s vortexing with 30 s breaks on ice in between). Lysates were spun through linear sucrose gradients in a SW-40 rotor (10-50%, 137000g, 150 min, 4 °C) and fractions were analyzed by SDS-PAGE followed by immuno-blotting using a Peroxidase-Anti-Peroxdiase (PAP) Soluble Complex antibody against Protein A. For RNase treatment, 0.3 mg/ml RNase A were incubated with lysate for 30 min on ice.

## 2.9 Native pullouts of Ski complex bound ribosomal complexes using TAP-tagged Ski3

Native TAP-pullouts were performed using Dynabeads® M-270 Epoxy (Life Technologies) with yeast strains expressing C-terminally TAP-tagged Ski3. Purifications were essentially performed as described before (Defenouillère et al., 2013, Oeffinger et al., 2007). Cultures were harvested at 0.9-1.0 $OD_{600}$, resuspended in lysis buffer (20 mM HEPES pH 7.4, 100 mM KOAc, 10 mM $MgCl_2$, 1 mM DTT, 0.5 mM PMSF, 10 $\mu$g/ml cycloheximide) and lysed by glass bead disruption (10x 30 s vortexing with 30 s breaks on ice in between). Incubation with 300 $\mu$l IgG-coupled magnetic Dyna/-beads® was performed for 12 h at 4 °C with slow tilt rotation. TAP-tagged Ski3 and all associated ribonucleoprotein complexes were eluted with 200 units of AcTEV Protease (Thermo Fisher) for 180 min at 17 °C.

## 2.10 *In vitro* reconstitution of Ski complex with CMV-stalled overhang RNCs

Yeast ribosomes were stalled on a DP120 mRNA with a CMV-stalling sequence. RNCs were prepared as described above for NS-RNCs. Constructs were designed to have a 0, 10, 20 or 50 nt overhang at the 3' end on the ribosome by adding additional

nucleotides after the stalling sequence (10 nt to account for the distance between A-site and the entry site of the ribosome and 0, 10, 20 or 50 nt for the respective 3' overhang construct).

*In vitro* binding assays were performed using 2 pmol RNCs and 5-fold molar excess of purified Ski complex as described above. Protein gels were stained with SYPRO Orange and gel bands were quantified using Imagequant (GE Healthcare Life Sciences) and the rollingball method for background subtraction. To account for slight variations in the amount of used RNCs in each lane, the quantified values for the Ski2 and Ski3 double band were normalized by dividing though the quantified value for a ribosomal band (see fig. S7D; band is marked with an asterisk). The normalized Ski binding ratio was plotted in a bar plot. This experiment was performed as a duplicate (N = 2).

## 2.11 Targeted ribosomal profiling on the native ribosome-Ski complexes

Ribosomal profiling was performed essentially as described before (Ingolia et al., 2009). RPF and RNA samples were prepared from the Ski3-TAP strain as shown in Fig. 3.16. All data was processed by Vivekanandan Shanmuganathan and Markus Pech (Beckmann lab, Gene Center LMU, Munich).

For RNA, cell lysate (for control) or purified ribosome-Ski complexes were used for RNA extraction using a miRNeasy mini Kit (Qiagen). Total RNA was depleted of ribosomal RNA by using the Ribo-Zero rRNA Removal Kit for Human/Mouse/Rat (Epicentre). rRNA depleted total RNA was heat fragmented and sample preparation was continued as given in the ARTseq™ Ribosome Profiling Kit.

For RPFs, the cell lysate (for control) or purified ribosome-Ski complexes were treated with 40 units per $A_{260}$ of RNase I (Ambion) at 25 °C for 45 min in a shaker at 500 rpm followed by 5 min incubation on ice with SUPERase-In (Ambion). The lysate (control) was applied to 10-30% sucrose gradients and centrifuged at 121000 g for 3.5 h to separate 80S monosomes from residual polysomes, which withstood the nuclease treatment. The 80S peak was isolated and ribosomes pelleted by centrifugation. For ribosome-Ski complexes, the sucrose gradients were omitted, since already the purified complexes showed reproducible 80S monosomes only. Instead, ribosomes were pelleted through a sucrose cushion.

80S were split in ribosome-dissociation buffer (20 mM Tris, 400 mM KCl, 2 mM $MgCl_2$, 1 mM DTT and 1 mM puromycin) and subunits were pelleted again by centrifugation. The supernatant from this centrifugation step was used as the source for RPFs. RPFs were further purified and size selected in a 15% denaturing urea-PAGE gel for fragments between 26-62 nucleotides using markers. Gel extracted fragments were precipitated and processed as given in the protocol (ARTseq™ Ribosome Profiling Kit, Epicentre, WI, USA) for library preparation and high-throughput sequencing. Sequencing was performed on an Illumina HiSeq 1500.

## 2.12 Bioinformatical analysis of RPFseq and RNAseq datasets

Reads mapping to ribosomal RNA, tRNA, small nuclear and nucleolar RNA were removed. Remaining reads were mapped to the yeast genome using Tophat (v2.0.8b) (Trapnell et al., 2009) and only uniquely mapped reads were used for length distribution and further bioinformatic analysis.

For plotting the relative positions of reads in the ORFs, we used multiple mapping of two positions. Consequently, only reads with a maximum of two positions within the genome were taken to avoid partial coverage due to overlapping genes or duplicated sequences within the coding regions. The 'per nucleotide coverage' in the ORFs for all genes was calculated. Afterwards, each gene was split into ten equal segments. The 'per nucleotide coverage' mean values of each segment were then divided by the entire gene mean. Subsequently, the mean values across the genome for all segment ratios were calculated. These values were averaged, standard deviations were calculated and plotted. The same was done for a single dataset of total RNA.

The codon correlation plot was done as described before (Presnyak et al., 2015), only that the correlation was calculated with the footprint count ratio instead of mRNA half-life. Briefly, the footprint count ratio between pulldown and control were calculated. Then Spearman correlation values were calculated between the footprint ratio and codon occurrence across the genome for all codons. Optimal and non-optimal codons were adapted from Presnyak et al (Presnyak et al., 2015).

For the codon occupancy in A-, P- and E-site, only uniquely mapped reads were used for further bioinformatic analysis. For identifying the P-site position within the footprints, a meta-gene analysis using 5' end of the footprints around the start codon was performed. Based on this analysis, the first peak appeared 12 nucleotides upstream of the start codon. A-, P- and E-site codons for all footprints were assigned

by shifting 16, 13 and 10 nucleotides, respectively. The number of footprints per amino acid in each site was calculated by summing up the shifted footprints over the corresponding codons. To normalize the occurrence, the codons in the second position downstream of the A-site were summed up and the occurrence for each amino acid was calculated. The values for the amino acids in A-, P- and E-site where then divided by the occurrence for each corresponding amino acid in this second position accordingly. For all the footprints mapping to ORFs, the normalized occurrence of A-, P- and E-site amino acids were then plotted.

## 2.13 Cryo-EM, Single Particle Analysis and model building of the ribosome-Ski complex

Freshly prepared samples of the endogenous pullout from the genomically TAP-tagged Ski3 yeast strain were adjusted to 4 $A_{260}$/ml (80 nM 80S ribosomes) and applied to 2 nm pre-coated Quantifoil R3/3 holey carbon supported grids. Two datasets were collected on a Titan Krios TEM (FEI Company) equipped with a Falcon II direct electron detector at 300 keV under low dose conditions of about 28 e-/Å2 for 10 frames in total using the EPU software (FEI Company) and a defocus range of -0.7 to -4.0 $\mu$m. Magnification settings resulted in a pixel size of 1.084 Å/pixel. Contrast transfer function (CTF) estimation was performed with CTFFIND4 (Mindell and Grigorieff, 2003; Rohou and Grigorieff, 2015) and only micrographs that showed clear signal below 4.5 Å resolution were used. Automatic particle picking was performed with Gautomatch (http://www.mrc-lmb.cam.ac.uk/kzhang/). Both datasets were individually 2D classified using Relion (Scheres, 2012). Non-ribosomal particles were discarded resulting in 2 datasets with 175038 and 258426 particles, respectively. The vast majority of the particles were programmed ribosomes with tRNAs (>95%). Afterwards, both datasets were combined and 3D refinement was performed for subsequent movie processing and generation of shiny particles in Relion (Bai et al., 2015; Scheres, 2014). All shiny particles were then transferred to Frealign (Grigorieff, 2007)for 3D classification. First, the dataset was classified into 7 classes. Classes 1-3 contained poorly resolved 80S ribosomes with partial Ski complex density (total of 78878 particles, 18.2%). Class 4 contained 80S with eIF-5A in the E-site but no density for the Ski complex (182884 particles, 42.2%). Finally, classes 5-7 contained 80S with strong Ski complex density but differing in the position of the L1 stalk (classes 5-6 with L1 in, 152959 particles, 35.5%; class 7 with L1 out, 18742, 4.3%). Classes 5 and 6 were joined for a second round of 3D classification and particles with very low

scores were discarded. The second classification resulted in a low-resolved ribosome-Ski complex class (26574 particles, 18.0%) which was discarded and 2 classes displaying ribosome-Ski complexes with 2 different small subunit rolling states (59112 particles, 40.2% and 61516 particles, 41.8%). The higher populated of these classes was further subclassified resulting in 2 final classes with different Ski2 arch domain positions (31503 particles, 54.0% for the arch domain contacting the 40S subunit and 26814 particles, 46.0%, for the arch domain contacting Ski3). Final refinement was performed in Frealign resulting in a map at 3.8 Å resolution according to the gold standard criterium (FSC = 0.143). The map was sharpened with bfactor.exe from the Frealign package and used for interpretation. To address resolution heterogeneity and changes in local resolution, different low-pass filtered maps were generated for model building and refinement. Local resolution was calculated using ResMap.

For model building, the crystal structures and models for the *S. cerevisiae* ribosome (pdb code 4V88 for the 40S and 5GAK for the 60S; Ben-Shem et al., 2011; Schmidt et al., 2015) and of the *S. cerevisiae* Ski complex (4BUJ; Halbach et al., 2013) and the Ski2 insertion domain (4A4K; Halbach et al., 2012) were fitted as rigid bodies into the isolated and appropriately filtered electron densities using UCSF Chimera except for the flexible Ski3 N-terminal arm (residues 1-505) which was rigid body fitted individually. A- and P-site tRNAs were fitted based on the structure of eIF-5A bound to the ribosome that was modelled before (5GAK; Schmidt et al., 2015), the mRNA was modelled by extending the 3' end of the model mRNA in the mammalian POST-translocational state (EMD-2620 and pdb 4UJE; Budkevich et al., 2014). After rough fitting, flexible fitting and Jiggle Fitting in Coot (Emsley and Cowtan, 2004; Brown et al., 2015) was applied where necessary.

All models were subsequently combined and subjected to real-space refinement using PHENIX (Adams et al., 2010). After PHENIX refinement, the model was further subjected to reciprocal space refinement in REFMAC v5.8 (Murshudov et al., 1997) using restraints generated by ProSMART and LIBG as previously shown (Brown et al., 2015). Because of the difference in local resolution and to avoid overfitting, refinement weights and the resolution limit for REFMAC were estimated separately for the 60S subunit and the 40S-Ski complex part as described in Fernández et al., 2014. Additionally, the N-terminal arm of Ski3 (residues 1-170) was removed from the refinement since resolution in this part was 10 Å or lower. For the final model, only the rigid body fitted N-terminal arm of the crystal structure was used. $FSC_{average}$ was monitored throughout the refinement and the final model was validated using MolProbity. Cross-validation against overfitting was performed as described before

for both model refinements separately and is described in more detail in the Results section.

Figures were created with the PyMOL Molecular Graphics System (Version 1.7.4, Schrödinger, LLC) and with UCSF Chimera (Pettersen et al., 2004).

## 2.14 Cryo-EM, Single Particle Analysis and model building of the eIF-5A-80S structure

For the eIF-5A-80S structure, only the class containing eIF-5A bound to the ribosome without Ski complex was used and an extra dataset was collected. Data collection was performed as described before with a dose of 2.4 e- /Å$^{-2}$ per frame for 13 frames in total. Data were collected at a defocus range between -0.8 and -3.4 $\mu$m. Only micrographs that showed clearly visible Thon rings below 5.5 Å on the level of the rotationally averaged power spectra profiles were used for further analysis. Automatic particle detection was performed by the program SIGNATURE (Chen and Grigorieff, 2007). Initial *in silico* sorting of the dataset consisting of 246555 particles in total was performed using the SPIDER software package (Frank et al., 1996). Classes were obtained by competitive projection matching in SPIDER (Leidig et al., 2014). The vast majority (>95%) of the particles we found were programmed with tRNAs. This dataset could be subdivided into two main classes, both containing A- and P-tRNAs and either with or without the Ski complex (76816 and 88640 particles, respectively). The large number of ribosomal particles without density for the Ski complex suggests that the Ski complex was not stably bound to these particles. To our surprise, both classes contained ribosome-bound eIF-5A. Nevertheless, only the class without Ski complex displayed a highly resolved density for eIF-5A that allowed model building. The density for eIF-5A in the Ski complex bound ribosome class was partially disordered and the density for the factor was fragmented. For high-resolution refinement, the dataset containing the eIF-5A particles was further cleaned by removing particles with low cross-correlation. The cleaned dataset (62532 particles) was then processed further using Relion. To do this, the particle boxes were extracted using the coordinates obtained by SIGNATURE and normalized in Relion. The contrast transfer function (CTF) estimation was repeated using CTFFIND3 and the dataset was subjected to auto-refinement in Relion using a ribosomal reference low-pass filtered to 70 Å. After auto-refinement, the dataset was subjected to movie processing and the particle-polishing feature in Relion. Here, only the first 8 frames

were used for the calculations, resulting in an accumulated dose of 24 e-/Å$^{-2}$. Subsequent auto-refinement of "shiny" particles resulted in a final reconstruction of 3.9 Å resolution according to a gold standard FSC cutoff of 0.143. This map was sharpened using automatic b-factor estimation in RELION and used for interpretation and model building. Local resolution was calculated using ResMap and maps were visualized in UCSF Chimera. RELION data were processed on the Leibnitz-Rechenzentrum (LRZ) Munich.

For modeling the large ribosomal subunit (LSU), the crystal structure of the yeast ribosome (PDB ID 4V88; Ben-Shem et al., 2011) was taken as a template. Peptidyl A- and decacylated P-tRNA were modeled based on the crystal structure of the *Thermus thermophilus* 70S ribosome in the post-catalysis state of peptide bond formation (containing dipeptidyl-tRNA in the A site and deacylated tRNA in the P site, PDB ID 1VY5; Polikanov et al., 2014) and for eIF-5A a homology model (based on Kim et al., 1998) was generated using HHPred (Soding et al., 2005). All structures were roughly fitted into the map using UCSF Chimera. Flexible fitting and, where necessary, de novo model building was done in Coot followed by real space refinement in PHENIX. For the rRNA and the tRNAs, geometry restrictions were calculated using the "PDB to 3D restraints" database prior to PHENIX refinement.

The eIF-5A homology model was obtained after a multiple alignment using HHPred. This model was subjected to geometry minimization using PHENIX and remodeled in Coot. The well-resolved hypusine-containing $\beta$3-$\beta$4 loop (residues 47-54) was modeled de novo and for the N-terminal extension (NTE; res 1-16) a poly-Ala model was generated. For uL16, the loop containing residues 103-111 (not present in the yeast ribosome X-ray structure) was modeled de novo. The L1 stalk in the eIF-5A position was remodeled and a poly-alanine model for uL1 was generated using uL1 from the human 80S ribosome as a template (PDB 5AJ0; Behrmann et al., 2015). In a final step, all models were combined and subjected to real-space refinement using the PHENIX software.

# 3 Results

## 3.1 *In vitro* characterization of Ski7 and Ski complex binding to the ribosome

An open question concerning general 3'-to-5' degradation and mRNA quality control is the exact function of the Ski proteins in these processes (Anderson and Parker, 1998; Araki et al., 2001; van Hoof et al., 2000). Both Ski7 and the Ski complex are essential for exosomal function, except for the GTPase domain of Ski7 that is only needed in NSD (Araki et al., 2001). The current working model suggests that Ski7 can act as an adaptor between the exosome and the Ski complex by interacting with both factors via its N-terminal domains N1 and N2 (van Hoof et al., 2002). The Ski complex is believed to funnel mRNA into the exosome for degradation (Halbach et al., 2013). In NSD (and possibly NGD), Ski7 is believed to bind to the ribosome with its GTPase domain akin to Hbs1 to help recognize nonstop (or no-go) decay targets. Since Hbs1 works in concert with Dom34, a cofactor reaching into the A-site, it was suggested that a similar A-site factor might exist for Ski7 as well (Shoemaker and Green, 2012). With the purpose of understanding their role in NSD and 3'-to-5' mRNA decay, we set out to characterize the interactions of Ski7 and the Ski complex with 80S ribosomes *in vitro*. We generated *bona fide* ribosomal nonstop decay targets by generating ribosome nascent chain complexes (RNCs) stalled within the poly-$A_{50}$ tail of a DP120 reporter mRNA lacking a stop-codon (NS-RNCs; see Methods for details). Binding to RNCs was tested via *in vitro* reconstitution assays with endogenously purified wildtype or mutant Ski proteins.

### 3.1.1 Generation of *bona fide* NSD target RNCs

*Bona fide* NSD targets were purified by *in vitro* translation of a reporter DP120-poly-$A_{50}$ mRNA in a cell-free *S. cerevisiae* translation system. RNCs were purified via an

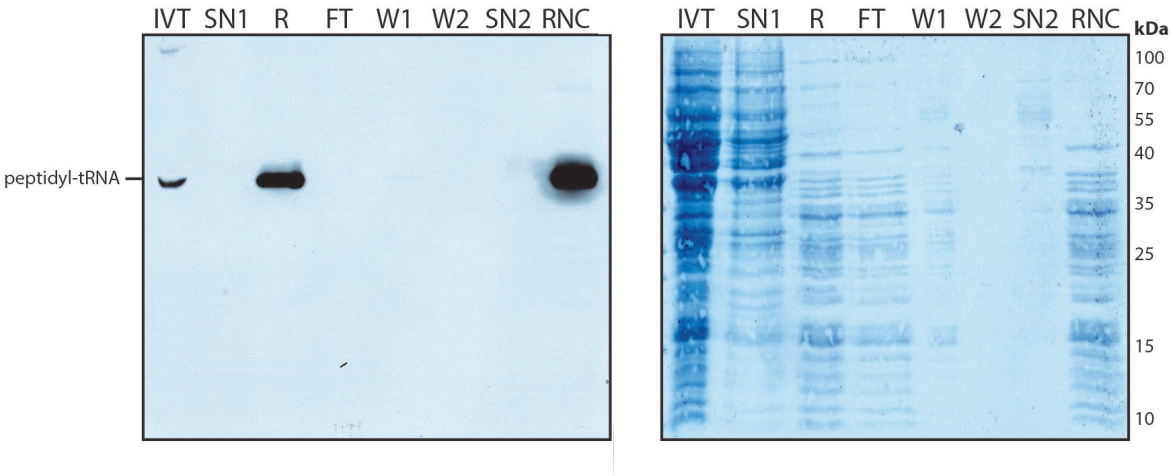


FIGURE 3.1: **Preparation of NS-RNCs.** Left: Western Blot of the NS-RNC purification. IVT = In vitro translation reaction; SN1 = supernatant first centrifugation step; R = total ribosomes (pellet from first centrifugation step); FT = flow-through of Talon beads purification; W1/W2 = Wash fraction; SN2 = supernatant second centrifugation step; RNC = purified RNCs (pellet from second centrifugation step). Loaded amounts in percent of total fractions were 0.25% IVT, 0.25% SN1, 1.0% R, 0.5% FT, 5.0% W1, 5.0% W2, 5.0% SN2 and 8.25% RNCs. A clear signal for peptidyl-tRNA is visible in the IVT, the total ribosomes R and RNC fraction. Right: PVDF membrane of SDS-PAGE of RNC preparation visualized after Amido Black staining. The enrichment of RNCs was estimated to be around 5x from comparing the strength of the protein bands in the R and RNC fractions and the signal for the peptidyl-tRNA on the Western Blot.

N-terminal $His_6$-tag on the nascent chain and analysed with SDS-PAGE and Western Blot (Fig. 3.1) as described before (Beckmann et al., 2001; Halic et al., 2004).

Eluted RNCs showed high purity and concentration in the final elution sample, ranging generally between 30-50 $A_{260}$/ml depending on the preparation (equal to 1.8-3.0 $A_{260}$ per 400$\mu$l of translation extract). The enrichment factor of RNCs in the elution fraction was estimated to be approximately 5 (the applied amounts of ribosomes in the R and RNC fraction were almost identical while the signal on the Western Blot was approximately 5 times stronger for the RNC fraction) for the purification. These RNCs were used for subsequent *in vitro* reconstitution assays with purified Ski7 and Ski complex constructs.

### 3.1.2 *In vitro* reconstitution of Ski7 and Ski complex bound NS-RNCs

Endogenously purified Ski7 and Ski complex constructs were prepared by Felix Halbach and Eva Kowalinski (Conti lab, Max Planck Institute of Biochemistry, Martinsried) as described (Halbach et al., 2012, Halbach et al., 2013; Kowalinski et al., 2015). For *in vitro* reconstitutions, 5 or 10 times molar excess of protein ligand versus RNCs was used. Binding was analysed by pelleting through a sucrose cushion and visualization by SDS-PAGE (Fig. 3.2).

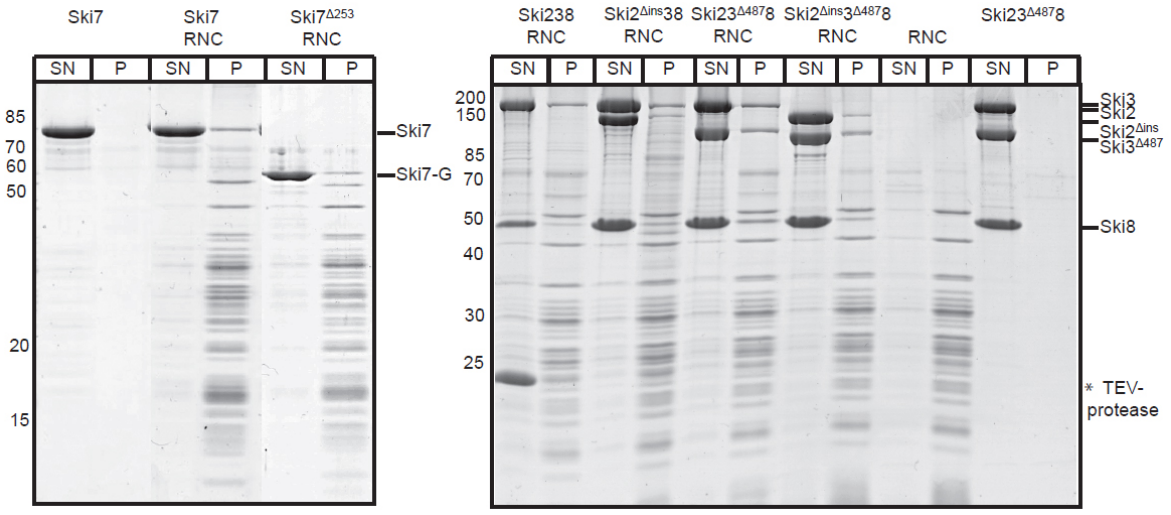


FIGURE 3.2: ***In vitro* reconstitution of ribosomal Ski complexes.** SN = supernatant; P = pellet. SDS gels were stained with SYPRO Orange and visualized with a Typhoon FLA 900 Fluoresence Bioimager. 2 pmol of RNCs were loaded. Left panel: Reconstitution with 10 times molar excess of Ski7 constructs. Ski7 alone did not pellet, whereas a clear band for Ski7 and Ski7$^{\Delta 253}$ is seen when reconstituting with NS-RNCs. Right panel: Reconstitution with 5 times molar excess of Ski complex constructs. Ski complex alone did not pellet in our assays (lane 11 and 12). In contrast, all Ski complex constructs bound to NS-RNCs as indicated by the additional bands in the pellet fractions.

*In vitro* reconstitutions resulted in clear binding of full-length Ski7 to NS-RNCs (Fig. 3.2, left panel). Also, the GTPase domain alone (Ski7$^{\Delta 253}$) could be bound to the RNCs, whereas Ski7 alone did not pellet in our assay. Surprisingly, the Ski complex also bound to the RNCs (Fig. 3.2, right panel). Binding was observed with full-length Ski complex, Ski complex missing the arch/insertion domain of Ski2 (Ski2$^{\Delta ins}$38), a construct with a truncated N-terminal arm of Ski3 (Ski23$^{\Delta 487}$8) and when combining both truncations (Ski2$^{\Delta ins}$3$^{\Delta 487}$8). Ski complex alone did not pellet by itself. These

data suggest that Ski7 with its GTPase domain and, surprisingly, the Ski complex can bind to ribosomes stalled by DP120-poly-$A_{50}$ mRNA *in vitro*. Notably, when using empty gradient purified yeast 80S ribosomes instead of RNCs, the Ski complex did not pellet anymore under medium salt concentrations (300 mM KOAc), whereas it still bound to nonstop RNCs (Fig. 3.3). This indicates that nonstop ribosomal complexes or at least ribosomes containing an mRNA are the preferred target.

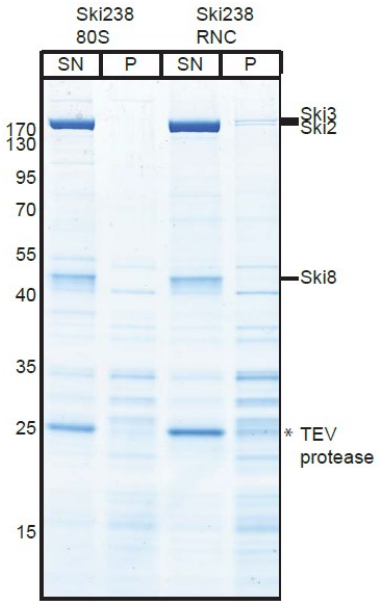


FIGURE 3.3: ***In vitro* reconstitution of Ski complex with empty 80S ribosomes and NS-RNCs.** SN = supernatant; P = pellet. 2 pmol of RNCs and ribosomes were loaded. Figure shows the SDS gel after Simply Blue staining. In the presence of 300 mM KOAc, Ski complex (used in 5 times molar excess) did not bind to empty 80S ribosomes, but only to prepared RNCs as indicated by the extra bands in the pellet fraction.

## 3.2 *In vivo* characterization of Ski7 and Ski complex binding to the ribosome

Our initial *in vitro* results suggest that both the Ski complex and Ski7 stably interact with ribosomes. However, so far no further evidence under more native conditions was given. To this end, polysome profile analysis was performed using *S. cerevisiae* strains with either genomically tandem affinity purification (TAP)-tagged Ski7 or Ski3 to analyze their ribosome-binding behavior in the cell. All tagged proteins were tested for activity in NSD using a non-stop reporter by Quentin Defenouillère (Jacquier lab, Pasteur Institut, Paris; see Schmidt et al., 2016).

### 3.2.1 Polysome profile analysis of Ski3- and Ski7-TAP strains

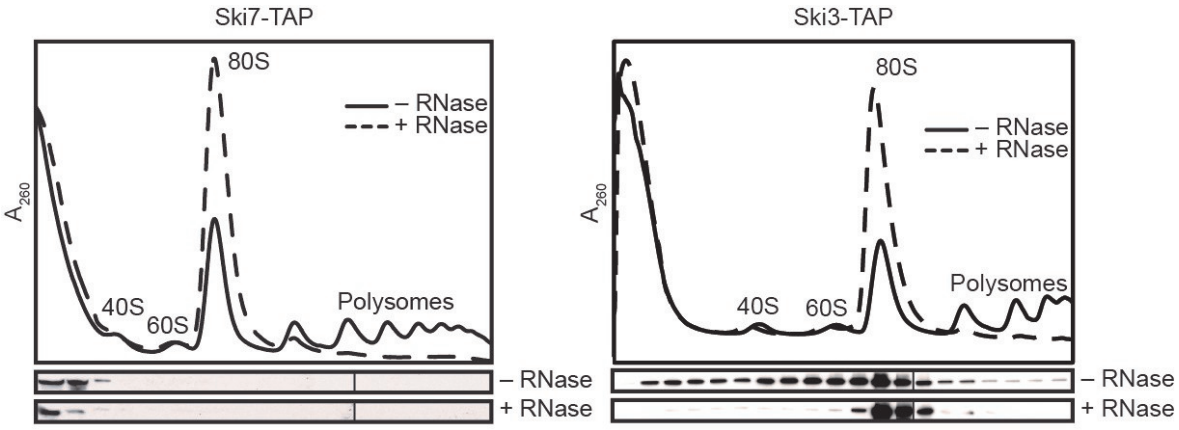


FIGURE 3.4: **Polysome profile analysis.** Polysome profiles from cells expressing TAP-tagged Ski7 or Ski3 with and without RNase treatment. Fractions were analysed by immunoblotting using an $\alpha$-Protein A antibody against the TAP tag. Ski7 was only detectable in the low-molecular fractions of the gradients. In contrast, Ski complex co-migrated with ribosomes and was exclusively found in the 80S fraction after RNase treatment.

For polysome profile analysis, strains were harvested in mid-log phase (0.9-1.0 $OD_{600}$) under physiological conditions and lysates were applied on linear 10-50% sucrose gradients to separate ribosomal fractions. All fractions were subsequently analysed by Western Blot using an $\alpha$-TAP antibody to investigate the presence of the TAP-tagged protein (Fig. 3.4). To our surprise, Ski7 was almost exclusively found in the upper (low molecular) fractions of the gradient. We basically could not detect any signal for Ski7-TAP in the ribosomal fractions as would be expected from a ribosome binding factor. In contrast, we detected a strong signal throughout the ribosomal fractions for Ski3-TAP, showing a prominent peak in the 80S fractions, whereas very little Ski3-TAP signal could be found in the upper fractions of the gradient. To check that this co-migration is not the result of the Ski complex unspecifically binding to mRNA, we treated our lysates with RNase A. This resulted in the collapse of all polysomal fractions into a single 80S peak where Ski3-TAP selectively and exclusively was detected. Thus, our polysome gradient analysis suggests that the Ski complex, not Ski7, stably interacts with ribosomes.

Notably, a nonstop reporter assay was performed by Quentin Defenouillère (Jacquier lab, Pasteur Institut, Paris) as part of this project to further verify this interaction. This assay confirmed the association of Ski complex specifically to NSD ribosomes *in vivo*

even in the absence of Ski7 and Dom34 or Hbs1. For experimental data, please refer to Schmidt et al., 2016.

### 3.2.2 Purification of native ribosome-Ski complexes from a Ski3-TAP strain

From our polysome profile analysis and the nonstop reporter assay, we concluded that Ski complex rather than Ski7 is targeting ribosomes in the cell. To test if the Ski complex is indeed forming a stable complex with ribosomes, we established a purification protocol for native ribosome-Ski complexes with the further goal to perform mass spectrometry analysis and cryo-EM.

We optimized the purification protocol using magnetic IgG-coupled Dynabeads® based on established protocols (Defenouillère et al., 2013; Oeffinger et al., 2007). The purification was analysed and monitored by SDS-PAGE and Western Blot (Fig. 3.5).

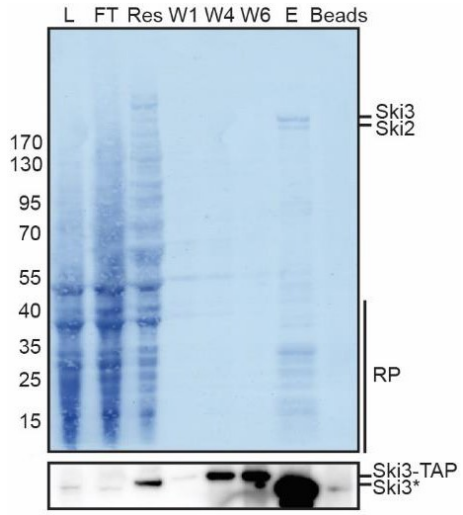


FIGURE 3.5: **Purification of native ribosome-Ski complexes from strains containing TAP-tagged Ski3.** Simply Blue stained SDS gel and Western Blot of the native pullouts using wild-type yeast cells with genomically TAP-tagged Ski3. Western Blots were performed with an $\alpha$-CAB antibody against the calmodulin part of the TAP tag. Purifications were carried out with Dynabeads® from 20 L of yeast culture. L = lysate; FT = flow-through; Res = resuspended beads after first harvest; W1/W4/W6 = wash fractions; E = elution after TEV cleavage; Beads = bead fraction after boiling in SDS sample buffer. Final elution fraction contains Ski complex and co-purified ribosomes (RP). Successful TEV cleavage was confirmed by Western Blot (cleaved Ski3 is indicated with an asterisk).

As expected from the previous experiments, Ski3-TAP can be co-purified with ribosomes (Fig. 3.5). The elution fraction contained pure native ribosome-Ski complexes indicated by the two high-molecular weight bands for Ski2 and Ski3 at approximately 170 and 190 kDa and the characteristic ribosomal band pattern visible in the low-molecular range (RPs). The estimated yields from 20 L of yeast culture ranged from 3.0-7.0 $A_{260}$ depending on the preparation. Western blotting confirmed successful cleavage of the Ski3-TAP protein by TEV protease as visualized by the shifting signal (Ski3* corresponds to the cleaved protein) in the elution fraction. Mass-spectrometry analyses confirmed the presence of all Ski complex subunits in our sample alongside large amounts of ribosomal proteins (see Appendix Table A.1). These data further confirm the interaction of the Ski complex with ribosomes under native conditions in the cell and allowed us to perform further biochemical and structural analysis.

## 3.3 Medium-resolution structures of *in vitro* reconstituted NS-RNC-Ski complexes

The *in vitro* reconstitutions showed successful binding of both Ski7 and Ski complex to the prepared RNCs. However, only Ski complex showed stable binding in the performed polysome profile analysis and nonstop reporter experiments *in vivo*. We therefore questioned whether Ski7 is only transiently, if at all, binding to ribosomes for NSD. For screening the interactions of both Ski7 and the Ski complex with ribosomes, we set out to obtain a medium-resolution cryo-EM structure of the *in vitro* reconstituted samples with full-length Ski7 and Ski complex to NS-RNCs. Samples were prepared as for the reconstitution assays and collected with a Titan Krios TEM equipped with a TemCam-F816 CMOS camera. The resulting datasets were processed with SPIDER as described before (Becker et al., 2011; Frank et al., 1996; Leidig et al., 2014).

Processed samples with Ski7 and NS-RNCs did not reveal any additional densities beside the ribosome in our medium resolution reconstructions (data not shown). The dataset resulted essentially in partially P-site tRNA containing ribosomes without any indication of the factor bound to it. From these reconstructions, we could not verify Ski7 binding to ribosomes or analyse any interactions. Further sample preparations using different buffer conditions and also truncated Ski7$^{\Delta 253}$ failed in obtaining any structural data about Ski7 on the ribosome, suggesting that under given conditions Ski7 is not stably interacting with the ribosome, but might rather transiently bind to it. This hypothesis is substantiated by the findings from the nonstop reporter assay

and the polysome profile analysis. Additionally, it is possible that other factors like the Ski complex or the exosome are needed to tightly bind Ski7 to our RNCs. Thus, the binding observed in our reconstitution assays might be the result of the high molecular excess in the sample, forcing Ski7 onto the ribosome.

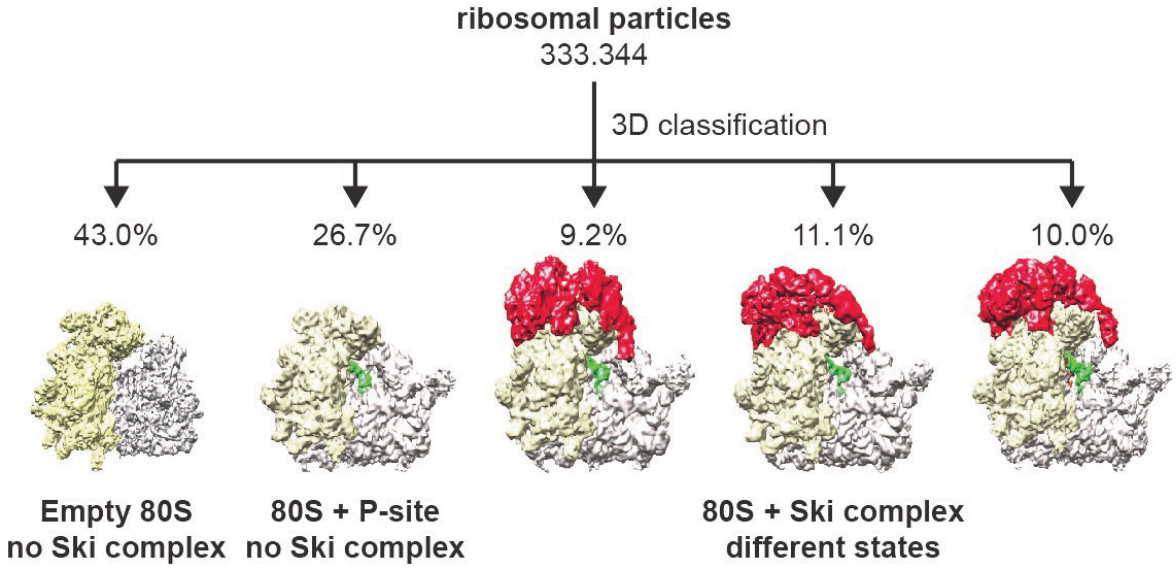


FIGURE 3.6: **Classification of the *in vitro* reconstituted NS-RNC-Ski complex medium-resolution dataset.** Classification was performed by competitive projection matching in SPIDER. Two classes that did not contain any density for the Ski complex (empty and programmed ribosomes) were separated from three classes showing Ski complex occupancy. These three classes (containing 30.3% of all particles) showed flexibility in the Ski complex and were almost evenly split between three different binding states.

In contrast, we obtained a strong density for the Ski complex on the ribosome (Fig. 3.6 and Fig. 3.7). Initial *in silico* 3D classification revealed that the dataset contained approximately 43% ribosomes that were not programmed with tRNA and 27% of particles that were not occupied by the Ski complex (Fig. 3.6). Additionally, we separated three different binding states of the Ski complex in the Ski complex containing particles. Rigid body docking of the model from the crystal structure into the best resolved class revealed that the Ski complex binds to the 40S subunit, closely resembling its native state (Fig. 3.7A). Only the N-terminal arm of Ski3 was largely displaced in our reconstructions. However, detailed interactions could not be seen due to lower local and overall resolution and also due to flexibility of the Ski complex on the ribosome (Fig. 3.7B). Nevertheless, these first reconstructions confirmed our newly found ribosome-Ski complex interaction from the *in vitro* and *in vivo* assays,

leading us to investigate the interactions of the Ski complex with the ribosome more closely.

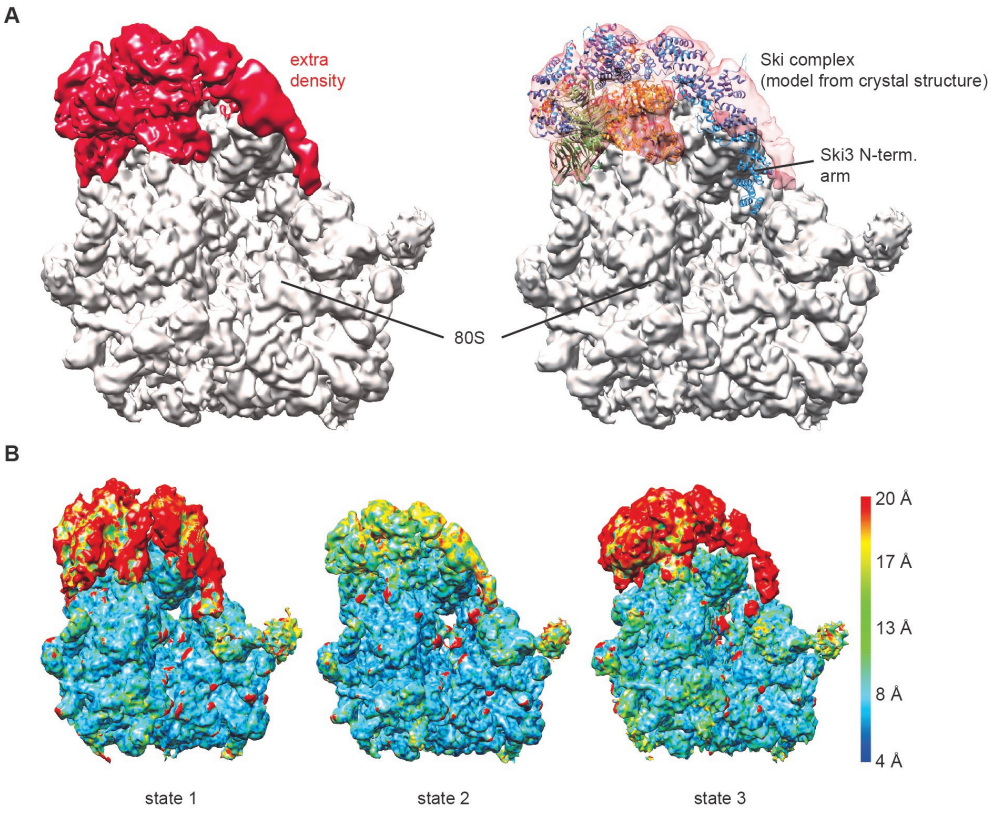


FIGURE 3.7: **Medium-resolution reconstruction of the in vitro reconstituted NS-RNC-Ski complex.** (**A**) Left panel: The reconstructions revealed a large extra density (shown in red) on the 40S subunit beside the density for the ribosome. Right panel: Initial fitting of the model from the crystal structure of the Ski complex into the best resolved NS-RNC-Ski complex map. The model overall fits into the observed density, only the N-terminal arm of Ski3 displays a larger conformational change in our reconstruction. (**B**) All three separated states from the 3D classification coloured according to their local resolution. The Ski complex shows high flexibility in all states with a local resolution ranging from 10-20 Å.

## 3.4 High-resolution structure of a native ribosome-Ski complex

The structural data from the *in vitro* reconstituted complexes revealed a Ski complex occupancy on the ribosome of approximately 30%. Moreover, only around 60% of ribosomes were programmed with tRNA, resulting most likely from the lower programming rate expected from *in vitro* translation reactions. Since the *in vitro* reconstituted samples also displayed strong heterogeneity and flexibility of the Ski complex, we aimed to gain cryo-EM data on the natively purified sample instead. These complexes should have the advantage of showing higher Ski complex occupancy on ribosomes compared to the reconstituted sample. Additionally, natively purified samples often result in more stable complexes, thus higher resolution for cryo-EM. Purified ribosome-Ski complexes were applied to Quantifoil carbon-supported holey grids and data was collected on a FEI Titan TEM equipped with a Falcon II direct electron detector. Grid and ice-quality was checked by manual inspection and micrographs showing no high-frequency information beyond 4.5 Å (as estimated by CTFFIND4 (Rohou and Grigorieff, 2015)) were discarded. After manual inspection of the micrographs, this resulted in two datasets containing 5259 and 3834 images. Both datasets were joined for data processing in Relion (Scheres, 2012) and Frealign (Grigorieff, 2007).

### 3.4.1 Data processing

Initial 2D classification in Relion resulted in 433464 ribosomal particles that were subjected to movie processing (Bai et al., 2013; Scheres, 2014). All following processing steps were then performed in Frealign, using the shift- and radiation-corrected "shiny particles" from the Relion movie processing feature.

An initial 3D classification revealed that basically all ribosomal particles contained A- and P-site tRNAs in contrast to the relatively low programming rate of the *in vitro* dataset (Fig. 3.8). This suggests that our purification yielded active complexes and not stalled artifacts that did not partake in translation. Furthermore, a high heterogeneity in the obtained ribosomal particles could be seen, as expected for natively purified complexes. We obtained three classes with 80S ribosomes and poorly resolved Ski complex, each containing around 5-7% of all particles of the dataset. Furthermore, three classes with strong Ski complex density on the ribosome could be separated. Two of these classes containing approximately 35% of all particles were

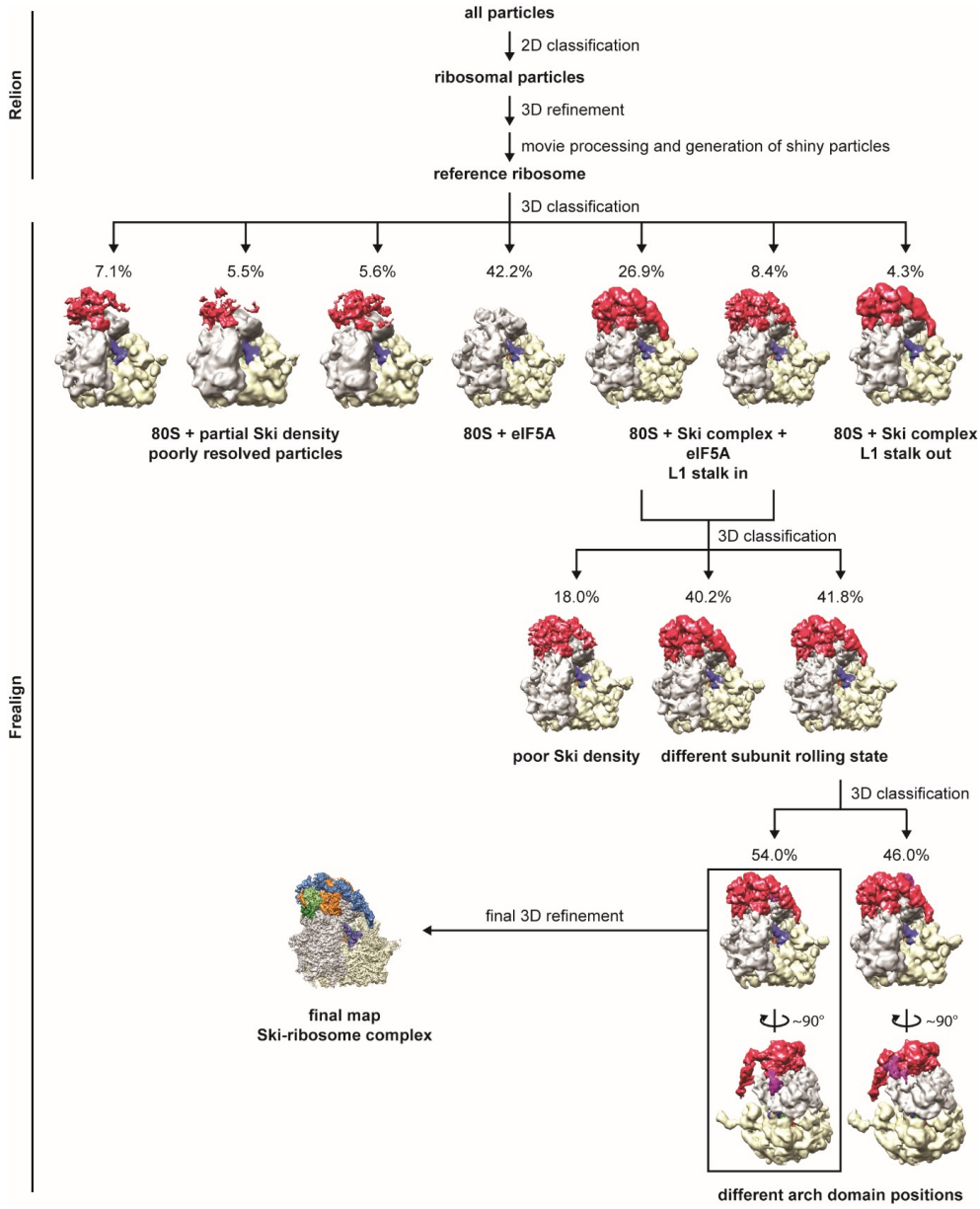


FIGURE 3.8: **Classification of the native ribosome-Ski complex purification dataset.** Non-ribosomal particles were excluded after 2D classification in Relion and particles were subjected to movie processing. Shift and radiation corrected ("shiny") particles were used for further processing in Frealign. The first 3D classification step resulted in 7 ribosomal classes with only programmed ribosomes containing A- and P-site tRNAs. 3 classes showed strong Ski complex density but differed in the position of the L1 stalk. One class did not contain Ski complex but only eIF-5A bound to the E-site of the ribosome. Classes with strong Ski complex density and L1 stalk in the inside position were joined (35.5% of total particles) and subjected to further 3D classification which resulted in one class with poor Ski complex density and two classes that showed different subunit rolling states. The larger of these (41.8%) was taken for a final 3D classification that sorted out two different conformational states of the Ski2 arch domain, either contacting the N-terminal arm of Ski3 (46.0%) or the 40S subunit (54.0%). The latter was refined to high resolution and used for model building and structural analysis.

essentially identical and joined for further processing. The third class containing 4% of particles showed a difference in the position of the L1 stalk compared to the other Ski complex containing classes. Since this class only contained very few particles, it was discarded for further processing. Surprisingly, we also obtained a large class (42%) of ribosomes showing no density for the Ski complex but displaying a strong density in the E-site corresponding to eIF-5A which will be discussed in chapter 3.7 further below. Notably, eIF-5A was present in all ribosomal classes except the Ski complex containing class with the L1 stalk in the outward position.

A second round of 3D classification of the joined "good" Ski complex containing classes resulted in two classes with strong Ski complex density differing in the 40S subunit rolling state (Budkevich et al., 2014) and a smaller class containing particles with poor Ski complex density that was discarded. The larger of the subunit rolling classes was then used for a final 3D classification, resulting in two populations with different conformations of the Ski2 arch domain, either contacting the N-terminal arm of Ski3 (46%) or the 40S subunit (54%). The latter was used for the final 3D refinement, resulting in a reconstruction at an overall resolution of 3.8 Å according to the gold standard criterium (FSC=0.143 according to Scheres, 2012; Fig. 3.9A).

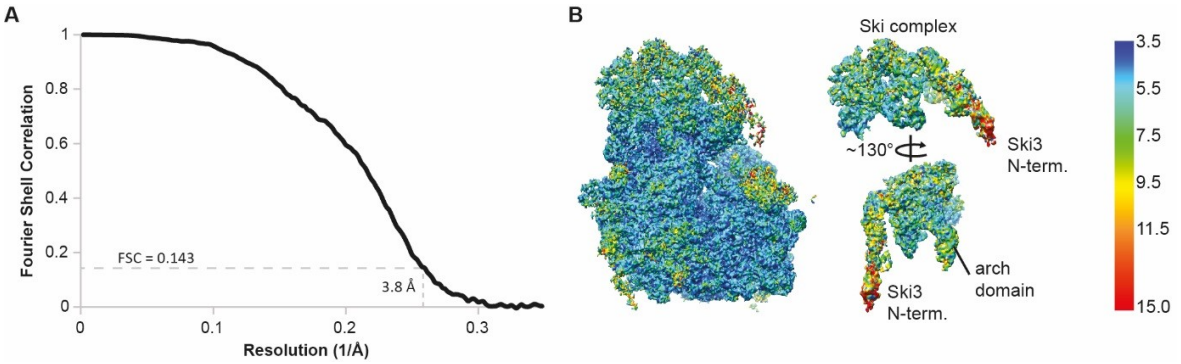


FIGURE 3.9: **Resolution determination and local resolution for the native ribosome-Ski complex reconstruction.** (**A**) The final class was refined to an overall resolution of 3.8 Å according to the gold standard criterium. (**B**) Final map for the entire ribosome-Ski complex and Ski complex alone coloured by local resolution as estimated by Resmap (Kucukelbir et al., 2014). Resolution ranged from 3.5 Å in the inner core of the ribosome and most of the Ski-ribosome interaction points to approximately 6-7 Å for the outer part of the Ski complex. The N-terminal arm of Ski3 showed high flexibility due to lack of stabilizing contacts to the ribosome and was thus resolved below 10 Å.

Local resolution varied between 3.5 Å for the ribosome and most of the ribosomal contact sites of the Ski complex to over 10 Å for the more flexible parts such as the stalk, some expansion segments and the N-terminal arm of Ski3 (Fig. 3.9B). This

allowed us to build an atomic model for almost the complete Ski complex bound to the ribosome based on previously published crystal structures (Ben-Shem et al., 2011; Halbach et al., 2012, Halbach et al., 2013). The final model contains the entire 80S ribosome, the Ski complex, 34 nucleotides of mRNA, A- and P-site tRNAs and eIF-5A (deposited under PDB-ID 5MC6). In particular, our reconstruction allowed modelling of almost all ribosomal interaction sites and the entire arch domain of Ski2 and its connection to the helical domain. Additionally, we could visualize the so-called basic loop of Ski2, as well as several connecting loops in $Ski8_{OUT}$ which contacted the ribosome, that were not present in the crystal structures.

### 3.4.2 Model building and validation

For the model building process, a refinement and structure validation pipeline was established, based on previous publications (Amunts et al., 2014; Brown et al., 2015; Fernández et al., 2014). This pipeline includes initial fitting in Coot (Emsley and Cowtan, 2004) and subsequent refinement of the model against the map in real space (using Phenix; Adams et al., 2010) and reciprocal space (using REFMAC; Murshudov et al., 1997) without adjusting amplitudes or phases of the cryo-EM map. To avoid distortions of secondary structure features and protein domains during the refinement process, protein and RNA restraints were generated via Phenix or ProSMART/LIBG and, if necessary, adjusted manually, and carefully monitored throughout the refinement processes. For a complete overview of the model building process, please refer to Appendix Table A.2.

To validate our atomic model and structural data, we first calculated the Fourier Shell correlation (FSC) of our model against the final map (Fig. 3.10). This so-called $FSC_{average}$ is a measure of how well the model fits into the observed density. Ideally, FSC values should maintain higher values (around 0.3-0.5) up to the estimated resolution (= resolution used during the refinement) and the plotted FSC curve should be void of any harsh drop-offs. To check for potential overfitting of the atomic model during refinement, the atoms of the final model were randomly displaced by 0.5 Å to remove any model bias and subsequently refined in REFMAC against the first half-map from the gold-standard determination. After refinement, the FSC of this newly refined model against the first half-map and against the second half-map was calculated, resulting in $FSC_{work}$ and $FSC_{test}$ respectively (Fig. 3.10). When comparing these FSC curves, a large discrepancy indicates overfitting during the refinement process.

During the model building process, we observed that refinement of the entire ribosome-Ski complex model always resulted in overfitting as indicated by $FSC_{work}$

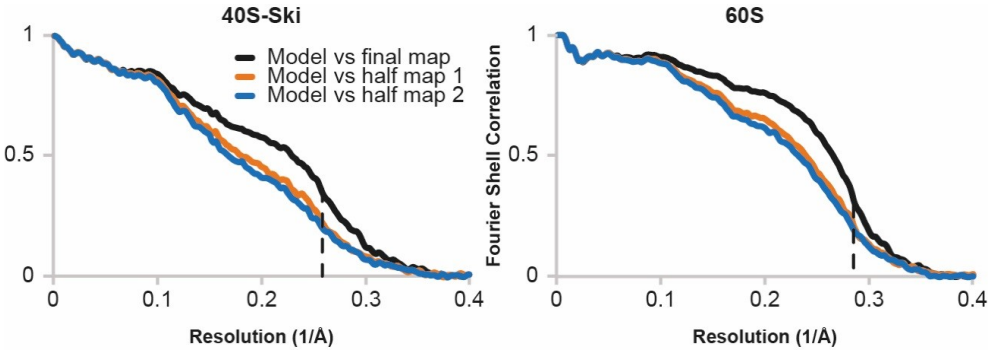


FIGURE 3.10: **Model validation and overfitting analysis of the molecular models containing the 60S (60S) and the 40S-bound Ski complex (40S-Ski).** Fourier shell correlations (FSCs) were calculated between the final refined model and the final map to gain the $FSC_{average}$ (black). The absence of harsh drop-offs and values around 0.4 even beyond the estimated resolution indicate good fits of the models to the map. For overfitting analysis, the atoms of the refined model were displaced and the model was refined against one of the two half maps from the gold standard resolution determination. FSCs were then calculated between the displaced refined model and the first half map ($FSC_{work}$; orange) and the second half map ($FSC_{test}$; blue). A high similarity between both FSC plots suggests that no overfitting was performed during model refinement.

and $FSC_{test}$ which probably originated from differences in the local resolution of the 60S compared to the 40S subunit and particularly the outer regions of the Ski complex. Thus, we split our model for refinement containing either the 60S subunit or the 40S subunit with the Ski complex. Additionally, the most N-terminal part of Ski3 (residues 1-170) showing the highest flexibility and therefore the lowest resolution was removed from refinement and only fit as a rigid body for the final model. Both parts were refined individually at 3.8 Å (60S) and 4.2 Å (40S-Ski) to account for the local resolution differences, resulting in atomic models free of any overfitting and good fits according to the FSC plots and the $FSC_{average}$ values of 0.79 and 0.83 for the 40S-Ski and 60S model, respectively (Fig. 3.10). Final model statistics were calculated with Molprobity (Chen et al., 2010) and are summarized in Appendix Table A.2.

### 3.4.3 Overall architecture of the ribosome-Ski complex

The atomic model reveals how the Ski complex interacts with the ribosome (Fig. 3.11 and Fig. 3.12). The overall architecture of the Ski complex itself is essentially as observed before and the overall binding mode is consistent with the medium-resolution

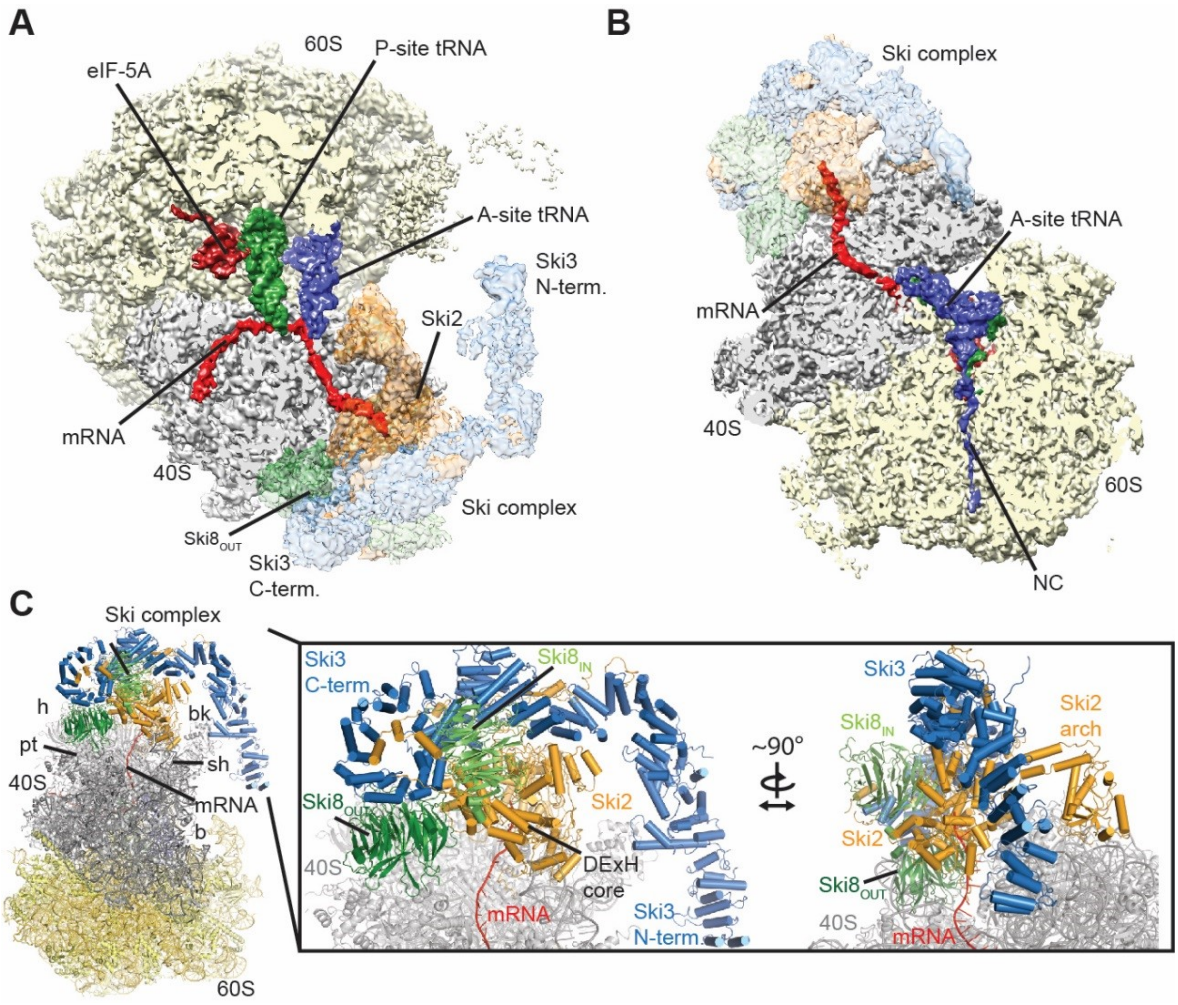


FIGURE 3.11: **Cryo-EM structure of the yeast ribosome-Ski complex.** (**A** and **B**) Top and side view of the ribosome-Ski complex showing densities low-pass filtered to local resolution for the Ski subunits, A-site and P-site tRNA, eIF-5A, mRNA and the nascent polypeptide chain (NC). (**C**) Overall structure of the Ski complex bound to the 80S. The mRNA is shown in red. The zoom-in panel show two orthogonal views of the interactions of the Ski complex with the head of the 40S. General structural features of the Ski complex and the 40S subunit are indicated (h = head; b = body; bk = beak; pt = platform; sh = shoulder).

structure from *in vitro* reconstituted NS-RNC-Ski complexes (Fig. 3.11A and B). The Ski complex binds to the 40S subunit of the ribosome and positions itself directly over the entry of the mRNA channel (Fig. 3.11A-C). It contacts the ribosome via Ski2, the N-terminal arm of Ski3 and $Ski8_{OUT}$. The RecA2 domain of Ski2 binds to the 40S head via uS3 and eS10 (Fig. 3.12A). Additionally, it contacts two flipped out bases at the tip of rRNA helix 16 (h16; U494 and U495) out via several charged residues (R622, N650-N654) to engage the ribosome (Fig. 3.12A and B). Ski3 is contacting the 40S via the beak protein eS12 (Fig. 3.12C). Interestingly, the contact site is at

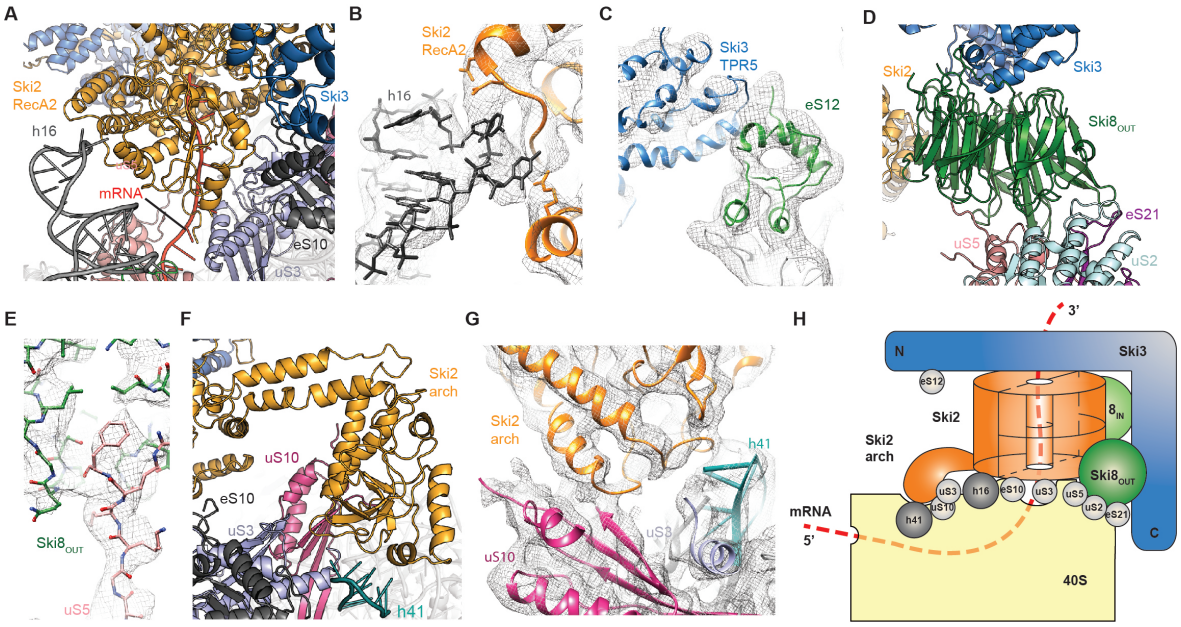


FIGURE 3.12: **Interactions of the Ski complex with the ribosome.** (**A**) The RecA2 domain of Ski2 binds to the tip of rRNA h16 and contacts uS3 and uS10 on the 40S head. (**B**) Close-up view with electron density of the h16 interactions with Ski2 RecA2. (**C**) Close-up view with electron density of the interaction of the N-terminal arm of Ski3 with the 40S beak protein eS12. Ski3 binds via TPR5 where the regular TPR motif is disrupted. (**D**) $Ski8_{OUT}$ interacts with the 40S platform via loops at the bottom surface. It is sandwiched between Ski2, Ski3 and r-proteins uS2, uS5 and eS21. (**E**) Close-up view on the interaction of the C-terminal tail of uS5 and $Ski8_{OUT}$. The otherwise disordered N-terminal tail is completely stabilized and resolved in our structure. (**F**) Interactions of the Ski2 arch domain with the 40S head. The arch domain binds via r-proteins uS3, uS10 and rRNA h41. (**G**) Close-up view with electron density of the arch domain interactions with the 40S head. (**H**) Schematic overview of the Ski complex interactions with the 40S subunit.

TPR5, thus at the position where the regular TPR motif of the Ski3 N-terminal arm is disrupted by a split B helix (Halbach et al., 2013). Ski8 is sandwiched between Ski3 and the 40S platform proteins uS2, uS5 and eS21 (Fig. 3.12D). The $\beta$ propeller binds to the ribosome via several linker loops (loop 1C-1D with eS21; loops 2A-2B, 5A-5B, 6A-6B and 6C-6D with uS5; loop 7A-7B with uS2) at the bottom surface, stabilizing the C-terminal tail of uS5 that is usually disordered but could be fully modelled in our structure (residues 249-254; Fig. 3.12E). Finally, the arch domain of Ski2 is extending from the helical domain and binds to the 40S head via rRNA helix 41 and r-proteins uS3 and uS10 (Fig. 3.12F and G). All of these interactions firmly lock the Ski complex on the small subunit and position the helicase core directly over the

mRNA entry channel (Fig. 3.12H).

### 3.4.4 Binding of the Ski complex to the ribosome induces conformational changes

We could observe that the Ski complex and the ribosome undergo conformational changes upon binding (Fig. 3.13). rRNA h16 is in an unusual bent conformation, moving by about 25 Å after being contacted by the Ski2 RecA2 domain (Fig. 3.13A). The N-terminal arm of Ski3 displays its proposed flexibility after binding to the 40S beak by also moving 30 Å into a more open and extended conformation when compared to the crystal structure (Fig. 3.13B). Finally, the largest movement is seen for the Ski2 arch domain (Fig. 3.13C). It is found in an open position when compared to that observed in the crystal structure of Ski2 alone or the homologous DExH helicase Mtr4 (Weir et al., 2010). We found that it flexes outward by about 30° while

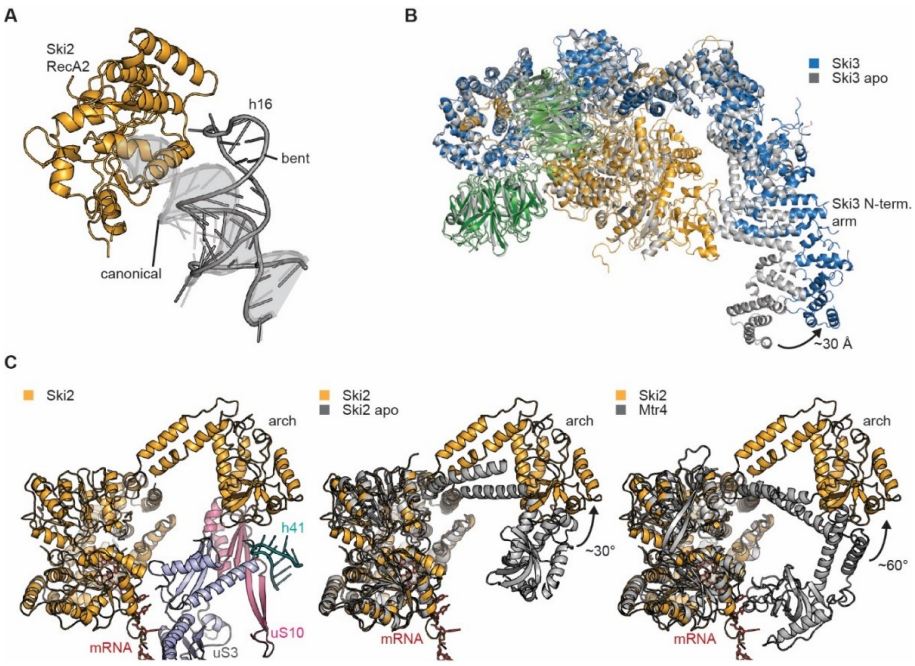


FIGURE 3.13: **Conformational changes of the ribosome and Ski complex upon binding.** (**A**) Binding of Ski2 RecA2 induces a conformational change of h16 which is shifted by approximately 25 Å compared to its canonical position (indicated in light gray). (**B**) Movement of the N-terminal arm of Ski3. Binding to the ribosome shifts the arm by about 30 Å compared to the crystal structure. (**C**) Movement of the Ski2 arch domain. The arch domain moves away from the RNA entry of the helicase during binding to h41, uS3 and uS10 (left panel) when compared to the crystal structure (middle panel) or the homologous helicase Mtr4 (Weir et al., 2010) (right panel).

moving away from the RNA helicase channel entry. Thus, ribosome binding changes the conformation of the two structural elements previously shown to auto-inhibit the RNA-dependent ATPase activity of the Ski complex (Halbach et al., 2013). This suggests that ribosome binding of the Ski complex automatically results in an active and open confirmation of Ski2 where RNA can access the helicase core.

### 3.4.5 The 3' end of the mRNA is directly channelled into the Ski2 helicase

Strikingly, we could observe density for mRNA extending much further than the approximately 28 nucleotides that was observed for ribosomes (Fig. 3.14A) (Budkevich et al., 2014; Jenner et al., 2005). Upon close inspection, we saw that the mRNA extended from its canonical path in the 40S into the helicase core of the Ski2 subunit (Fig. 3.14A and B). The 3' end exits the 40S subunit through a constriction formed by uS3, uS5 and eS30 and passes a small gap between the ribosome and the Ski complex (Fig. 3.14B). It then threads into the Ski2 helicase through an opening formed by the helical domain and RecA2, contacting the basic loop of Ski2 (residues 545 to 606) beforehand (Fig. 3.14C). At the entry site into Ski2, the unwinding $\beta$-hairpin loop contacts the mRNA and bends the nucleotide as it enters the helicase channel (Fig. 3.14C and D). This loop has been shown to be important for RNA unwinding in other DExH helicases and is proposed to be important for the helicase processivity (Büttner et al., 2007). When comparing the mRNA path with that observed for Mtr4 (Weir et al., 2010), four nucleotides follow essentially the same path (Fig. 3.14D). Thus, binding of the Ski complex to the ribosome leads to an elongated mRNA binding tunnel where the mRNA 3' end is threaded into the helicase core of Ski2. This suggests that the helicase complex actively engages ribosomes to possibly extract and funnel mRNA into the exosome for subsequent 3'-to-5' degradation.

## 3.5 Biochemical characterization of the mRNA-Ski complex interaction

The structural data suggest that the Ski complex interacts with the mRNA 3' end extending from the ribosome. To characterize the influence of the length of the 3' overhang, we designed recruitment assays with different mRNA overhang constructs and checked the binding ratio of the Ski complex (Fig. 3.15). To that end, we used a CMV

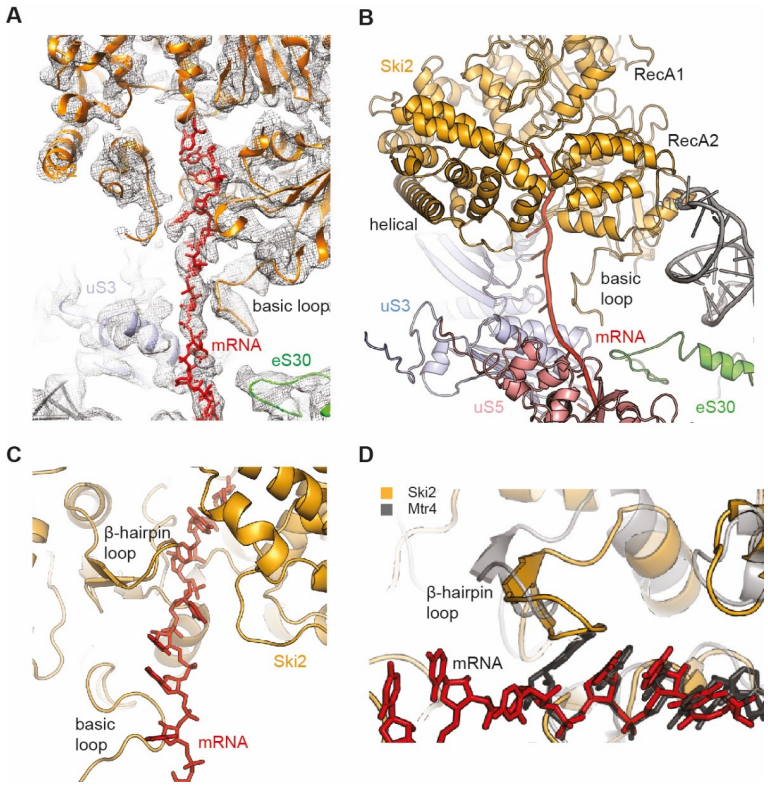


FIGURE 3.14: **mRNA threading from the ribosome into the Ski2 helicase.** (**A**) Model and electron density for the mRNA entry site occupied by the Ski complex. Density for the mRNA extended far outside of the canonical path in the 40S. The mRNA leaves through a constriction formed by uS3 and eS30 and is passing through a gap while being contacted by the Ski2 basic loop. It then enters the Ski2 helicase by an opening formed by RecA2 and the helical domain of Ski2. (**B**) Close-up view of the model of the mRNA path into the Ski2 helicase core. (**C**) Close-up view of the opening formed between the Ski2 RecA2 domain (including the basic loop) and the helical domain (including the $\beta$-hairpin loop). Both loops contact the mRNA while it enters the helicase core. (**D**) Comparison of the mRNA path for the ribosome-bound Ski complex and Mtr4. The path inside Ski2 is essentially the same while the $\beta$-hairpin loop bends the mRNA nucleotide when it enters the helicase core in our structure.

reporter to stall the ribosome at a precise position on a DP120 reporter mRNA (Matheisl et al., 2015). Constructs were designed as such that different lengths of 3' mRNA overhangs extend from the entry site of the ribosomal mRNA tunnel. These overhang constructs were then used for *in vitro* reconstitution assays with 5 times molar excess of purified Ski complex. After pelleting through a sucrose cushion, pellet and supernatant samples were analysed by Western Blot and bands were quantified using Imagequant. To account for slightly differing amounts of RNCs and Ski complex, the Ski protein bands were normalized against ribosomal bands for quantification (for

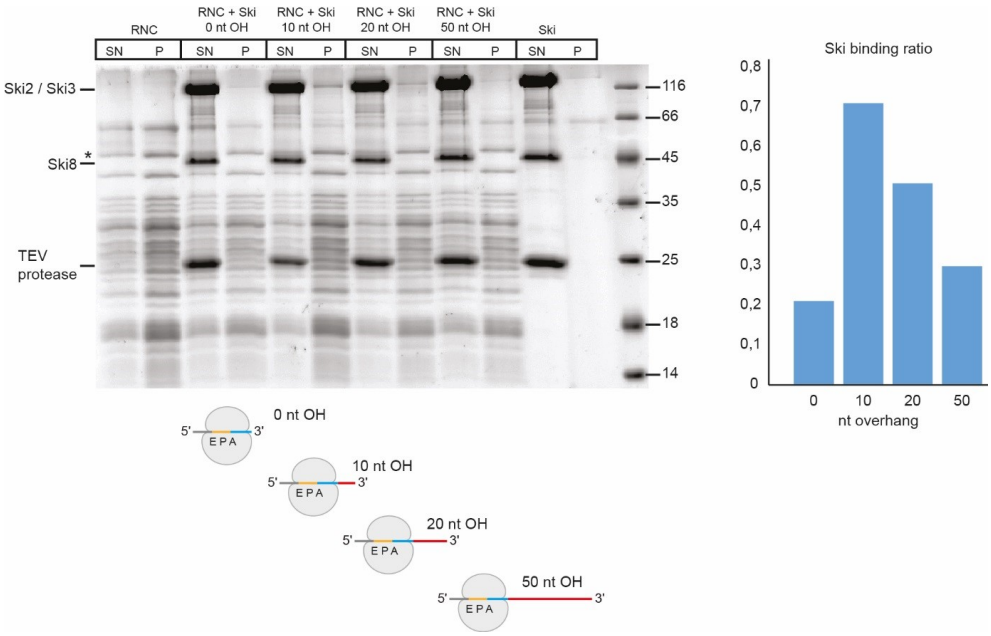


FIGURE 3.15: **Biochemical analysis of the 3' mRNA binding by the Ski complex.** Example SDS gel after SYPRO Orange staining of the *in vitro* reconstitution using recombinantly purified Ski complex and different overhang RNC constructs (shown schematically on the bottom). Each construct presents a different length of 3' mRNA overhang. The binding ratio was estimated by quantifying bands with Imagequant and normalizing the Ski2/Ski3 double band versus a ribosomal band (indicated with an asterisk). The experiment was performed as a duplicate and binding ratios were calculated and plotted in a bar diagram (right panel). As can be seen, the Ski complex has a higher affinity towards ribosomes presenting a short 10-20 nucleotide 3' mRNA overhang.

details see Methods) and the experiment was carried out as a duplicate.

A clear preference towards a certain 3' mRNA overhang length is visible from the recruitment assay. Whereas very little Ski complex was bound to RNCs that presented no 3' mRNA overhang, the binding ratio was significantly increased for a short 10 nucleotide long fragment extending from the ribosome. For 20 and 50 nucleotides, the binding ratio decreased again, with 50 nucleotides being almost at the level of 0 nucleotides. These data suggest that the Ski complex prefers short 3' mRNA overhangs between 10-20 nucleotides for ribosome binding. Arguably, this effect is explained by the necessity of threading the mRNA end into the Ski2 helicase core which is more difficult with longer overhangs. Notably, the interactions between Ski2 and the mRNA 3' end seem to significantly contribute to the stable binding of the Ski complex to ribosomes, since without any overhang, the binding ratio is at a very low level which is in line with the *in vitro* reconstitution where no Ski complex was bound to empty 80S ribosomes (see 3.1.2).

## 3.6 Analysis of mRNAs associated with ribosome-Ski complexes by targeted ribosome profiling

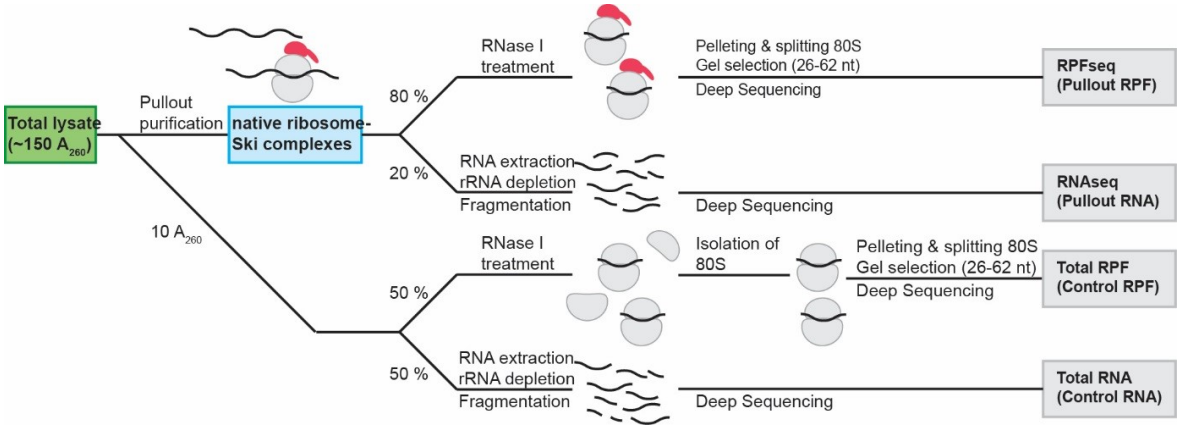


FIGURE 3.16: **Overview of the sample preparation for the targeted profiling.** Control samples were generated from the total lysate, pullout samples from purified ribosome-Ski complexes. For the pullout samples, the additional isolation of 80S could be omitted since it exclusively contained 80S monosomes.

To verify the mRNA binding *in vivo*, we performed targeted ribosome profiling on our natively purified ribosome-Ski complexes (Fig. 3.16). In short, profiling allows to gain information about the nature and translation status of mRNAs in a cell with the help of deep sequencing tools. This allows to gain insights into the position of ribosomes on individual mRNAs and to monitor different translation and degradation events on a global scale in the cell. In targeted profiling, a specific purified population of ribosomal complexes is used instead of the total lysate of a cell (Fig. 3.16). For a detailed explanation about ribosome profiling, please refer to Ingolia et al., 2009. All profiling data was processed by Vivekanandan Shanmuganathan and Markus Pech (Beckmann lab, Gene Center Munich).

In our experiment, we used natively purified ribosome-Ski complexes to analyse the composition of mRNAs and to gain insights into the targeting process of the Ski complex to ribosome-associated mRNAs (Fig. 3.17). First, we analysed whether the 3' mRNA overhang binding of the Ski complex is also visible under native conditions by checking the RNase protection length from our purified complexes (Fig. 3.17A). We found that beside the characteristic 28-30 nucleotide peak corresponding to the protection length of the ribosome, a second peak is observable at 35-40 nucleotides.

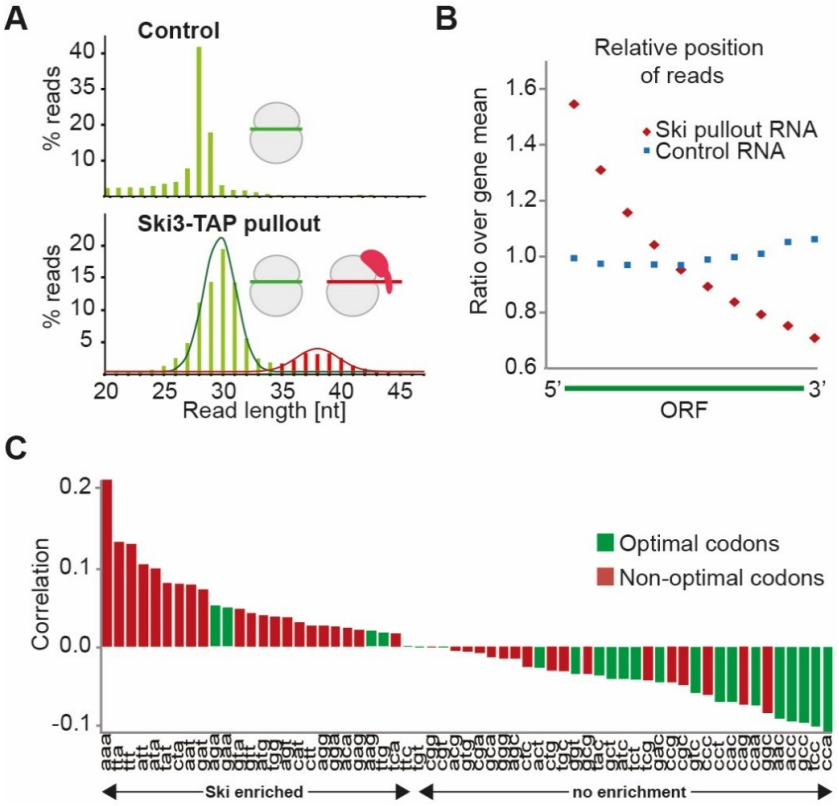


FIGURE 3.17: **Biochemical features of the Ski-ribosome interactions with the mRNA 3' end.** (**A**) Length distribution of ribosome-protected footprints (RPFs) from native 80S ribosomes and the Ski3-TAP pullout samples. In the pullout sample, an additional peak with an extended protection length of 10 nucleotides could be detected. (**B**) Relative positional distribution of RNA reads from 5' to 3' over the ORFs in the respective mRNA of the Ski pullout compared with that of control mRNA. Whereas an even positional distribution of ribosomes was visible in the control, the pullout contained more ribosomes at the 5' part of mRNAs. (**C**) Codon correlation plot ranked by Ski enrichment (stop codons were removed). Spearman correlation values were calculated between the footprint ratio (Ski3-TAP pullout against control) and codon occurrence across the genome for all codons according to Presnyak et al., 2015. A strong bias of non-optimal codons in the Ski-ribosomes associated mRNAs was detected.

This exactly corresponds to the protection length that would be expected from the ribosome (28-30 nt) plus Ski complex (9-10 nt) and fits the observation from the structural data where 34 nucleotides are clearly visible. This confirms that Ski complexes engage ribosomes in the cell and that the 3' mRNA overhang is actively threaded into the Ski2 helicase core. Additionally, when analysing the position of ribosomes on the ribosome-Ski complex associated mRNAs, we found a strong bias of ribosomes sitting on the more 5' part of mRNAs and fewer ribosomes at the 3' part (Fig. 3.17B). This

argues in favour of ribosome-Ski complexes being engaged in ongoing 3'-to-5' mRNA degradation where shortening of mRNAs from the 3' end is expected. Finally, when analysing the codon composition of target mRNAs, we found a strong correlation between codon optimality and Ski complex presence (Fig. 3.17C). In mRNAs that were associated with ribosome-Ski complexes, a strong bias towards non-optimal codons could be detected. This further suggests an involvement of ribosome-Ski complexes in 3'-to-5' mRNA degradation since non-optimal codons have been reported to significantly reduce the half-life of mRNAs (Presnyak et al., 2015). Thus, mRNAs with high non-optimal codon content are prime targets for degradation.

Collectively, we could show that the Ski complex binds to ribosomes *in vivo* and *in vitro*. Here, the Ski complex resembles an open conformation where the mRNA is bound to the Ski2 helicase. Biochemical analysis of the 3' mRNA overhang revealed that a short 10-20 nucleotide fragment extending from the ribosome may act as a recruitment signal for the Ski complex. Targeted profiling revealed that this Ski-ribosome intermediate might not be limited to quality control, but represent a general decay intermediate in mRNA turnover.

## 3.7 High-resolution structure of eIF-5A bound to the ribosome

During data processing and 3D classification, we made the surprising discovery that almost all ribosomes had eIF-5A bound and that a larger number of ribosomal particles did not contain Ski complex, but only eIF-5A bound to the E-site. Since Ski3-TAP was used as bait protein, these ribosomes probably had the Ski complex bound to them initially but lost it during the purification or grid making process. eIF-5A, which contains a unique modification called hypusine (at K51 in yeast) that is essential for its activity, is implicated in the rescue of ribosomes stalled on poly-proline stretches (Dever et al., 2015; Gutierrez et al., 2013), therefore we did not expect it to find at such large quantities in our dataset. It consists of two domains (domain I and domain II) while missing domain III that is present only in the bacterial homologue EF-P. Additionally, eukaryotic eIF-5A contains an N-terminal extension (NTE) that is not present in its prokaryotic or archaeal counterparts. Our discovery raised some questions on whether eIF-5A might have some additional functions in quality control pathways or recognition and rescue of stalled ribosomes in general. Moreover, the exact mechanism of ribosome rescue by eIF-5A is not understood. Our structural data allowed us to build a complete atomic model of eIF-5A on the ribosome to gain

insights into its rescue function. Moreover, biochemical analysis revealed that eIF-5A might have a broader use in eukaryotic translation as anticipated before.

### 3.7.1 Data processing and resolution determination

3D refinement of the eIF-5A containing 80S class resulted in a structure at an overall resolution of 3.9 Å according to the gold standard criterium (Fig. 3.18A). Local resolution ranged from 3.5 Å in the inner core to roughly 4.5 Å on the outer surface of the ribosome. Most importantly, eIF-5A was mostly well resolved below 4 Å, including domain I with the $\beta$3-$\beta$4 loop containing the hypusine moiety (Fig. 3.18B). Only the NTE displayed some flexibility which is reflected in its lower resolution compared to the rest of the protein. This allowed us to build a complete atomic model based on a homology model from archaeal eIF-5A (Kim et al., 1998; PDB 2EIF) for structural analysis. The model was assembled and adjusted manually in Coot and subjected to Phenix real space refinement.

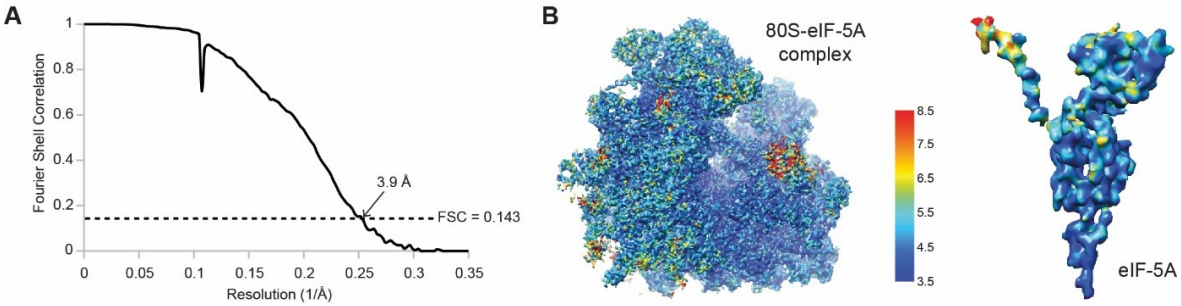


FIGURE 3.18: **Resolution determination and local resolution for the ribosome-bound eIF-5A reconstruction.** (**A**) The final map was refined to an overall resolution of 3.9 Å according to the gold standard criterium. (**B**) Final map and eIF-5A alone coloured by local resolution as estimated by Resmap. Resolution ranged mostly from 3.5 Å to 4.5 Å. eIF-5A was well resolved below 4 Å with the exception of the NTE that displayed higher flexibility.

### 3.7.2 Overall structure of eIF-5A bound to the ribosome

Overall, eIF-5A binds in a similar position on the ribosome to that observed for bacterial EF-P (Fig. 3.19A and B). The factor resembles its unbound form closely with the exception of the $\beta$3-$\beta$4 loop which readjusts upon binding (Fig. 3.19C). Domain I of eIF-5A (Fig. 3.19D) mostly interacts with the 25S rRNA of the LSU (Fig. 3.20A). The main interactions are with nucleotides within rRNA helices 74 (h74) and 93 (h93), as well as helix 68 (h68) and helix 70 (h70). In contrast, domain II shows

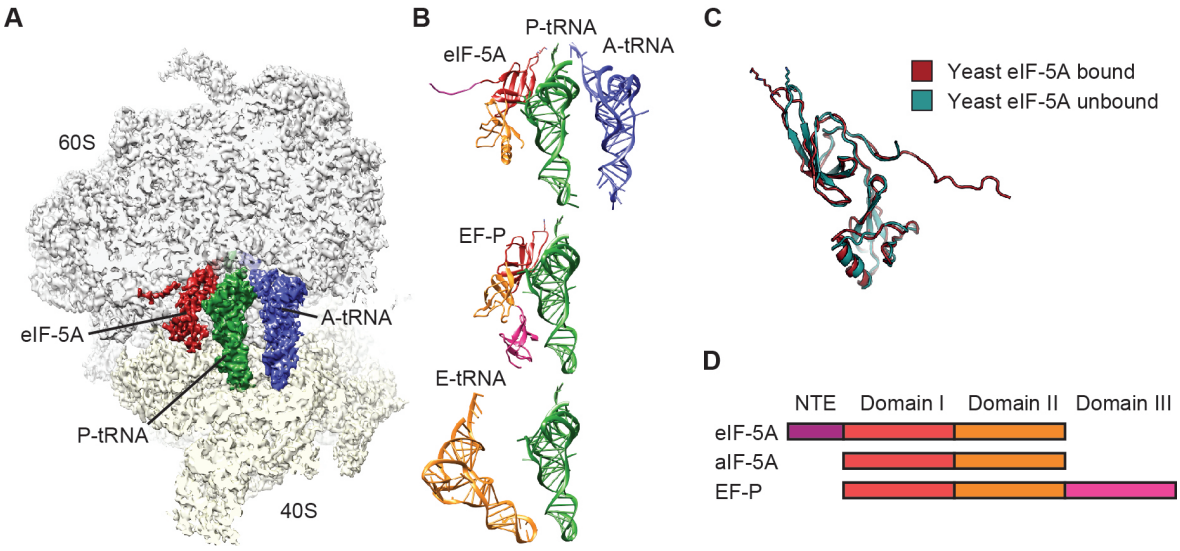


FIGURE 3.19: **Cryo-EM structure of eIF-5A bound to the yeast ribosome.** (**A**) Transverse section of the cryo-EM map of the eIF-5A-80S complex, showing densities for the 40S and 60S subunit, A-site tRNA, P-site tRNA and eIF-5A. The map reveals the binding site of eIF-5A to the E-site of the ribosome. (**B**) Comparison of ribosome binding positions of eIF-5A, EF-P and E-site tRNA, relative to A-tRNA and P-tRNA. The domains of eIF-5A and EF-P are coloured according to (**D**). (**C**) Comparison of bound and unbound eIF-5A structures from yeast. (**D**) Schematic representation of the domain structures of eIF-5A, aIF-5A and EF-P.

no interactions with rRNA and contacts r-proteins uL1 and eL42 (Fig. 3.20A and B). Here, domain II is inserted between domains 1 and 2 of uL1 (Fig. 3.20B). The NTE, which was not visible in previous crystal structures due to flexibility, is sandwiched between uL1 and eL42 and probably stabilized by these interactions (Fig. 3.20C). uL1, the NTE and eL42 adopt the overall secondary structure of an extended $\beta$-sheet formed by all three proteins. In general, the L1 stalk is largely shifted inwards due to its interaction with domain II from eIF-5A and is further stabilized by the NTE (Fig. 3.20D and E). This closed conformation of the L1 stalk was also observed for EF-P bound to the bacterial ribosome (Blaha et al., 2009). The specific interactions of the NTE (which is only present in eukaryotes; see Fig. 3.19D) with uL1 and eL42 might explain the observed shift in domain I of eIF-5A when compared to ribosome-bound archaeal IF-5A or bacterial EF-P (Fig. 3.20F). Finally, the $\beta$3-$\beta$4 loop of domain I inserts into a pocket formed by ribosomal rRNA, namely h74 and h93, and P-site tRNA (Fig. 3.20G). Here, a network of hydrogen bonds is observed including nucleotides 2806-2808 and 2963-2968 and the mostly positively charged residues of the $\beta$3-$\beta$4 loop (S47, T49, H52, H54; Fig. 3.20H). In contrast, there are no other interactions with the P-site tRNA with the exception of a weak hydrogen bond of R27

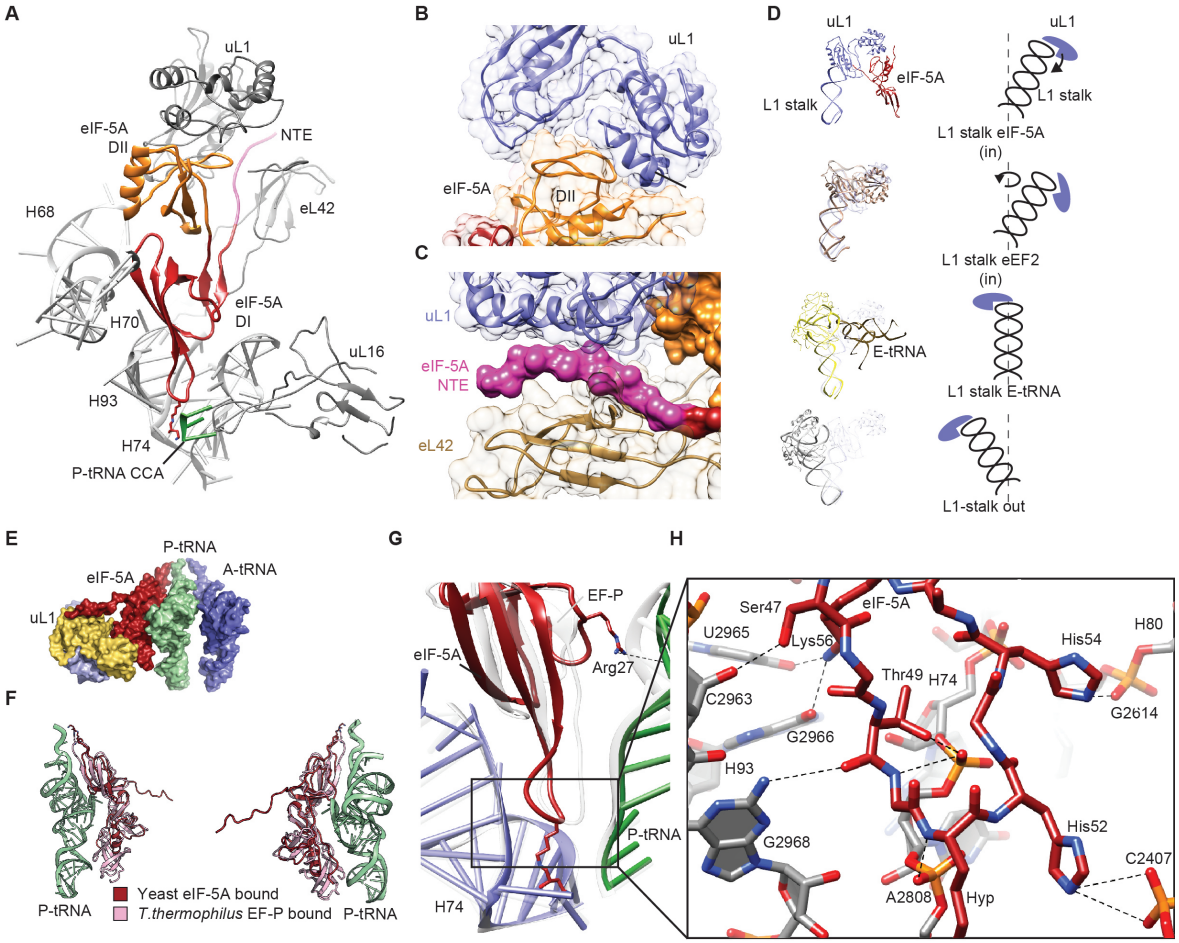


FIGURE 3.20: **Interactions of eIF-5A with the yeast ribosome.** (**A**) Molecular model for the interaction of domains I (DI) and II (DII) as well as the NTE of eIF-5A with rRNA and ribosomal protein components of the ribosome. (**B**) View of the domain II interaction with uL1. Domain II of eIF-5A inserts into the cleft between domains 1 and 2 of uL1. (**C**) Surface representation of the NTE of eIF-5A sandwiched between ribosomal proteins uL1 and eL42. (**D**) Comparison and schematic representation of the L1 stalk position between eIF-5A bound ribosomes (top), eEF2- bound ribosomes (second row), E-site tRNA bound ribosomes (third row) and empty E-site (bottom). (**E**) Surface representation of eIF-5A interacting with uL1. (**F**) Structure comparison between 80S-bound eIF-5A and 70S-bound EF-P. (**G**) Comparison of the ribosome binding position of domain I, P-site tRNA and h74 relative to EF-P, P-tRNA and h74 of the bacterial EF-P complex (shown in light gray). R27 of eIF-5A makes a potential hydrogen bond to the P-site tRNA whereas no other interaction could be detected between eIF-5A and the P-site tRNA. The $\beta$3-$\beta$4 loop is shifted away from the P-tRNA compared to EF-P. (H) Possible hydrogen bond interactions (dashed lines) between domain I of eIF-5A with 25S rRNA h74, h80 and h93.

to G4-C5, whereas a multitude of contacts were observed for EF-P with P-site tRNA (Blaha et al., 2009). This difference might explain why eIF-5A and EF-P have been shown to differ in function.

### 3.7.3 The hypusine residue contacts the CCA-end of the P-site tRNA

The cryo-EM reconstruction contained the complete electron density for the hypusine residue at the tip of the $\beta$3-$\beta$4 loop (Fig. 3.21A). We observed that it inserts deeply into a pocket formed by the CCA-end of the P-site tRNA and h74 while forming two stabilizing hydrogen bonds with U2807 and A2808. With its extended side chain, the hypusine then contacts the CCA-end of the P-site tRNA and forms a hydrogen bond between its terminal 4-amino group and A76 (Fig. 3.21B). Even though we did not detect any contacts in our structure, we note that the hydroxyl group of the hypusine residue could potentially form contacts to rRNA in the vicinity (mostly h74) which might explain its necessity in higher eukaryotes compared to yeast.

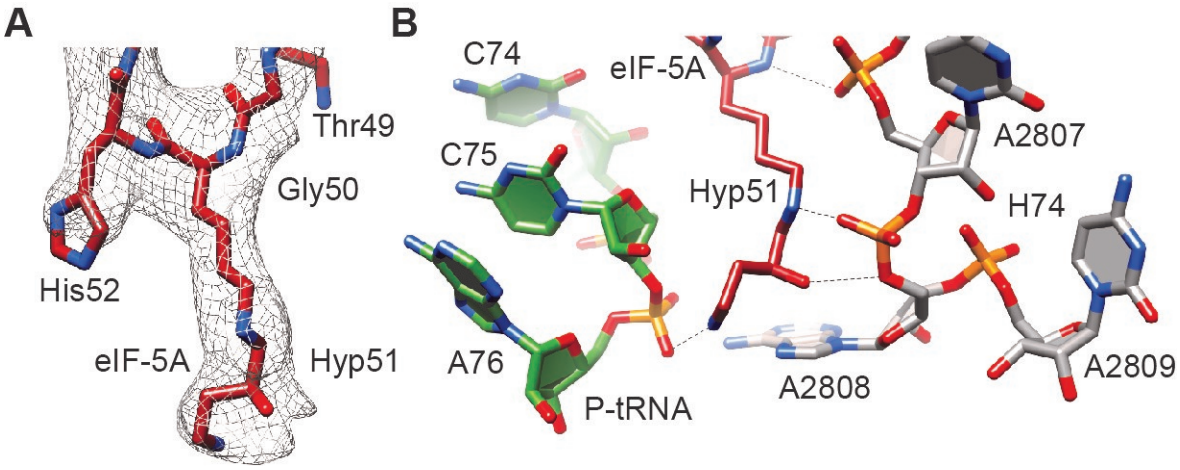


FIGURE 3.21: **Interaction of the hypusine of eIF-5A in the PTC of the ribosome.** (**A**) Molecular model and electron density for the hypusine (Hyp51) residue at the tip of the $\beta$3-$\beta$4 loop in domain I of eIF-5A. (**B**) Potential hydrogen bonds between the hypusine, rRNA h74 and the CCA-end of the P-site tRNA. The terminal amino group contacts A76 of the P-tRNA.

### 3.7.4 eIF-5A binding stabilizes a specific loop of uL16 for peptide-bond formation

Since the sample contained a mixture of different polypeptide chains, the NC is only resolved at backbone level. However, our reconstruction clearly indicates that the NC is attached to the A-site tRNA, resulting in a pre-translocation post-peptide transfer state (Fig. 3.22A and B). Interestingly, we saw that the eukaryotic-specific loop of uL16 (residues 104-110) was completely stabilized and resolved in our structure compared to other 80S structures (Behrmann et al., 2015; Ben-Shem et al., 2011) where it was disordered (Fig. 3.22C). This stabilization is most likely the result of several interactions between uL16 and the A- and P-site tRNAs. We detected hydrogen bonds between D108 and A76, as well as R109 and G73 of the P-tRNA (Fig. 3.22C). Additionally, C104 contacts C72 of the A-site tRNA, which seems to be essential for loop stabilization since it is not resolved in presence of only P-site tRNA. This stabilization might be necessary for peptide-bond formation since the prokaryotic r-protein L27 substitutes for the loop of uL16 but adopts a similar position that is important for the PTC activity (Polikanov et al., 2014).

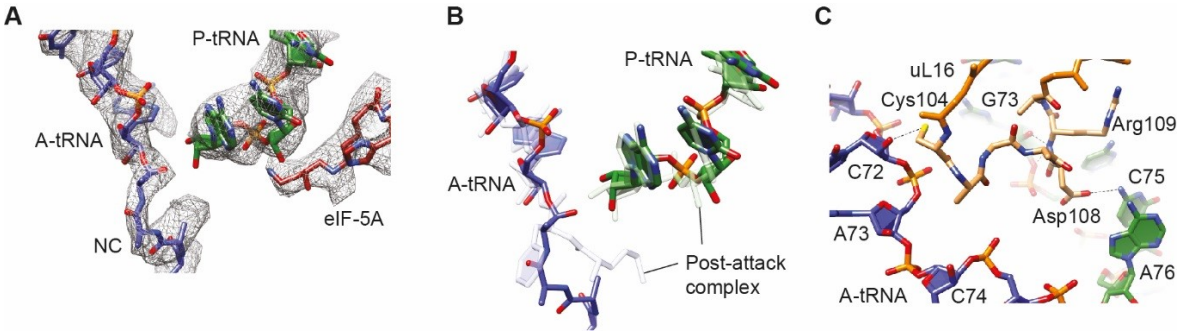


FIGURE 3.22: **The nascent chain and uL16 in the eIF-5A bound ribosomal structure.** (**A**) Electron density and molecular model for the CCA-ends of the P-site and A-site tRNA with the NC as well as eIF-5A. The NC is attached to the A-site tRNA. (**B**) Comparison of A-tRNA and P-tRNA from the eIF-5A-80S complex with A- and P-site tRNAs from post-attack complexes. (**C**) Potential hydrogen bond interactions between A- and P-site tRNA and uL16 leading to the stabilization of a loop of uL16 (residues 104-110).

### 3.7.5 eIF-5A binds to ribosomes with a vacant E-site

Finally, we wondered about the presence of eIF-5A in our Ski3-TAP pullout sample. The binding of eIF-5A to quality control and mRNA degradation intermediates could indicate a yet unidentified role of the factor in these pathways. To analyse this possibility, we performed deep-sequencing analysis of the associated mRNAs to investigate their codon composition (Fig. 3.23A). All sequencing analysis was performed by Vivekananadan Shanmuganathan (Beckmann lab, Gene Center LMU, Munich). We found an overall even distribution of codons in the P- and E-site and only slight enrichment of phenylalanine, histidine and proline codons in the A-site. This suggests that we did not specifically enrich poly-proline stalled or initiation complexes with eIF-5A. Upon close inspection, we found that the addition of cycloheximide could be a possible explanation for eIF-5A's presence. In our structure, we detected that cycloheximide does not clash with eIF-5A bound to the E-site, as it does with E-site tRNA (Fig. 3.23B). Thus, binding of cycloheximide to the E-site might generate ideal targets for eIF-5A, namely ribosomes stalled with P-site tRNA and an empty E-site. This is further indicated by the presence of eIF-5A in the Ski complex containing structure (see above) and the fact that mass spectrometry analysis of pullouts from Ski3-TAP strains without the addition of cycloheximide did not reveal any eIF-5A (data not shown). Thus, eIF-5A could bind to the E-site of the ribosome as soon as it is vacant.

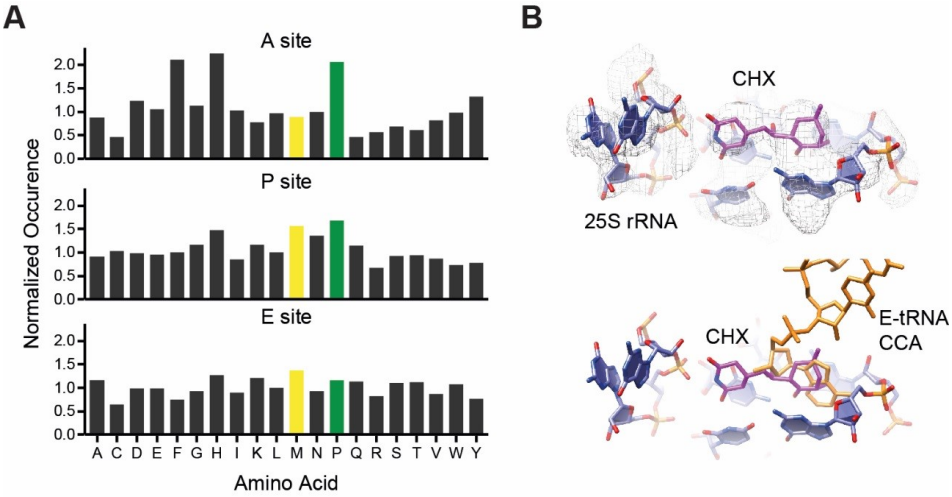


FIGURE 3.23: **Codon analysis and cycloheximide (CHX) presence in the eIF-5A-80S complex.** (**A**) Representation of codons positioned in the A-site, P-site and E-site of eIF-5A-80S complexes. Only a slight enrichment of phenylalanine, histidine and proline codons in the A-site can be detected. (**B**) Atomic model and electron density for CHX bound to the E-site. While eIF-5A can still bind (upper panel), CHX crashes with the CCA-end of E-site tRNA (lower panel).

Collectively, we present the structure of eIF-5A bound to the E-site of the 80S ribosome. Our reconstruction reveals that the unique hypusine modification is essential for eIF-5A's function by reaching deep towards the PTC. The amino group at the tip of the hypusine residue contacts the CCA-end of the P-site tRNA for stabilization. Additional stabilization of a specific uL16 loop and the A-site tRNA allow proper peptide bond formation, explaining eIF-5A's role as a rescue and translation elongation promoting factor. Furthermore, analysis of the codon composition in the A-, P- and E-sites together with the structural data reveal that eIF-5A binds specifically to ribosomes with a vacant E-site, thus identifying its target by monitoring tRNA occupancy.

# 4 Discussion

## 4.1 Ski complex links the mRNA translation and degradation machineries

Even though it is long known that mRNA translation and degradation are mutually interdependent pathways, direct evidence for this interplay was rather rare. First studies in 2003 from Sheth and colleagues suggested that only non-translating mRNAs are targeted for 5'-to-3' degradation and that the translation status of an mRNA would ultimately determine if it is targeted for degradation or not (Sheth et al., 2003). Nevertheless, the actual process of mRNA degradation (and protein degradation for that matter) was mostly viewed as isolated except for quality control of aberrant mRNAs that had been shown to be initiated co-translationally on the ribosome. Only recently, reports from the Coller and Steinmetz labs showed that 5'-to-3' mRNA degradation can indeed happen for translating mRNAs and that decapping and Xrn1-dependent degradation are occurring on translating polysomes (Hu et al., 2009, Hu et al., 2010; Pelechano et al., 2015). Around the same time, the RQC was discovered and it was also shown that protein degradation of aberrant peptides is often directly linked to translational events and ribosome stalling (Brandman et al., 2012; Defenouillère et al., 2013). These findings ultimately changed the view of the connection between translation and degradation in the field. Since then, most studies were focusing on 5'-to-3' mRNA degradation, considering that it is the major mRNA turnover pathway in yeast, whereas very little is known in comparison about the exosome-dependent 3'-to-5' degradation pathway and its connection to translation. The findings presented in this dissertation show for the first time that the same level of interconnection that has been shown for Xrn1-dependent degradation and translation also exists for the 3'-to-5' degradation pathway. Our data suggest that the Ski complex acts as a physical link between the mRNA translation and degradation machineries and that Ski complex binding to the ribosome is possibly the first step in initiating 3'-to-5' degradation. Moreover, we highlight the first structural evidence of

the connection of mRNA degradation and translation, something that was missing so far for both degradation pathways.

Our finding that the Ski complex and not Ski7 associates stably with 80S ribosomes was initially rather surprising since the Ski complex does not resemble any known ribosome binding factor and was never predicted to bind to it in previous screenings. Since both Ski7 and the Ski complex are needed for 3'-to-5' mRNA degradation (Araki et al., 2001; van Hoof et al., 2000), the current working model states that mRNAs are channeled into the exosome by the Ski complex and that Ski7 acts as an adaptor protein to mediate the interactions between both complexes (Araki et al., 2001; Frischmeyer et al., 2002; van Hoof et al., 2002). In case of mRNA quality control, Ski7's resemblance to other translational GTPases like Hbs1 or eRF3 led to the hypothesis that Ski7 would bind ribosomes to recognize targets for NSD via its C-terminal GTPase domain. All our findings contradict the proposed function of Ski7 and suggest a different mechanism altogether. Our *in vitro* reconstitutions and the nonstop reporter assay show that the Ski complex interacts with ribosomes even in absence of Ski7 and other quality control factors like Dom34 and Hbs1 arguing that Ski complex binding to ribosomes is occurring upstream and independent of these factors. We therefore propose a two-component model where a ribosome-Ski complex recruits a preassembled exosome-Ski7 complex to degrade the associated mRNA (Fig. 4.1). This model would explain why Ski7 only would show transient binding to ribosomes and could never really be visualized in our attempts where possible stabilizing factors like the exosome and the Ski complex were not present.

## 4.2 Ribosome binding activates the helicase complex for mRNA threading

What impact has ribosome binding on the Ski complex? Our structure reveals that several interactions and conformational changes position the Ski complex on the small subunit of the ribosome so that the helicase channel entry of Ski2 is perfectly aligned with the mRNA entry channel of the ribosome. This alignment allows the threading of the mRNA 3' end into the helicase core directly on the ribosome which was also proven biochemically. Threading is facilitated by rearrangements of the arch domain of Ski2 and the N-terminal arm of Ski3. These two elements were proposed to allosterically regulate helicase activity by forming a lid to prevent access to the helicase core and were shown to be more flexible compared to the rest of the complex (Halbach et al., 2013). Both elements display large conformational changes

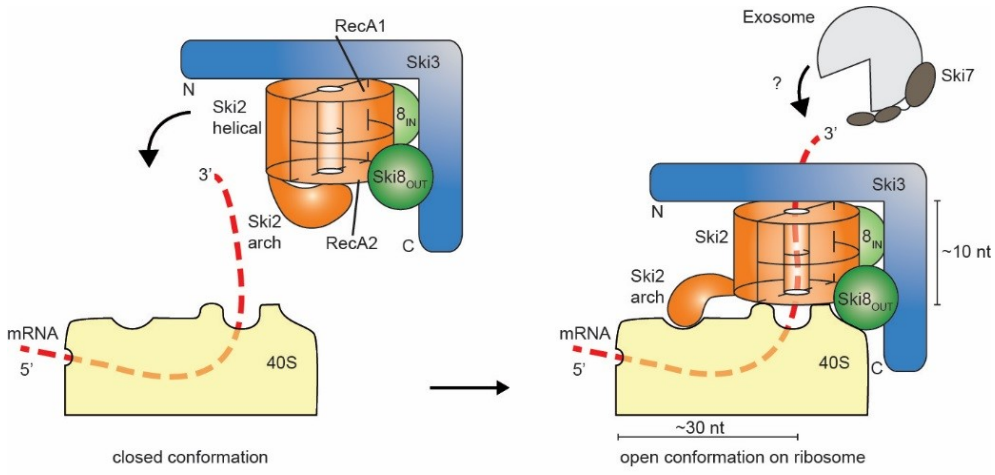


FIGURE 4.1: **Model for ribosome-binding of the Ski complex in 3'-to-5' mRNA decay.** The Ski complex binds to ribosomes to thread the associated mRNA into its helicase core. Subsequently, this ribosome-Ski complex can bind with a preassembled exosome-Ski7 complex to degrade the mRNA.

when binding to the ribosome and move into an open position away from the helicase channel entry. For the N-terminal arm of Ski3, TPR5 interacts with the 40S beak at the position where the regular TPR motif is disrupted by a split B helix. Halbach et al suggested that this would allow increased flexibility in the N-terminal arm (Halbach et al., 2013), therefore it is tempting to speculate that this interruption is needed for ribosome binding to allow the arm to move into its outward position. The arch domain also moves outward into an open conformation since its previous position is occupied by 40S head proteins uS3 and uS10 and rRNA h41 compared to the Ski2 crystal structure. This large outward movement is made possible by the long flexible connection to the helical domain of Ski2 consisting of two parallel alpha-helices. The increased flexibility is substantiated by our finding of a second population of ribosome-Ski complexes with the arch domain binding to the N-terminal arm of Ski3 (see Fig. 3.8), showing that it can rotate by about 180° around the double helix linker. Notably, in this second population the arch domain is also positioned far away from the helicase entry. We thus suggest that the increased flexibility of both the arch domain and the N-terminal arm of Ski3 is used to automatically generate an open and active conformation of the Ski complex upon ribosome binding as compared to a more closed conformation when being isolated from the ribosome. Therefore, Ski complex binding to the ribosome leads to a conformation where a substrate mRNA can be threaded into the Ski2 helicase, therefore "activating" the helicase complex (Fig. 4.1).

## 4.3 The 3' mRNA end as an anchor for Ski complex binding

Our presented structure gives insights into how the Ski complex can be guided to appropriate ribosomal targets. This recruitment needs to be a highly precise process since there are much less copies of the Ski complex in the cell than ribosomes (Ghaemmaghami et al., 2003) and because it would be highly detrimental to recruit an RNA helicase that locks onto the mRNA to an actively translating ribosome. Our data suggest that a short 10-20 nucleotide long extended 3' mRNA overhang on the ribosome seems to act as a recruitment signal (Fig. 3.15). This preference for short mRNA extensions might be due to the necessity of threading the mRNA into the Ski2 helicase core. Since the Ski complex shows no lateral openings in its structure, threading of long RNA extensions while binding to the ribosome would pose a significant challenge. Additionally, mRNA binding seems to significantly increase stability since binding is substantially weaker to ribosomes lacking mRNA completely (Fig. 3.3). An interesting fact is that short 3' overhangs created by an endonucleolytic cleavage are hallmarks of NSD and NGD where so-called primary and secondary targets are created (Shoemaker and Green, 2012). For NGD, it was already proven that the 5' substrate, which would include a short 3' overhang, is targeted by 3'-to-5' mRNA degradation (Doma and Parker, 2006). Since endonuclease events are occurring in both quality control pathways, having the 3' overhang as a recruitment signal seems to be a likely model. Furthermore, this model is substantiated by the polysome profile analysis of the Ski3-TAP strain presented in this thesis (Fig. 3.4). After RNase A digestion, all the signal for Ski3-TAP collapsed into the 80S fraction. While this was expected for the signal in the polysome fraction, it is initially surprising to see for the lower molecular fractions. The disappearance of the signal from the free unbound and ribosomal subunit fractions would be explained by RNase A generating short 3' mRNA overhangs on the 80S ribosomes which in turn leads to sequestering of the Ski complex in the lysate. For general turnover, 3'-to-5' degradation is much less frequent, but also only very few endonucleolytic events are detected (Harigaya and Parker, 2012) . Furthermore, since mRNAs are translated from 5' to 3', yet exosome-dependent degradation occurs from 3' to 5', the ribosome would act as a roadblock at some point which would need to be removed. This fact could explain why 5'-to-3' degradation evolved to be the major turnover pathway in yeast and other eukaryotic organisms.

Another possibility for recruitment would be the recognition of targets by specific

modifications. Recent studies have shown that ubiquitination of r-proteins seems to act as a major initiation signal for protein quality control (Brandman et al., 2012; Higgins et al., 2015; Sitron et al., 2017; Sundaramoorthy et al., 2017). Ubiquitinations of uS3, eS10 and uS10 have been shown to be important for initial ribosome stalling and binding of necessary factors for the RQC response. It is possible that similar ubiquitination events are recognized by the Ski complex, however we didn't detect any ubiquitin densities in our structure. Nevertheless, we note that uS3 and uS10 are both interacting with the Ski complex and could serve as recognition sites. An interesting aspect is also the involvement of the Ski2 arch domain in recruitment of the Ski complex to ribosomes. It has been shown that the arch domain of the Ski2-related helicase Mtr4 binds to specific conserved LFX$\phi$D motifs (with X being any and $\phi$ being a hydrophobic amino acid) on adapter proteins, thus recruiting the helicase to its pre-ribosomal target (Thoms et al., 2015). This specific interaction is conducted by the KOW domain found in the Mtr4 arch domain. The KOW domain is absent in Ski2 and uS3 and uS10 that interact with the Ski2 arch domain do not contain an LFX$\phi$D motif, however the involvement of the arch domain in recruiting the Ski complex to the ribosome is still a possibility. Nevertheless, we note that recruitment via a short 3' mRNA overhang seems to be the most likely model which is in line with our *in vitro* recruitment assays and previous findings investigating quality control pathways.

## 4.4 Ski complex binding to ribosomes - the first step in ribosome-associated 3'-to-5' mRNA degradation

What is the function of the Ski complex bound to the ribosome? From previous studies, it is known that the Ski complex forms an elongated mRNA binding tunnel together with the exosome, leading to the proposal that it can actively channel RNA into it for degradation (Halbach et al., 2013). The data presented here indicate that this binding tunnel might be even further extended by the ribosome. It is tempting to suggest that the formation of a "super complex" would be the next step as proposed above, where the exosome with Ski7 binds to a ribosome-Ski complex, forming an over 70 nucleotide long mRNA binding tunnel. The Ski complex could then actively extract the mRNA from the ribosome in a processive reaction by using energy from ATP hydrolysis and thread it into the exosome for degradation. This model seems likely by looking at other steps in RNA and protein degradation processes where more examples for active substrate threading are found. For example, beside that RNAs

are threaded into the exosome by the Ski complex, proteins are threaded into the proteasome through its 19S cap structure by different ATPases like Cdc48 (Tomko and Hochstrasser, 2013). Likewise, the bacterial RNA and protein degradation complexes PNPase or RNase PH and ClpP, respectively, show barrel-like architectures similar to the exosome and the proteasome, where substrates are actively threaded to the active site via a central channel (Alexopoulos et al., 2012; Garneau et al., 2007; Tomko and Hochstrasser, 2013). Therefore, energy-consuming active substrate threading seems to be a reoccurring principle used in degradation processes in the cell. Notably, threading of the substrate through a narrow channel makes it necessary that proteins or RNAs are unwound, thus threading might be necessary to make the target more accessible. Therefore, it would make sense to have a helicase to channel RNA into the exosome to start with.

Some questions are left open regarding the steps after Ski complex binding to ribosomes and possible channeling of the mRNA into the exosome. First, the Ski complex must be released from the ribosome. It is unclear at which point the disassembly occurs. However, it would be likely that Ski7 binding to the ribosome-Ski complex could signal for the Ski complex's release after the RNA is fed into the exosome (see also further below). Second, the ribosome must be recycled. It is unclear whether the ribosome splitting system Dom34/Hbs1 and ABCE1 can also rescue ribosomes that were targeted by the Ski complex. We note that in our structure the binding site for Hbs1 would be accessible even when Ski complex is bound, nevertheless the A-site is still occupied by peptidyl-tRNA. Thus, Dom34 cannot access its binding site to recruit the splitting ATPase ABCE1. To remove the A-site, it would either have to be actively extracted (since drop-off seems unlikely when the NC is still attached) or another translocation step needs to occur to move it to the P-site, thus freeing the A-site for Dom34. Further investigations have to elucidate the mechanism of ribosome recycling in 3'-to-5' mRNA decay. Third, the function of Ski7 needs to be evaluated. Since the GTPase domain is only needed for quality control (Araki et al., 2001), it seems likely that Ski7 primarily acts as an adaptor by binding to the Ski complex and the exosome in 3'-to-5' mRNA degradation. Due to our findings, it is most likely that Ski7 is not part of recognizing the target for NSD by binding to a stalled ribosome, but rather acts afterwards to possibly check Ski complex association to the ribosome, to signal the start of active mRNA threading by the Ski complex and/or to release it from the 80S. For this, the GTPase domain could transiently interact with the ribosome to signal any of these processes. It is intriguing to think that Ski7's GTPase domain might always be needed when 3'-to-5' degradation is started

on the ribosome and that two pathways exist, one degrading "free" mRNAs and one targeting mRNAs associated to ribosomes. Since NSD and secondary targets (5' target after endonucleolytic cleavage) in NGD are always involving a stalled ribosome and are exclusively relying on exosome-dependent degradation, it explains why for these pathways Ski7's GTPase domain was shown to be important. When looking at general mRNA turnover, however, 3'-to-5' degradation is only a minor pathway which could explain why a ribosome-associated population that also requires the Ski7 GTPase domain was overlooked in previous studies. Since Ski7 was proposed to be a pseudo GTPase that always resembles the GTP-bound active state (Kowalinski et al., 2015), GTP hydrolysis would not be important for this signaling. It remains to be answered what the exact role of Ski7 is in ribosome-associated co-translational mRNA degradation. Finally, the exact order of events needs to be investigated, since many of the proposed processes could work at several timepoints. So far, it seems only clear that Ski complex binding to ribosomes is the first step in initiating the pathway.

## 4.5 The role of ribosome-Ski complexes in general mRNA turnover

As already mentioned before, it is an interesting aspect whether the Ski complex only initiates 3'-to-5' mRNA degradation in quality control co-translationally or if this is also the case for general mRNA turnover. It seems likely that the Ski complex binds to the ribosome for mRNA quality control, targeting specifically ribosomes that are stalled on aberrant mRNAs via their 3' mRNA overhang. But is this also the case for general 3'-to-5' mRNA turnover? The fact that very little unbound Ski3 was detected in our polysome profile analysis hints that co-translational initiation of 3'-to-5' mRNA degradation might not only occur in quality control pathways, but also in general mRNA turnover. In addition, our targeted profiling suggests the involvement of ribosome-Ski complexes in on-going general 3'-to-5' mRNA decay (Fig. 3.17). We could not detect a specific enrichment of nonstop or no-go decay targets in our experiment. The shift of ribosomes towards the more 5' part of mRNAs indicates that these mRNAs are already degraded from the 3' end since our control showed an even distribution of ribosomes over the respective mRNAs. Additionally, analyzed mRNAs were enriched in non-optimal codons. Even though it is not entirely clear how these mRNAs are degraded, only few codon combinations seem to give rise to specific mRNA and protein quality control responses, whereas the majority seems to be targeted by general turnover pathways (Gamble et al., 2016; Letzring et al., 2010;

Presnyak et al., 2015). Thus, it is very likely that our ribosome-Ski complex structure is an intermediate step in general 3'-to-5' degradation, stabilized possibly by the lack of ATP in our buffers or because additional factors are not present. Notably, as mentioned above, it is possible that two separate pathways for general turnover exist where either non-translating or ribosome-associated mRNAs are targeted. This idea is encouraged when looking also at Xrn1-dependent 5'-to-3' degradation. It was shown that 5'-to-3' degradation can either happen in P-bodies or co-translationally on polysomes (Hu et al., 2009; Pelechano et al., 2015; Sheth et al., 2003). Thus, it would not be surprising to see a similar principle also for 3'-to-5' mRNA degradation.

Taken together, we present evidence that the Ski complex can link mRNA translation and degradation by binding to ribosomes which leads to threading of mRNAs into the helicase that are still associated. The length of the 3' mRNA overhang seems to dictate whether the Ski complex is recruited to the ribosome to initiate 3'-to-5' mRNA degradation, possibly by actively removing mRNA from the ribosome to channel it into the exosome. Since earlier studies could show that the human ortholog of Ski2 seems to colocalize with 40S subunits and 80S ribosomes in HeLa cells (Qu et al., 1998), it is very likely that the direct link we identified here might operate broadly in different mRNA decay pathways and different species.

## 4.6 eIF-5A – a so far unknown factor involved in quality control?

Originally, eIF-5A was identified as a factor helping to form the first peptide bond during translation and thus was initially characterized as an initiation factor (Glick and Ganoza, 1975). Following studies, however, made clear that eIF-5A's role was much more versatile than originally anticipated, making the term initiation factor somewhat misleading. These studies could show that eIF-5A's major function was rather not found in initiation, but in rescuing ribosomes, particularly those that were stalled on poly-proline stretches (Gutierrez et al., 2013). Further evidence was found that eIF-5A also has some additional function in peptide bond formation in general, giving rise to the thought that it has a primary role in promoting translation elongation (Saini et al., 2009). The fact that eIF-5A was present in all our ribosomal particles raised the question if it is also involved in quality control and initiation of mRNA degradation. Did we identify a yet another unanticipated role of eIF-5A in these processes?

Our analysis of the codon composition in A-, P- and E-site highlights that our purification does not specifically enrich initiation complexes with methionine in the P-site or poly-proline stalled ribosomes which argues in favor of eIF-5A being involved in other processes than rescuing poly-proline stalled ribosomes or initiation (Fig. 3.23A). The fact that in absence of cycloheximide eIF-5A was not detected by mass spectrometry in otherwise equally purified samples hints towards the notion, that cycloheximide binding to the E-site influences binding of eIF-5A. Our structural data reveals that while cycloheximide clashes with the CCA-end of an E-site tRNA, eIF-5A can accommodate while the antibiotic is bound (Fig. 3.23B). This finding suggests that eIF-5A can bind to ribosomes when the E-site is vacant, a state that is to be expected when translation elongation is slowed down/paused or translocation did not take place yet. In combination with newer findings that eIF-5A acts as a general promotor of elongation and peptide-bond formation that can alleviate stalling on many motifs and not only poly-proline tracts (Schuller et al., 2017), this argues in favor of a model where eIF-5A is recruited specifically to ribosomes that struggle during elongation by binding to an empty E-site. The fact that eIF-5A is one of the highest expressed proteins in yeast (approximately 274000 copies per cell; Ghaemmaghami et al., 2003) is in line with this model. Due to the high copy number in the cell, eIF-5A should always be available for binding and kinetics are in favor of accommodation to the E-site. Therefore, eIF-5A could recognize its targets by screening the E-site for tRNA presence to assist in peptide bond formation. The absence of eIF-5A from other purifications using cycloheximide, i.e. RNC preparations, might be explained by the very quick purification under mild conditions compared to these protocols. Since it is known that E-site tRNAs are removed by higher salt conditions during washing steps, it would not be surprising if also bound eIF-5A would be removed. The fact that more recent natively purified complexes from our lab also resulted in eIF-5A binding to the E-site substantiates this hypothesis.

## 4.7 The hypusine stabilizes tRNAs in P- and A-site to assist in peptide bond formation

It's been long known that translation elongation slow-down can occur when translating specific amino acids or on specific codons within an mRNA. Proline was identified to be a bad donor and acceptor during peptide bond formation due to its unusual geometry and that poly-proline attached to the P-site tRNA leads to destabilization of the tRNA and even peptidyl-tRNA drop-off (Doerfel et al., 2013; Johansson et al.,

2011; Muto and Ito, 2008; Pavlov et al., 2009; Wohlgemuth et al., 2008). Moreover, recent studies could identify several codon combinations that cause severe ribosome stalling (Gamble et al., 2016; Letzring et al., 2010). These codons often have been shown to contain a wobble base pair in the third position with the respective tRNA, leading to the idea that tRNA accommodation is slowed down and that the geometry in the PTC is not ideal for peptide bond formation because of this weaker interaction compared to a normal Watson-Crick base pair. Many of these stallings can be rescued by eIF-5A (Schuller et al., 2017), but how can this be achieved by a single factor? Several models were proposed with eIF-5A either being directly or indirectly involved in the peptide bond formation. Our structure argues in favor of eIF-5A being not directly involved in the bond formation process. The results discussed in this work show that the accommodation to the E-site allows the insertion of the $\beta$3-$\beta$4 loop containing the critical hypusine residue into a pocket that reaches towards the PTC of the ribosome. Thereby, the loop is stabilized by multiple hydrogen bond interactions and the hypusine at the tip contacts the CCA-end of the P-site tRNA (Fig. 3.21). Notably, this interaction is only possible because of the extended nature of the hypusine residue, explaining why this post-translational modification is critical to eIF-5A's function in elongation and rescue. Furthermore, a specific loop of uL16 might play an important role in eIF-5A's function (Fig. 3.22). In bacteria, the position of the uL16 loop is occupied by bL27 which in turn was shown to be involved in a proton wire that couples A-site tRNA binding to peptide bond formation (Polikanov et al., 2014). We identified that the uL16 loop is stabilized in the eIF-5A bound structure. This stabilization is achieved by a hydrogen bond network formed between the residues in the uL16 loop, the CCA-ends of both A-site and P-site tRNA and the hypusine residue of eIF-5A. We propose that the interaction of the hypusine residue with the P-site CCA-end and subsequent stabilization of the uL16 loop and the A-site tRNA allows proper peptide bond formation by stabilizing the geometry in the PTC. eIF-5A could act as a "repair factor" by idealizing the geometry and stabilizing the P-site tRNA in the PTC which would allow translation to be continued. This stabilization model would also explain why eIF-5A could stimulate translation elongation in general, since the CCA-end that is contacted by the hypusine is interchangeable between all tRNAs.

## 4.8 The structure of eIF-5A on the ribosome reveals differences to EF-P

When comparing eIF-5A with its prokaryotic homologue EF-P, several differences can be detected. While eIF-5A was identified to be important for multiple steps in translation as discussed above, EF-P has so far only been implicated in the rescue of poly-proline stalled ribosomes. This more specific function might also be reflected in the structural data. Where DI of EF-P shows multiple contacts with the P-site tRNA (Blaha et al., 2009), basically recognizing whether a prolyl-tRNA is accommodated or not, eIF-5A does not show any of these interactions and DI is rather moved away from the P-tRNA (Fig. 3.20). This could explain why eIF-5A acts on a broad spectrum of tRNAs and is not only functioning when prolyl-tRNA is bound to the P-site. The eukaryote-specific NTE of eIF-5A might hereby be the reason why DI is shifted away from the P-site when compared to archaeal IF-5A or EF-P. The interaction of the NTE with uL1 and eL42 could induce a shift that is transferred to DI and the $\beta$3-$\beta$4 loop. This shift would of course not be seen in EF-P where no NTE is present. In contrast, the function of the prokaryote-specific DIII is not clear as of now and our structure does not contain any insights into its role in prokaryotic ribosome rescue.

In summary, our structure of eIF-5A bound to the ribosome reveals how eIF-5A can rescue stalled ribosomes and promote translation elongation. The critical hypusine residue contacts the CCA-end of the P-site tRNA, thereby stabilizing it. This leads to the stabilization of a loop in uL16 which in turn contacts the A-tRNA CCA-end. This chain of events stabilizes the overall geometry in the PTC, allowing for successful peptide bond formation. Furthermore, eIF-5A seems to bind to ribosomes with an empty E-site, which is a hallmark of ribosomes that are slowed down or paused in translocation and translation elongation. Thus, eIF-5A selects its target by scanning the E-site for tRNA occupancy. This mechanism would also explain the recent findings that eIF-5A might act much more broadly in promoting translation elongation (Schuller et al., 2017), specifically for "slow" codons.

# 5 Outlook

The findings presented in this thesis are the first structural insight into how mRNA translation and 3‘-to-5‘ degradation are directly coupled, laying the groundwork for following research in this field. Yet, many open questions remain to be answered to fully understand this pathway.

First, the exact role of the Ski complex bound to the ribosome remains to be investigated, with particular focus on its processivity and possible function in extracting mRNAs from the ribosome. Concomitantly, Ski7’s role in quality control and ribosome-associated mRNA decay needs to be revisited. In this regard, an interesting target for structural studies would be the proposed "super complex" formed of a ribosome-Ski complex with an exosome-Ski7 complex. First insights of the interactions of Ski7 with the exosome could be gained recently (Kowalinski et al., 2015), but it is not clear how this assembly contacts the ribosome-bound Ski complex as of now.

Second, further research should be focusing on whether the Ski complex binds ribosomes also for general mRNA turnover. Our profiling data suggests that the natively purified complexes are indeed intermediates of common mRNA decay, thus arguing that a ribosome-associated degradation pathway might exist. Insights into Ski7’s exact function in either quality control or turnover and more in-depth profiling analysis in different genetic strain backgrounds could shed some light onto the subject.

Third, an exact order of events for ribosome-associated mRNA degradation must be established. Here, it needs to be investigated what happens after Ski7 and the exosome interact with the Ski complex and how ribosome recycling occurs in this pathway. It is likely that Dom34 and ABCE1 are involved in this process, however it is currently unknown what their exact target would be and at what point exosome-Ski7 binding and ribosome splitting is happening.

Finally, the existence of ribosome-Ski complexes in other eukaryotic organisms needs to be investigated. Both the exosome and the Ski complex are conserved from

yeast to human (Makino et al., 2013; Halbach et al., 2013). Earlier findings already showed that the human orthologue of Ski2 seems to associate with 40S subunits and 80S ribosomes (Qu et al., 1998). Since 3‘-to-5‘ degradation and quality control are common to all eukaryotic cells, purifying similar complexes from higher eukaryotic organisms would yield answers about the conservation of these pathways.

A recently published study on eIF-5A bound to a eukaryotic ribosome confirmed our findings of the overall position of the factor and its contact to the CCA-end of the P-site tRNA (Melnikov et al., 2016). With the newer reports in mind that eIF-5A seems not to be limited to rescue poly-proline stalled ribosomes, but rather alleviates many stalling events in the cell (Schuller et al., 2017), it would be interesting to investigate eIF-5A’s target recognition further. Our data suggests that scanning of an empty E-site might dictate whether eIF-5A is binding or not and could thus turn the factor into a "timing sensor" for translation that detects slowed down ribosomes. Another factor known to be targeting slow ribosomes is Dhh1, therefore insights into possible interactions between these factors could elucidate the topic. Notably, both proteins would be expected to compete for binding to the E-site (or the ribosome *per se*) since eIF-5A acts as a rescue factor whereas Dhh1 was implicated with the degradation of mRNAs (Radhakrishnan et al., 2016). Therefore, it is possible that these factors could determine the fate of the ribosome-associated mRNA. Since most observed stalling events were happening on specific codon combinations and poly-basic stallers, further research should be conducted towards the exact mechanism of stalling for these mRNAs. With high-resolution cryo-EM, it should be possible to detect any changes in the PTC or tunnel interactions that cause stalling in these cases.

# Appendix

TABLE A.1: Mass spectrometry analysis of the native ribosome-Ski complex pullout.

| | | Accession | Score | Mass | Matches | sign. | Signals | sign. | emPAI |
|---|---|---|---|---|---|---|---|---|---|
| 1 | 1 | SKI2_YEAST | 4032 | 146651 | 137 | 137 | 48 | 48 | 3,47 |
| 2 | 1 | SKI3_YEAST | 4032 | 164707 | 131 | 131 | 47 | 47 | 2,31 |
| 3 | 1 | GBLP_YEAST | 1140 | 34898 | 37 | 37 | 15 | 15 | 4,13 |
| 4 | 1 | HSP76_YEAST | 1106 | 66668 | 31 | 31 | 17 | 17 | 1,49 |
| 4 | 2 | HSP75_YEAST | 1095 | 66732 | 30 | 30 | 17 | 17 | 1,49 |
| 5 | 1 | SSZ1_YEAST | 996 | 58316 | 25 | 25 | 13 | 13 | 1,28 |
| 6 | 1 | SKI8_YEAST | 920 | 44717 | 28 | 28 | 9 | 9 | 1,52 |
| 7 | 1 | PYR1_YEAST | 916 | 246198 | 29 | 29 | 17 | 17 | 0,25 |
| 8 | 1 | RL8B_YEAST | 861 | 28151 | 32 | 32 | 12 | 12 | 4,97 |
| 8 | 2 | RL8A_YEAST | 728 | 28164 | 25 | 25 | 10 | 10 | 2,82 |
| 9 | 1 | RS3_YEAST | 842 | 26543 | 25 | 25 | 12 | 12 | 4,25 |
| 10 | 1 | RS6A_YEAST | 828 | 27037 | 26 | 26 | 12 | 12 | 3,52 |
| 11 | 1 | RS3A1_YEAS1 | 825 | 28783 | 29 | 29 | 12 | 12 | 4,18 |
| 11 | 2 | RS3A2_YEAS1 | 776 | 28852 | 28 | 28 | 12 | 12 | 4,14 |
| 12 | 1 | RL4A_YEAST | 754 | 39125 | 30 | 30 | 13 | 13 | 2,39 |
| 13 | 1 | IMDH3_YEAST | 735 | 56948 | 17 | 17 | 6 | 6 | 0,57 |
| 14 | 1 | RS5_YEAST | 734 | 25080 | 19 | 19 | 9 | 9 | 2,49 |
| 15 | 1 | RL19A_YEAST | 732 | 21691 | 23 | 23 | 7 | 7 | 3,23 |
| 16 | 1 | RL7A_YEAST | 703 | 27621 | 25 | 25 | 11 | 11 | 2,92 |
| 17 | 1 | EF1A_YEAST | 652 | 50400 | 29 | 29 | 12 | 12 | 1,59 |
| 18 | 1 | RS20_YEAST | 638 | 13899 | 16 | 16 | 6 | 6 | 3,66 |
| 19 | 1 | RS8A_YEAST | 628 | 22590 | 16 | 16 | 6 | 6 | 1,63 |
| 20 | 1 | RS14A_YEAST | 619 | 14585 | 21 | 21 | 10 | 10 | 9,11 |
| 21 | 1 | C1TC_YEAST | 590 | 102540 | 19 | 19 | 12 | 12 | 0,46 |
| 22 | 1 | RL23A_YEAST | 581 | 14578 | 16 | 16 | 4 | 4 | 3,36 |

| | | | | | | | | | |
|---|---|---|---|---|---|---|---|---|---|
| 23 | 1 | RS4A_YEAST | 561 | 29449 | 24 | 24 | 14 | 14 | 4,56 |
| 24 | 1 | XRN1_YEAST | 558 | 175692 | 20 | 20 | 11 | 11 | 0,25 |
| 25 | 1 | RL20A_YEAST | 539 | 20424 | 16 | 16 | 6 | 6 | 1,91 |
| 26 | 1 | RS17A_YEAST | 538 | 15836 | 17 | 17 | 6 | 6 | 2,88 |
| 27 | 1 | EF2_YEAST | 534 | 93686 | 11 | 11 | 7 | 7 | 0,27 |
| 28 | 1 | RL16A_YEAST | 530 | 22187 | 14 | 14 | 5 | 5 | 1,33 |
| 28 | 2 | RL16B_YEAST | 370 | 22235 | 12 | 12 | 6 | 6 | 1,33 |
| 29 | 1 | RLA0_YEAST | 514 | 33696 | 17 | 17 | 8 | 8 | 1,33 |
| 30 | 1 | RS9A_YEAST | 504 | 22429 | 12 | 12 | 5 | 5 | 1,31 |
| 30 | 2 | RS9B_YEAST | 396 | 22285 | 12 | 12 | 5 | 5 | 1,32 |
| 31 | 1 | SC160_YEAST | 499 | 134955 | 18 | 18 | 11 | 11 | 0,3 |
| 32 | 1 | ZUO1_YEAST | 489 | 49047 | 13 | 13 | 9 | 9 | 0,8 |
| 33 | 1 | CLU_YEAST | 481 | 145304 | 15 | 15 | 8 | 8 | 0,22 |
| 34 | 1 | K6PF1_YEAST | 466 | 108587 | 10 | 10 | 6 | 6 | 0,2 |
| 35 | 1 | RL3_YEAST | 460 | 43844 | 12 | 12 | 5 | 5 | 0,66 |
| 36 | 1 | RL35A_YEAST | 459 | 13958 | 16 | 16 | 5 | 5 | 2,7 |
| 37 | 1 | RLI1_YEAST | 458 | 69095 | 10 | 10 | 5 | 5 | 0,26 |
| 38 | 1 | RL30_YEAST | 457 | 11408 | 13 | 13 | 6 | 6 | 5,32 |
| 39 | 1 | RL1A_YEAST | 449 | 24698 | 13 | 13 | 7 | 7 | 1,75 |
| 40 | 1 | RS12_YEAST | 447 | 15462 | 14 | 14 | 7 | 7 | 3,02 |
| 41 | 1 | RL12A_YEAST | 442 | 17869 | 15 | 15 | 5 | 5 | 1,82 |
| 42 | 1 | GLYM_YEAST | 440 | 53881 | 8 | 8 | 4 | 4 | 0,27 |
| 43 | 1 | RL36A_YEAST | 438 | 11117 | 13 | 13 | 5 | 5 | 4,07 |
| 44 | 1 | RL25_YEAST | 434 | 15748 | 11 | 11 | 4 | 4 | 1,18 |
| 45 | 1 | RL13B_YEAST | 433 | 22511 | 19 | 19 | 9 | 9 | 3 |
| 45 | 2 | RL13A_YEAST | 332 | 22540 | 13 | 13 | 9 | 9 | 2,48 |
| 46 | 1 | RS7B_YEAST | 431 | 21621 | 12 | 12 | 5 | 5 | 1,37 |
| 46 | 2 | RS7A_YEAST | 271 | 21609 | 12 | 12 | 5 | 5 | 1,74 |
| 47 | 1 | RS2_YEAST | 412 | 27490 | 14 | 14 | 6 | 6 | 1,23 |
| 48 | 1 | RS15_YEAST | 404 | 15992 | 14 | 14 | 4 | 4 | 4,65 |
| 49 | 1 | RL10_YEAST | 395 | 25573 | 21 | 21 | 7 | 7 | 1,67 |
| 50 | 1 | RL14A_YEAST | 394 | 15215 | 12 | 12 | 4 | 4 | 1,74 |
| 50 | 2 | RL14B_YEAST | 360 | 15201 | 11 | 11 | 4 | 4 | 1,74 |
| 51 | 1 | RS13_YEAST | 393 | 17018 | 10 | 10 | 4 | 4 | 1,07 |
| 52 | 1 | RS19A_YEAST | 392 | 15907 | 14 | 14 | 6 | 6 | 2,2 |
| 53 | 1 | K6PF2_YEAST | 375 | 105179 | 7 | 7 | 4 | 4 | 0,13 |

| | | | | | | | | | |
|---|---|---|---|---|---|---|---|---|---|
| 54 | 1 | RL5_YEAST | 375 | 33751 | 13 | 13 | 5 | 5 | 0,76 |
| 55 | 1 | RL15A_YEAST | 352 | 24464 | 13 | 13 | 5 | 5 | 1,16 |
| 56 | 1 | RRP44_YEAST | 344 | 114491 | 10 | 10 | 6 | 6 | 0,18 |
| 57 | 1 | RSSA1_YEAS1 | 343 | 28064 | 13 | 13 | 6 | 6 | 1,45 |
| 58 | 1 | HSC82_YEAST | 337 | 80850 | 6 | 6 | 4 | 4 | 0,17 |
| 59 | 1 | RS22A_YEAST | 336 | 14674 | 9 | 9 | 4 | 4 | 1,31 |
| 60 | 1 | RS23A_YEAST | 318 | 16142 | 5 | 5 | 3 | 3 | 0,77 |
| 61 | 1 | HSP72_YEAST | 316 | 69599 | 11 | 11 | 6 | 6 | 0,38 |
| 62 | 1 | RL17B_YEAST | 313 | 20539 | 7 | 7 | 3 | 3 | 0,58 |
| 62 | 2 | RL17A_YEAST | 304 | 20537 | 7 | 7 | 3 | 3 | 0,58 |
| 63 | 1 | IF4F1_YEAST | 309 | 107264 | 10 | 10 | 6 | 6 | 0,2 |
| 64 | 1 | RL9A_YEAST | 302 | 21613 | 9 | 9 | 4 | 4 | 1,06 |
| 64 | 2 | RL9B_YEAST | 295 | 21701 | 8 | 8 | 4 | 4 | 0,77 |
| 65 | 1 | CSL4_YEAST | 298 | 31849 | 6 | 6 | 3 | 3 | 0,35 |
| 66 | 1 | RS24A_YEAST | 297 | 15319 | 15 | 15 | 7 | 7 | 3,96 |
| 67 | 1 | NAT1_YEAST | 296 | 99299 | 9 | 9 | 6 | 6 | 0,21 |
| 68 | 1 | MPG1_YEAST | 288 | 39712 | 9 | 9 | 6 | 6 | 0,62 |
| 69 | 1 | RS18A_YEAST | 287 | 17084 | 13 | 13 | 5 | 5 | 1,95 |
| 70 | 1 | RL2A_YEAST | 286 | 27392 | 11 | 11 | 6 | 6 | 1,23 |
| 71 | 1 | RS16A_YEAST | 282 | 15838 | 8 | 8 | 4 | 4 | 1,17 |
| 72 | 1 | RRP5_YEAST | 279 | 193700 | 8 | 8 | 5 | 5 | 0,09 |
| 73 | 1 | RL31A_YEAST | 279 | 12945 | 13 | 13 | 6 | 6 | 5,49 |
| 74 | 1 | RL33A_YEAST | 277 | 12147 | 9 | 9 | 4 | 4 | 1,72 |
| 74 | 2 | RL33B_YEAST | 102 | 12161 | 5 | 5 | 3 | 3 | 1,1 |
| 75 | 1 | RL26A_YEAST | 274 | 14225 | 10 | 10 | 5 | 5 | 1,93 |
| 76 | 1 | ERF1_YEAST | 258 | 49203 | 8 | 8 | 4 | 4 | 0,3 |
| 77 | 1 | RLA4_YEAST | 255 | 11043 | 6 | 6 | 4 | 4 | 1,98 |
| 78 | 1 | RL27A_YEAST | 254 | 15522 | 9 | 9 | 4 | 4 | 1,2 |
| 79 | 1 | RLA1_YEAST | 253 | 10901 | 4 | 4 | 1 | 1 | 0,74 |
| 80 | 1 | RL11A_YEAST | 251 | 19764 | 7 | 7 | 3 | 3 | 0,6 |
| 81 | 1 | PDC1_YEAST | 251 | 61685 | 7 | 7 | 4 | 4 | 0,3 |
| 82 | 1 | BFR1_YEAST | 247 | 54606 | 9 | 9 | 6 | 6 | 0,42 |
| 83 | 1 | RL24B_YEAST | 245 | 17537 | 8 | 8 | 3 | 3 | 1,02 |
| 84 | 1 | RL6A_YEAST | 239 | 19949 | 6 | 6 | 4 | 4 | 0,86 |
| 84 | 2 | RL6B_YEAST | 233 | 19974 | 5 | 5 | 3 | 3 | 0,59 |
| 85 | 1 | PABP_YEAST | 233 | 64475 | 8 | 8 | 5 | 5 | 0,28 |

| | | | | | | | | | |
|---|---|---|---|---|---|---|---|---|---|
| 86 | 1 | IF2G_YEAST | 223 | 58400 | 6 | 6 | 3 | 3 | 0,18 |
| 87 | 1 | RL38_YEAST | 222 | 8821 | 8 | 8 | 4 | 4 | 2,83 |
| 88 | 1 | SKI7_YEAST | 222 | 85183 | 7 | 7 | 3 | 3 | 0,16 |
| 89 | 1 | RLA2_YEAST | 219 | 10739 | 5 | 5 | 3 | 3 | 1,3 |
| 90 | 1 | ARB1_YEAST | 210 | 68506 | 6 | 6 | 3 | 3 | 0,15 |
| 91 | 1 | RL22A_YEAST | 209 | 13685 | 5 | 5 | 3 | 3 | 1,44 |
| 91 | 2 | RL22B_YEAST | 163 | 13818 | 4 | 4 | 3 | 3 | 0,94 |
| 92 | 1 | RPA2_YEAST | 202 | 136682 | 5 | 5 | 3 | 3 | 0,07 |
| 93 | 1 | TY1AB_YEASX | 199 | 199337 | 8 | 8 | 5 | 5 | 0,08 |
| 94 | 1 | DED1_YEAS7 | 199 | 65741 | 5 | 5 | 4 | 4 | 0,22 |
| 95 | 1 | RPA1_YEAST | 197 | 187683 | 7 | 7 | 5 | 5 | 0,09 |
| 96 | 1 | RRP4_YEAST | 195 | 39574 | 6 | 6 | 3 | 3 | 0,27 |
| 97 | 1 | EIF3C_YEAS7 | 195 | 93391 | 3 | 3 | 2 | 2 | 0,07 |
| 98 | 1 | RL18A_YEAST | 194 | 20608 | 6 | 6 | 3 | 3 | 0,57 |
| 99 | 1 | NOP3_YEAST | 190 | 45437 | 4 | 4 | 2 | 2 | 0,15 |
| 100 | 1 | STM1_YEAST | 187 | 29977 | 4 | 4 | 3 | 3 | 0,37 |
| 101 | 1 | RS27B_YEAST | 184 | 9145 | 7 | 7 | 3 | 3 | 2,66 |
| 102 | 1 | G3P1_YEAST | 183 | 35842 | 4 | 4 | 3 | 3 | 0,3 |
| 103 | 1 | METK1_YEAST | 177 | 42077 | 3 | 3 | 2 | 2 | 0,16 |
| 104 | 1 | NOP58_YEAS7 | 173 | 56978 | 4 | 4 | 2 | 2 | 0,12 |
| 105 | 1 | ENO2_YEAST | 169 | 46942 | 4 | 4 | 2 | 2 | 0,15 |
| 106 | 1 | URA7_YEAST | 167 | 65125 | 4 | 4 | 3 | 3 | 0,16 |
| 107 | 1 | EIF2A_YEAST | 165 | 71774 | 3 | 3 | 3 | 3 | 0,14 |
| 108 | 1 | RL21A_YEAST | 164 | 18288 | 7 | 7 | 4 | 4 | 0,97 |
| 109 | 1 | SRO9_YEAST | 155 | 48031 | 4 | 4 | 3 | 3 | 0,22 |
| 110 | 1 | NEW1_YEAST | 155 | 134932 | 5 | 5 | 4 | 4 | 0,1 |
| 111 | 1 | RRP46_YEAST | 151 | 24848 | 5 | 5 | 3 | 3 | 0,46 |
| 112 | 1 | RS25A_YEAST | 145 | 12032 | 5 | 5 | 3 | 3 | 1,74 |
| 113 | 1 | RL43A_YEAST | 144 | 10369 | 4 | 4 | 2 | 2 | 0,78 |
| 114 | 1 | RLA3_YEAST | 138 | 10661 | 2 | 2 | 1 | 1 | 0,32 |
| 115 | 1 | RL32_YEAST | 134 | 14762 | 4 | 4 | 2 | 2 | 0,51 |
| 116 | 1 | RS28A_YEAST | 131 | 7587 | 3 | 3 | 2 | 2 | 1,16 |
| 117 | 1 | RRP42_YEAST | 129 | 29094 | 2 | 2 | 1 | 1 | 0,11 |
| 118 | 1 | SUB2_YEAST | 126 | 50620 | 2 | 2 | 1 | 1 | 0,07 |
| 119 | 1 | RPAB4_YEAST | 124 | 7939 | 2 | 2 | 1 | 1 | 0,44 |
| 120 | 1 | TCPQ_YEAST | 123 | 61965 | 4 | 4 | 2 | 2 | 0,11 |

| | | | | | | | | | |
|---|---|---|---|---|---|---|---|---|---|
| 121 | 1 | IF2B_YEAST | 123 | 31840 | 2 | 2 | 1 | 1 | 0,1 |
| 122 | 1 | RL28_YEAST | 121 | 16711 | 2 | 2 | 1 | 1 | 0,2 |
| 123 | 1 | ADH1_YEAST | 119 | 37282 | 2 | 2 | 1 | 1 | 0,09 |
| 124 | 1 | RBG1_YEAST | 116 | 40904 | 2 | 2 | 1 | 1 | 0,08 |
| 125 | 1 | RPAC1_YEAST | 116 | 37948 | 3 | 3 | 2 | 2 | 0,18 |
| 126 | 1 | RS21B_YEAST | 113 | 9811 | 4 | 4 | 3 | 3 | 1,49 |
| 127 | 1 | NUG1_YEAST | 112 | 57787 | 3 | 3 | 2 | 2 | 0,12 |
| 128 | 1 | FBRL_YEAST | 109 | 34615 | 2 | 2 | 1 | 1 | 0,1 |
| 129 | 1 | RRP45_YEAST | 109 | 34510 | 5 | 5 | 3 | 3 | 0,32 |
| 130 | 1 | NCBP1_YEAST | 109 | 100183 | 2 | 2 | 1 | 1 | 0,03 |
| 131 | 1 | RS29B_YEAST | 108 | 6951 | 4 | 4 | 2 | 2 | 1,28 |
| 132 | 1 | IF4A_YEAS7 | 107 | 44840 | 3 | 3 | 2 | 2 | 0,15 |
| 133 | 1 | KPYK1_YEAST | 102 | 54909 | 6 | 6 | 5 | 5 | 0,34 |
| 134 | 1 | CBF5_YEAST | 102 | 55184 | 3 | 3 | 2 | 2 | 0,12 |
| 135 | 1 | SNU13_YEAST | 99 | 13731 | 2 | 2 | 1 | 1 | 0,25 |
| 136 | 1 | RS30A_YEAST | 96 | 7114 | 4 | 4 | 2 | 2 | 1,25 |
| 137 | 1 | RS11A_YEAST | 94 | 17852 | 4 | 4 | 2 | 2 | 0,41 |
| 138 | 1 | SEC16_YEAST | 92 | 241719 | 2 | 2 | 1 | 1 | 0,01 |
| 139 | 1 | RS26A_YEAST | 92 | 13724 | 4 | 4 | 2 | 2 | 0,56 |
| 140 | 1 | EIF3A_YEAST | 92 | 110333 | 5 | 5 | 3 | 3 | 0,09 |
| 141 | 1 | C1TM_YEAST | 92 | 106607 | 5 | 5 | 4 | 4 | 0,13 |
| 142 | 1 | ILVB_YEAST | 91 | 75061 | 2 | 2 | 1 | 1 | 0,04 |
| 143 | 1 | PPB_YEAST | 91 | 63136 | 2 | 2 | 1 | 1 | 0,05 |
| 144 | 1 | GPP1_YEAST | 89 | 28100 | 2 | 2 | 1 | 1 | 0,12 |
| 145 | 1 | PMG1_YEAST | 86 | 27592 | 2 | 2 | 1 | 1 | 0,12 |
| 146 | 1 | NSR1_YEAST | 85 | 44566 | 3 | 3 | 2 | 2 | 0,15 |
| 147 | 1 | IF4E_YEAST | 84 | 24239 | 2 | 2 | 2 | 2 | 0,3 |
| 148 | 1 | TBB_YEAST | 84 | 51233 | 2 | 2 | 1 | 1 | 0,06 |
| 149 | 1 | IF2P_YEAST | 83 | 112599 | 2 | 2 | 1 | 1 | 0,03 |
| 150 | 1 | NOP56_YEAST | 78 | 57057 | 2 | 2 | 1 | 1 | 0,06 |
| 151 | 1 | RS10A_YEAST | 75 | 12732 | 4 | 4 | 2 | 2 | 1,04 |
| 152 | 1 | VATB_YEAST | 75 | 57770 | 2 | 2 | 1 | 1 | 0,06 |
| 153 | 1 | RRP41_YEAST | 73 | 27543 | 3 | 3 | 2 | 2 | 0,26 |
| 154 | 1 | RRP40_YEAST | 73 | 26939 | 2 | 2 | 1 | 1 | 0,12 |
| 155 | 1 | EF3A_YEAST | 68 | 116727 | 2 | 2 | 2 | 2 | 0,06 |
| 156 | 1 | SEC13_YEAST | 68 | 33194 | 2 | 2 | 1 | 1 | 0,1 |

| | | | | | | | | | |
|---|---|---|---|---|---|---|---|---|---|
| 157 | 1 | ERV46_YEAST | 66 | 46776 | 2 | 2 | 1 | 1 | 0,07 |
| 158 | 1 | KRE33_YEAST | 64 | 119615 | 2 | 2 | 1 | 1 | 0,03 |
| 159 | 1 | BRX1_YEAST | 64 | 33625 | 1 | 1 | 1 | 1 | 0,1 |
| 160 | 1 | VPH1_YEAST | 64 | 95866 | 2 | 2 | 1 | 1 | 0,03 |
| 161 | 1 | RL34A_YEAST | 63 | 13859 | 2 | 2 | 1 | 1 | 0,25 |
| 162 | 1 | OLA1_YEAST | 63 | 44488 | 2 | 2 | 1 | 1 | 0,07 |
| 163 | 1 | AHA1_YEAST | 61 | 39582 | 1 | 1 | 1 | 1 | 0,08 |
| 164 | 1 | TM108_YEAST | 58 | 108339 | 1 | 1 | 1 | 1 | 0,03 |
| 165 | 1 | LCF4_YEAST | 56 | 77902 | 2 | 2 | 1 | 1 | 0,04 |
| 166 | 1 | TMA46_YEAST | 54 | 39831 | 2 | 2 | 1 | 1 | 0,08 |
| 167 | 1 | EIF3B_YEAS7 | 51 | 88616 | 2 | 2 | 1 | 1 | 0,04 |
| 168 | 1 | IF5A1_YEAST | 50 | 17217 | 2 | 2 | 1 | 1 | 0,2 |
| 169 | 1 | ILV6_YEAST | 49 | 34308 | 2 | 2 | 1 | 1 | 0,1 |
| 170 | 1 | ATN1_YEAST | 49 | 121193 | 1 | 1 | 1 | 1 | 0,03 |
| 171 | 1 | HAS1_YEAST | 49 | 56967 | 2 | 2 | 1 | 1 | 0,06 |
| 172 | 1 | YRA1_YEAST | 47 | 24940 | 2 | 2 | 1 | 1 | 0,13 |
| 173 | 1 | SC61G_YEAST | 44 | 8995 | 2 | 2 | 1 | 1 | 0,39 |
| 174 | 1 | RRP43_YEAST | 44 | 44269 | 1 | 1 | 1 | 1 | 0,07 |
| 175 | 1 | FAS1_YEAST | 42 | 229403 | 1 | 1 | 1 | 1 | 0,01 |
| 176 | 1 | VPS30_YEAST | 41 | 63564 | 2 | 2 | 1 | 1 | 0,05 |
| 177 | 1 | YKC3_YEAST | 40 | 32388 | 1 | 1 | 1 | 1 | 0,1 |
| 178 | 1 | AMPM1_YEAST | 39 | 44144 | 1 | 1 | 1 | 1 | 0,07 |
| 179 | 1 | SSD1_YEAST | 36 | 140211 | 1 | 1 | 1 | 1 | 0,02 |
| 180 | 1 | NACB1_YEAS7 | 35 | 17010 | 1 | 1 | 1 | 1 | 0,2 |
| 181 | 1 | YHI0_YEAST | 34 | 77851 | 1 | 1 | 1 | 1 | 0,04 |
| 182 | 1 | RIR1_YEAST | 33 | 100296 | 1 | 1 | 1 | 1 | 0,03 |
| 183 | 1 | TBA3_YEAST | 33 | 50290 | 1 | 1 | 1 | 1 | 0,07 |
| 184 | 1 | EF1G2_YEAST | 31 | 46605 | 1 | 1 | 1 | 1 | 0,07 |
| 185 | 1 | MBF1_YEAST | 31 | 16394 | 1 | 1 | 1 | 1 | 0,21 |

TABLE A.2: Model and refinement statistics for ribosome-Ski complex dataset.

| **DATA COLLECTION** | **Dataset 1** | **Dataset 2** |
|---|---|---|
| Particles | 175.038 | 258.426 |
| Pixel size [Å] | 1.084 | 1.084 |
| Defocus range [$\mu$m] | 0.7-2.5 | 0.7-4.0 |
| Voltage [keV] | 300 | 300 |
| Electron dose [$e^{-}$ Å$^{-2}$] | 28 | 28 |

| **MODEL REFINEMENT** | **40S-Ski** | **60S** |
|---|---|---|
| **Model composition** | | |
| Non-hydrogen atoms | 103.043 | 124.555 |
| Protein residues | 7.958 | 6.513 |
| RNA bases | 1.954 | 3.444 |
| **Refinement** | | |
| Resolution for refinement [Å] | 4.2 | 3.8 |
| Map sharpening B-factor [Å$^2$] | -115.3 | -115.3 |
| Average B-factor [Å$^2$] | 079.6 | 137.5 |
| $FSC_{average}$ | 0.79 | 0.83 |
| **R.m.s. deviations** | | |
| Bond lenght [Å] | 0.0070 | 0.0078 |
| Bond angles [°] | 1.13 | 1.24 |

| **VALIDATION** | **40S-Ski** | **60S** | **80S** |
|---|---|---|---|
| Molprobity score | 2.21 | 2.23 | 2.30 |
| Clashscore, all atoms | 3.07 | 3.37 | 4.08 |
| Good rotamers [%] | 96.16 | 95.84 | 96.01 |
| **Ramachandran Plot** | | | |
| Favored [%] | 84.29 | 86.65 | 85.35 |
| Outliers [%] | 3.15 | 2.69 | 2.94 |
| **Validation (RNA)** | | | |
| Good puckers [%] | 94.4 | 94.5 | 94.4 |
| Good backbone [%] | 58.7 | 66.4 | 63.6 |

# List of Abbreviations

| | |
|---|---|
| **$\mu$g** | Microgram |
| **$\mu$l** | Microliter |
| **$\mu$M** | Micromolar |
| **3D** | Three-dimensional |
| **aa-tRNA** | Aminoacyl-tRNA |
| **A-site** | Aminoacyl-site |
| **ATP** | Adenosine triphosphate |
| **CAT tail** | C-terminal Ala/Thr tail |
| **CC** | Cross-correlation |
| **CTF** | Contrast transfer function |
| **cryo-EM** | Cryo-electron microscopy |
| **DC** | Decoding center |
| **DHS** | Deoxhypusine synthetase |
| **DOHH** | Deoxyhypusine hydroxylase |
| ***D. melanogaster*** | Drosophila melanogaster |
| **DNA** | Deoxyribonucleic acid |
| **DTT** | Dithiothreitol |
| ***E. coli*** | Escherichia coli |
| **EF** | Elongation factor |
| **EJC** | Exon-junction complex |
| **ES** | Expansion segment |
| **E-site** | Exit-site |
| **FSC** | Fourier shell correlation |
| **GTP** | Guanosine triphosphate |
| ***H. sapiens*** | Homo sapiens |

| | |
|---|---|
| **HEAT** | Huntingtin, elongation factor 3, protein phosphatase 2A, Tor1 |
| **IF** | Initiation factor |
| **kDa** | Kilodalton |
| **LSU** | Large ribosomal subunit |
| **MDa** | Megadalton |
| **mg** | Milligram |
| **mM** | Millimolar |
| **mRNA** | Messenger RNA |
| **NC** | Nascent chain |
| **NGD** | No-go decay |
| **NMD** | Nonsense-mediated decay |
| **NSD** | Nonstop decay |
| **OD** | Optical density |
| **ORF** | Open reading frame |
| **PAGE** | Polyacrylamide gel electrophoresis |
| **PAP** | Poly-A polymerase |
| **PDB** | Protein data bank |
| **pre-rRNA** | precursor rRNA |
| **P-site** | Peptidyl-site |
| **PTC** | Peptidyl transferase center |
| **RF** | Release factor |
| **rpm** | Revolutions per minute |
| **RNP** | Ribonucleoprotein |
| **r-proteins** | Ribosomal proteins |
| **RQC** | Ribosome quality control |
| **rRNA** | Ribosomal RNA |
| **S (unit)** | Svedberg unit |
| ***S. cerevisiae*** | Saccharomyces cerevisiae |
| **SD** | Shine-Dalgarno |
| **SDS** | Sodium dodecyl sulfate |
| **snRNA** | small non-coding RNA |
| **SSU** | Small ribosomal subunit |
| **TAP** | Tandem affinity purification |
| **TC** | Ternary complex |
| **TE** | Tunnel exit |
| **TPR** | Tetratricopeptide repeat |

| | |
|---|---|
| **tRNA** | Transfer RNA |
| **Ub** | Ubiquitin |
| **UBL** | Ubiquitin-Like |
| **UPS** | Ubiquitin-proteasome system |
| **UTR** | Untranslated region |
| **WT** | Wild type |
| **YPD** | Yeast extract peptone dextrose |
| **YPG** | Yeast extract peptone glycerol |

# References

Adams, P. D. et al. (2010). “PHENIX: a comprehensive Python-based system for macromolecular structure solution.” In: *Acta Crystallographica. Section D, Biological crystallography* 66, pp. 213–221.

Agirrezabala, X. and J. Frank (2009). “Elongation in translation as a dynamic interaction among the ribosome, tRNA, and elongation factors EF-G and EF-Tu.” In: *Quarterly reviews of biophysics* 42, pp. 159–200.

Ahlberg, J et al. (1982). “Uptake and degradation of proteins by isolated rat liver lysosomes. Suggestion of a microautophagic pathway of proteolysis.” In: *Laboratory investigation; a journal of technical methods and pathology* 47, pp. 523–532.

Akashi, H (1994). “Synonymous codon usage in Drosophila melanogaster: Natural selection and translational accuracy”. In: *Genetics* 136, pp. 927–935.

Alexopoulos, J. A. et al. (2012). “ClpP: A structurally dynamic protease regulated by AAA+ proteins”. In: *Journal of Structural Biology* 179.2, pp. 202–210.

Alic, N. et al. (2007). “Selectivity and proofreading both contribute significantly to the fidelity of RNA polymerase III transcription”. In: *Proceedings of the National Academy of Sciences* 104, pp. 10400–10405.

Amm, I. et al. (2014). “Protein quality control and elimination of protein waste: The role of the ubiquitin-proteasome system”. In: *Biochimica et Biophysica Acta - Molecular Cell Research* 1843, pp. 182–196.

Amrani, N. et al. (2004). “A faux 3’-UTR promotes aberrant termination and triggers nonsense-mediated mRNA decay.” In: *Nature* 432, pp. 112–118.

Amunts, A. et al. (2014). “Structure of the Yeast Mitochondrial Large Ribosomal Subunit”. In: *Science* 343, pp. 1485–1489.

Anderson, J. S. J. and R. P. Parker (1998). “The 3’ to 5’ degradation of yeast mRNAs is a general mechanism for mRNA turnover that requires the SK12 DEVH box protein and 3’ to 5’ exonucleases of the exosome complex”. In: *EMBO Journal* 17, pp. 1497–1506.

Anger, A. M. et al. (2013). “Structures of the human and Drosophila 80S ribosome”. eng. In: *Nature* 497, pp. 80–85.

Araki, Y et al. (2001). “Ski7p G protein interacts with the exosome and the Ski complex for 3’-to-5’ mRNA decay in yeast.” In: *The EMBO journal* 20, pp. 4684–4693.

Armache, J.-P. et al. (2010). “Cryo-EM structure and rRNA model of a translating eukaryotic 80S ribosome at 5.5-A resolution.” eng. In: *Proceedings of the National Academy of Sciences of the United States of America* 107, pp. 19748–19753.

Arstila, A. U. and B. F. Trump (1968). “Studies on cellular autophagocytosis. The formation of autophagic vacuoles in the liver after glucagon administration.” In: *The American Journal of Pathology* 53, pp. 687–733.

Bai, X. C. et al. (2013). “Ribosome structures to near-atomic resolution from thirty thousand cryo-EM particles”. In: *eLife* 2013, pp. 2–13.

Bai, X. C. et al. (2015). “How cryo-EM is revolutionizing structural biology”. In: *Trends in Biochemical Sciences* 40, pp. 49–57.

Ban, N et al. (2000). “The complete atomic structure of the large ribosomal subunit at 2.4 A resolution”. In: *Science* 289, pp. 905–920.

Becker, T. et al. (2011). “Structure of the no-go mRNA decay complex Dom34-Hbs1 bound to a stalled 80S ribosome.” In: *Nature Structural & Molecular Biology* 18, pp. 715–720.

Becker, T. et al. (2012). “Structural basis of highly conserved ribosome recycling in eukaryotes and archaea.” In: *Nature* 482, pp. 501–506.

Beckmann, R. et al. (2001). “Architecture of the Protein-Conducting Channel Associated with the Translating 80S Ribosome”. In: *Cell* 107, pp. 361–372.

Behrmann, E. et al. (2015). “Structural snapshots of actively translating human ribosomes.” In: *Cell* 161, pp. 845–857.

Ben-Shem, A. et al. (2010). “Crystal structure of the eukaryotic ribosome.” In: *Science* 330, pp. 1203–1209.

Ben-Shem, A. et al. (2011). “The structure of the eukaryotic ribosome at 3.0 Å resolution.” In: *Science* 334, pp. 1524–1529.

Benard, L et al. (1999). “The ski7 antiviral protein is an EF1-alpha homolog that blocks expression of non-Poly(A) mRNA in Saccharomyces cerevisiae.” In: *Journal of Virology* 73, pp. 2893–2900.

Berg, P and E. J. Offengand (1958). “An Enzymatic Mechanism for Linking Amino Acids to RNA.” In: *Proceedings of the National Academy of Sciences of the United States of America* 44, pp. 78–86.

Bhushan, S. et al. (2010). “Structural basis for translational stalling by human cytomegalovirus and fungal arginine attenuator peptide.” In: *Molecular Cell* 40, pp. 138–146.

Bird, A. (2007). “Perceptions of epigenetics”. In: *Nature* 447, pp. 396–398.

Bischoff, L. et al. (2014). “Molecular Basis for the Ribosome Functioning as an L-Tryptophan Sensor”. In: *Cell Reports* 9, pp. 469–475.

Blaha, G. et al. (2009). “Formation of the First Peptide Bond: The Structure of EF-P Bound to the 70S Ribosome”. In: *Science* 325, pp. 966–970.

Blanchard, S. C. et al. (2004). “tRNA selection and kinetic proofreading in translation”. In: *Nature Structural & Molecular Biology* 11, pp. 1008–1014.

Boeck, R et al. (1996). “The yeast Pan2 protein is required for poly(A)-binding protein-stimulated poly(A)-nuclease activity.” In: *The Journal of Biological Chemistry* 271, pp. 432–438.

Bradatsch, B et al. (2012). “Structure of the pre-60S ribosomal subunit with nuclear export factor Arx1 bound at the exit tunnel”. eng. In: *Nat Struct Mol Biol* 19, pp. 1234–1241.

Brandman, O. and R. S. Hegde (2016). “Ribosome-associated protein quality control”. In: *Nature Structural & Molecular Biology* 23, pp. 7–15.

Brandman, O. et al. (2012). “A ribosome-bound quality control complex triggers degradation of nascent peptides and signals translation stress.” In: *Cell* 151, pp. 1042–1054.

Brown, A. et al. (2015). “Structural basis for stop codon recognition in eukaryotes”. In: *Nature* 524, pp. 493–496.

Brown, C. E. and A. B. Sachs (1998). “Poly(A) tail length control in Saccharomyces cerevisiae occurs by message-specific deadenylation.” In: *Molecular and Cellular Biology* 18, pp. 6548–59.

Brown, J. T. et al. (2000). “The yeast antiviral proteins Ski2p, Ski3p, and Ski8p exist as a complex in vivo.” In: *RNA* 6, pp. 449–457.

Budkevich, T. V. et al. (2014). “Regulation of the mammalian elongation cycle by subunit rolling: a eukaryotic-specific ribosome rearrangement.” In: *Cell* 158, pp. 121–131.

Büttner, K. et al. (2007). “Structural basis for DNA duplex separation by a superfamily-2 helicase.” In: *Nature Structural & Molecular Biology* 14, pp. 647–652.

Cech, T. R. (2000). “Structural biology. The ribosome is a ribozyme.” In: *Science* 289, pp. 878–879.

Chang, Y.-F. et al. (2007). “The Nonsense-Mediated Decay RNA Surveillance Pathway”. In: *Annual Review of Biochemistry* 76, pp. 51–74.

Chen, J. Z. and N Grigorieff (2007). “SIGNATURE: a single-particle selection system for molecular electron microscopy”. In: *Journal of Structural Biology* 157, pp. 168–173.

Chen, V. B. et al. (2010). “MolProbity: All-atom structure validation for macromolecular crystallography”. In: *Acta Crystallographica Section D: Biological Crystallography* 66.1, pp. 12–21.

Cheng, Y. (2015). “Single-Particle Cryo-EM at Crystallographic Resolution”. In: *Cell* 161, pp. 450–457.

Chiabudini, M. et al. In: *Molecular and Cellular Biology*, pp. 4062–4076.

Choe, Y.-J. et al. (2016). “Failure of RQC machinery causes protein aggregation and proteotoxic stress”. In: *Nature* 531, pp. 191–195.

Coller, J. and R. Parker (2005). “General translational repression by activators of mRNA decapping”. In: *Cell* 122, pp. 875–886. eprint: NIHMS150003.

Cosson, B. et al. (2002). “Poly(A)-binding protein acts in translation termination via eukaryotic release factor 3 interaction and does not influence [PSI(+)] propagation”. In: *Molecular Cell Biology* 22, pp. 3301–3315.

Crick, F. H. (1970). “Central dogma of molecular biology.” In: *Nature* 227, pp. 561–563.

Crick, F. H. et al. (1961). “General nature of the genetic code for proteins”. In: *Nature* 192, pp. 1227–1232.

Cui, Y et al. (1995). “Identification and characterization of genes that are required for the accelerated degradation of mRNAs containing a premature translational termination codon.” In: *Genes & Development* 9, pp. 423–436.

Czaplinski, K et al. (1995). “Purification and characterization of the Upf1 protein: a factor involved in translation and mRNA degradation.” In: *RNA* 1, pp. 610–623.

Czaplinski, K et al. (1998). “The surveillance complex interacts with the translation release factors to enhance termination and degrade aberrant mRNAs.” In: *Genes & development* 12, pp. 1665–77.

Defenouillère, Q. et al. (2013). “Cdc48-associated complex bound to 60S particles is required for the clearance of aberrant translation products.” In: *Proceedings of the National Academy of Sciences of the United States of America* 110, pp. 5046–5051.

Defenouillère, Q. et al. (2016). “Rqc1 and ltn1 prevent c-terminal alanine-threonine tail (cat-tail)-induced protein aggregation by efficient recruitment of cdc48 on stalled 60s subunits”. In: *Journal of Biological Chemistry* 291, pp. 12245–12253.

Dever, T. E. and R. Green (2012). “The elongation, termination, and recycling phases of translation in eukaryotes”. In: *Cold Spring Harbor Perspectives in Biology* 4, pp. 1–16.

Dever, T. E. et al. (2015). “The hypusine-containing translation factor eIF5A.” In: *Critical Reviews in Biochemistry and Molecular Biology* 49, pp. 413–425.

Dice, J. F. (1990). “Peptide sequences that target cytosolic proteins for lysosomal proteolysis.” In: *Trends in Biochemical Sciences* 15, pp. 305–309.

Dintzis, H. M. (1961). *Assembly of the Peptide Chains of Hemoglobin**.

Doerfel, L. K. et al. (2013). “EF-P Is Essential for Rapid Synthesis of Proteins Containing Consecutive Proline Residues”. In: *Science* 339, pp. 85–88.

Doma, M. K. and R Parker (2006). “Endonucleolytic cleavage of eukaryotic mRNAs with stalls in translation elongation”. In: *Nature* 440, pp. 561–564.

dos Reis, M. et al. (2004). “Solving the riddle of codon usage preferences: A test for translational selection”. In: *Nucleic Acids Research* 32, pp. 5036–5044.

Dziembowski, A. et al. (2007). “A single subunit, Dis3, is essentially responsible for yeast exosome core activity.” In: *Nature Structural & Molecular Biology* 14, pp. 15–22.

Eberle, A. B. et al. (2009). “SMG6 promotes endonucleolytic cleavage of nonsense mRNA in human cells.” In: *Nature Structural & Molecular Biology* 16, pp. 49–55.

Eckmann, C. R. et al. (2011). “Control of poly(A) tail length”. In: *Wiley Interdisciplinary Reviews: RNA* 2, pp. 348–361.

Emsley, P. and K. Cowtan (2004). “Coot: Model-building tools for molecular graphics”. In: *Acta Crystallographica Section D: Biological Crystallography* 60, pp. 2126–2132.

Fernández, I. S. et al. (2014). “Initiation of translation by cricket paralysis virus IRES requires its translocation in the ribosome”. In: *Cell* 157, pp. 823–831.

Franckenberg, S. et al. (2012). “Structural view on recycling of archaeal and eukaryotic ribosomes after canonical termination and ribosome rescue”. In: *Current Opinion in Structural Biology* 22, pp. 786–796.

Frank, J and R. K. Agrawal (2000). “A ratchet-like inter-subunit reorganization of the ribosome during translocation.” In: *Nature* 406, pp. 318–322.

Frank, J et al. (1996). “SPIDER and WEB: processing and visualization of images in 3D electron microscopy and related fields”. In: *Journal Structural Biology* 116, pp. 190–199.

Frank, J. et al. (1995). *A model of protein synthesis based on cryo-electron microscopy of the E. coli ribosome.*

Franks, T. M. and J. Lykke-Andersen (2008). “The Control of mRNA Decapping and P-Body Formation”. In: *Molecular Cell* 32, pp. 605–615.

Frischmeyer, P. A. et al. (2002). “An mRNA surveillance mechanism that eliminates transcripts lacking termination codons”. In: *Science* 295, pp. 2258–2261.

Frolova, L. et al. In: *RNA*.

Funakoshi, Y. et al. (2007). “Mechanism of mRNA deadenylation: evidence for a molecular interplay between translation termination factor eRF3 and mRNA deadenylases”. In: *Genes Dev* 21, pp. 3135–3148.

Gamble, C. E. et al. (2016). “Adjacent Codons Act in Concert to Modulate Translation Efficiency in Yeast”. In: *Cell* 166, pp. 679–690.

Gandhi, R. et al. (2008). “Depurination of Brome Mosaic Virus RNA3 in Vivo Results in Translation-dependent Accelerated Degradation of the Viral RNA”. In: *Journal of Biological Chemistry* 283, pp. 32218–32228.

Garneau, N. L. et al. (2007). “The highways and byways of mRNA decay.” In: *Nature Reviews. Molecular Cell Biology* 8, pp. 113–126.

Gatfield, D. and E. Izaurralde (2004). “Nonsense-mediated messenger RNA decay is initiated by endonucleolytic cleavage in Drosophila.” In: *Nature* 429, pp. 575–578.

Ghaemmaghami, S. et al. (2003). “Global analysis of protein expression in yeast”. In: *Nature* 425, pp. 737–741.

Glick, B. R. and M. C. Ganoza (1975). “Identification of a soluble protein that stimulates peptide bond synthesis.” In: *Proceedings of the National Academy of Sciences of the United States of America* 72, pp. 4257–4260.

Graille, M. et al. (2008). “Structure of Yeast Dom34: A protein related to translation termination factor Erf1 and involved in No-Go decay”. In: *Journal of Biological Chemistry* 283, pp. 7145–7154.

Grigorieff, N. (2007). “FREALIGN: high-resolution refinement of single particle structures.” In: *Journal of Structural Biology* 157, pp. 117–125.

Gutierrez, E. et al. (2013). “eif5A promotes translation of polyproline motifs”. In: *Molecular Cell* 51, pp. 35–45.

Halbach, F. et al. (2012). “The crystal structure of S. cerevisiae Ski2, a DExH helicase associated with the cytoplasmic functions of the exosome”. In: *RNA* 18, pp. 124–134.

Halbach, F. et al. (2013). “The yeast ski complex: crystal structure and RNA channeling to the exosome complex”. In: *Cell* 154, pp. 814–826.

Halic, M et al. (2004). “Structure of the signal recognition particle interacting with the elongation-arrested ribosome”. In: *Nature* 427, pp. 808–814.

Harigaya, Y. and R. Parker (2012). “Global analysis of mRNA decay intermediates in Saccharomyces cerevisiae”. In: *Proceedings of the National Academy of Sciences of the United States of America* 109, pp. 11764–9.

He, F et al. (1997). “Upf1p, Nmd2p, and Upf3p are interacting components of the yeast nonsense-mediated mRNA decay pathway.” In: *Molecular and Cellular Biology* 17, pp. 1580–1594.

Heuer, A. et al. (2017). “Structure of the 40S–ABCE1 post-splitting complex in ribosome recycling and translation initiation”. In: *Nature Structural & Molecular Biology* 24, pp. 453–460.

Higgins, R. et al. (2015). “The Unfolded Protein Response Triggers Site-Specific Regulatory Ubiquitylation of 40S Ribosomal Proteins”. In: *Molecular Cell* 59.1, pp. 35–49.

Hilal, T. et al. (2016). “Structural insights into ribosomal rescue by Dom34 and Hbs1 at near-atomic resolution”. In: *Nature Communications* 7, p. 13521.

Hinnebusch, A. G. and J. R. Lorsch (2012). “The mechanism of eukaryotic translation initiation: New insights and challenges”. In: *Cold Spring Harbor Perspectives in Biology* 4.

Hogg, J. R. and S. P. Goff (2010). “Upf1 senses 3’UTR length to potentiate mRNA decay.” In: *Cell* 143, pp. 379–89.

Houseley, J. and D. Tollervey (2006). “Yeast Trf5p is a nuclear poly(A) polymerase”. In: *EMBO Reports* 7, pp. 205–211.

Hsu, C. L. and A Stevens (1993). “Yeast cells lacking 5’–>3’ exoribonuclease 1 contain mRNA species that are poly(A) deficient and partially lack the 5’ cap structure.” In: *Molecular and Cellular Biology* 13, pp. 4826–4835.

Hu, W. et al. (2009). “Co-translational mRNA decay in Saccharomyces cerevisiae.” In: *Nature* 461, pp. 225–229.

Hu, W. et al. (2010). “Nonsense-mediated mRNA decapping occurs on polyribosomes in Saccharomyces cerevisiae.” In: *Nature structural & molecular biology* 17.2, pp. 244–7.

Inada, T. (2013). “Quality control systems for aberrant mRNAs induced by aberrant translation elongation and termination.” In: *Biochimica et Biophysica Acta* 1829, pp. 634–642.

Inada, T. and H. Aiba (2005). “Translation of aberrant mRNAs lacking a termination codon or with a shortened 3’-UTR is repressed after initiation in yeast.” In: *The EMBO Journal* 24, pp. 1584–1595.

Inagaki, Y et al. (2000). “Evolution of the eukaryotic translation termination system: origins of release factors.” In: *Molecular Biology and Evolution* 17, pp. 882–889.

Ingolia, N. T. et al. (2009). “Genome-wide analysis in vivo of translation with nucleotide resolution using ribosome profiling”. In: *Science* 324, pp. 218–223.

Ito-Harashima, S. et al. (2007). “Translation of the poly(A) tail plays crucial roles in nonstop mRNA surveillance via translation repression and protein destabilization by proteasome in yeast.” In: *Genes & Development* 21, pp. 519–524.

Jackson, R. J. et al. (2010). “The mechanism of eukaryotic translation initiation and principles of its regulation.” In: *Nature Reviews. Molecular Cell Biology* 11, pp. 113–127.

Jacobson, A and S. W. Peltz (1996). “Interrelationships of the pathways of mRNA decay and translation in eukaryotic cells.” en. In: *Annual Review of Biochemistry* 65, pp. 693–739.

Jalkanen, A. L. et al. (2014). “Determinants and implications of mRNA poly(A) tail size–does this protein make my tail look big?” In: *Seminars in Cell & Developmental Biology* 34, pp. 24–32.

Jenner, L. et al. (2005). “Translational operator of mRNA on the ribosome: how repressor proteins exclude ribosome binding.” In: *Science* 308, pp. 120–123.

Johansson, M. et al. (2011). “pH-sensitivity of the ribosomal peptidyl transfer reaction dependent on the identity of the A-site aminoacyl-tRNA.” In: *Proceedings of the National Academy of Sciences of the United States of America* 108, pp. 79–84.

Juszkiewicz, S. and R. S. Hegde (2017). “Initiation of quality control during poly(A) translation requires site-specific ribosome ubiquitination”. In: *Molecular Cell* 65, pp. 743–750.

Kalisiak, K. et al. (2016). “A short splicing isoform of HBS1L links the cytoplasmic exosome and SKI complexes in humans”. In: *Nucleic Acids Research*, gkw862.

Kaminishi, T. et al. (2007). “A Snapshot of the 30S Ribosomal Subunit Capturing mRNA via the Shine-Dalgarno Interaction”. In: *Structure* 15, pp. 289–297.

Kashima, I. et al. (2006). “Binding of a novel SMG-1–Upf1–eRF1–eRF3 complex (SURF) to the exon junction complex triggers Upf1 phosphorylation and nonsense-mediated mRNA decay”. In: *Genes & Development* 20, pp. 355–367.

Kervestin, S. et al. (2012). “Testing the faux-UTR model for NMD: analysis of Upf1p and Pab1p competition for binding to eRF3/Sup35p.” In: *Biochimie* 94, pp. 1560–1571.

Kim, K. K. et al. (1998). “Crystal structures of eukaryotic translation initiation factor 5A from Methanococcus jannaschii at 1.8 A resolution.” In: *Proceedings of the National Academy of Sciences of the United States of America* 95, pp. 10419–10424.

Kireeva, M. L. et al. (2008). “Transient Reversal of RNA Polymerase II Active Site Closing Controls Fidelity of Transcription Elongation”. In: *Molecular Cell* 30, pp. 557–566.

Kisselev, L. et al. (2003). “Termination of translation: interplay of mRNA, rRNAs and release factors?” In: *The EMBO Journal* 22, pp. 175–182.

Klauer, A. A. and A. van Hoof (2012). “Degradation of mRNAs that lack a stop codon: a decade of nonstop progress.” In: *Wiley Interdisciplinary Reviews. RNA* 3, pp. 649–660.

Kobayashi, T. et al. (2004). “The GTP-binding release factor eRF3 as a key mediator coupling translation termination to mRNA decay.” In: *The Journal of Biological Chemistry* 279, pp. 45693–45700.

Korostelev, A. (2011). “Structural aspects of translation termination on the ribosome”. In: *RNA* 17, pp. 1409–1421.

Korostelev, A. et al. (2008). “Crystal structure of a translation termination complex formed with release factor RF2”. In: *Proceedings of the National Academy of Sciences* 105, pp. 19684–19689.

Korostelev, A. et al. (2007). “Interactions and dynamics of the Shine Dalgarno helix in the 70S ribosome.” In: *Proceedings of the National Academy of Sciences of the United States of America* 104, pp. 16840–16843.

Kowalinski, E. et al. (2015). “Saccharomyces cerevisiae Ski7 Is a GTP-Binding Protein Adopting the Characteristic Conformation of Active Translational GTPases.” In: *Structure* 23, pp. 1336–43.

Kowalinski, E. et al. (2016). “Structure of a Cytoplasmic 11-Subunit RNA Exosome Complex”. In: *Molecular Cell* 63, pp. 125–134.

Kucukelbir, A. et al. (2014). “Quantifying the local resolution of cryo-EM density maps.” In: *Nature Methods* 11, pp. 63–65.

Kühlbrandt, W. (2014). “Cryo-EM enters a new era.” In: *eLife* 3, e03678.

Kuroha, K. et al. (2010). “Receptor for activated C kinase 1 stimulates nascent polypeptide-dependent translation arrest.” In: *EMBO Reports* 11, pp. 956–961.

Laemmli, U. K. (1970). “Cleavage of structural proteins during the assembly of the head of bacteriophage T4.” In: *Nature* 227, pp. 680–685.

Lagerkvist, U. (1978). “"Two out of three": an alternative method for codon reading.” In: *Proceedings of the National Academy of Sciences of the United States of America* 75, pp. 1759–1762.

LaGrandeur, T and R Parker (1999). “The cis acting sequences responsible for the differential decay of the unstable MFA2 and stable PGK1 transcripts in yeast include the context of the translational start codon.” In: *RNA* 5, pp. 420–433.

Le Hir, H et al. (2000). “The spliceosome deposits multiple proteins 20-24 nucleotides upstream of mRNA exon-exon junctions.” In: *The EMBO Journal* 19, pp. 6860–6869.

Lee, H. H. et al. (2007). “Structural and functional insights into Dom34, a key component of no-go mRNA decay”. In: *Molecular Cell* 27, pp. 938–950.

Leeds, P et al. (1991). “The product of the yeast UPF1 gene is required for rapid turnover of mRNAs containing a premature translational termination codon.” In: *Genes & Development* 5, pp. 2303–2314.

Leeds, P et al. (1992). “Gene products that promote mRNA turnover in Saccharomyces cerevisiae.” In: *Molecular and Cellular Biology* 12, pp. 2165–2177.

Leidig, C. et al. (2012). “Structural characterization of a eukaryotic chaperone—the ribosome-associated complex”. In: *Nature Structural & Molecular Biology* 20, pp. 23–28.

Leidig, C. et al. (2014). “60S ribosome biogenesis requires rotation of the 5S ribonucleoprotein particle.” In: *Nature Communications* 5, p. 3491.

Letzring, D. P. et al. (2010). “Control of translation efficiency in yeast by codon-anticodon interactions”. In: *RNA* 16, pp. 2516–2528.

Leung, E. K. Y. et al. (2011). “The Mechanism of Peptidyl Transfer Catalysis by the Ribosome”. In: *Annual Review of Biochemistry* 80, pp. 527–555.

Liu, Q. et al. (2006). “Reconstitution, Activities, and Structure of the Eukaryotic RNA Exosome”. In: *Cell* 127, pp. 1223–1237.

Loh, B. et al. (2013). “The SMG5-SMG7 heterodimer directly recruits the CCR4-NOT deadenylase complex to mRNAs containing nonsense codons via interaction with POP2”. In: *Genes & Development* 27, pp. 2125–2138.

Lu, J. and C. Deutsch (2008). “Electrostatics in the ribosomal tunnel modulate chain elongation rates.” In: *Journal of Molecular Biology* 384, pp. 73–86.

Lyumkis, D. et al. (2013). “Single-particle EM reveals extensive conformational variability of the Ltn1 E3 ligase.” In: *Proceedings of the National Academy of Sciences of the United States of America* 110, pp. 1702–1707.

Makino, D. L. et al. (2013). “Crystal structure of an RNA-bound 11-subunit eukaryotic exosome complex.” In: *Nature* 495, pp. 70–75.

Maquat, L. E. (2002). “Molecular biology. Skiing toward nonstop mRNA decay.” eng. In: *Science* 295, pp. 2221–2222.

Maquat, L. E. et al. (2010). “The pioneer round of translation: Features and functions”. In: *Cell* 142.3, pp. 368–374.

Matheisl, S. et al. (2015). “Structure of a human translation termination complex”. In: *Nucleic Acids Research* 43, pp. 8615–8626.

Melnikov, S. et al. (2012). “One core, two shells: bacterial and eukaryotic ribosomes.” In: *Nature Structural & Molecular Biology* 19, pp. 560–567.

Melnikov, S. et al. (2016). “Crystal Structure of Hypusine-Containing Translation Factor eIF5A Bound to a Rotated Eukaryotic Ribosome”. In: *Journal of Molecular Biology* 428, pp. 3570–3576.

Mindell, J. A. and N. Grigorieff (2003). “Accurate determination of local defocus and specimen tilt in electron microscopy.” In: *Journal of Structural Biology* 142, pp. 334–47.

Mitchell, P. and D. Tollervey (2003). “An NMD Pathway in Yeast Short Article Involving Accelerated Deadenylation and Exosome-Mediated 3 $\rightarrow$ 5 Degradation”. In: *Molecular Cell* 11, pp. 1405–1413.

Muhlrad, D and R Parker (1999). “Aberrant mRNAs with extended 3’ UTRs are substrates for rapid degradation by mRNA surveillance.” In: *RNA (New York, N.Y.)* 5.10, pp. 1299–307.

Muhlrad, D et al. (1994). “Deadenylation of the unstable mRNA encoded by the yeast MFA2 gene leads to decapping followed by 5’–>3’ digestion of the transcript.” In: *Genes & Development* 8, pp. 855–866.

Murshudov, G. N. et al. (1997). “Refinement of macromolecular structures by the maximum-likelihood method”. In: *Acta Crystallographica Section D: Biological Crystallography* 53, pp. 240–255.

Muto, H. and K. Ito (2008). “Peptidyl-prolyl-tRNA at the ribosomal P-site reacts poorly with puromycin.” In: *Biochemical and Biophysical Research Communications* 366, pp. 1043–1047.

Nedelsky, N. B. et al. (2008). “Autophagy and the ubiquitin-proteasome system: Collaborators in neuroprotection”. In: *Biochimica et Biophysica Acta - Molecular Basis of Disease* 1782, pp. 691–699.

Nissen, P et al. (2000). “The structural basis of ribosome activity in peptide bond synthesis.” In: *Science* 289, pp. 920–930.

Noble, C. G. and H. Song (2008). “Structural studies of elongation and release factors”. In: *Cellular and Molecular Life Sciences* 65, pp. 1335–1346.

Nogales, E. (2015). “The development of cryo-EM into a mainstream structural biology technique”. In: *Nature Methods* 13, pp. 24–27.

Noller, H. F. et al. (2002). “Translocation of tRNA during protein synthesis.” In: *FEBS Letters* 514, pp. 11–16.

Oeffinger, M. et al. (2007). “Comprehensive analysis of diverse ribonucleoprotein complexes.” In: *Nature Methods* 4, pp. 951–956.

Ogle, J. M. et al. (2001). “Recognition of Cognate Transfer RNA by the 30S Ribosomal Subunit”. In: *Science* 292, pp. 897–902.

Park, M. H. et al. (1981). “Identification of hypusine, an unusual amino acid, in a protein from human lymphocytes and of spermidine as its biosynthetic precursor”. In: *Proceedings of the National Academy of Sciences of the United States of America* 78, pp. 2869–2873.

Park, M. H. et al. (2010). “Functional significance of eIF5A and its hypusine modification in eukaryotes”. In: *Amino Acids*. Vol. 38, pp. 491–500.

Parker, R. (2012). “RNA degradation in Saccharomyces cerevisae.” In: *Genetics* 191, pp. 671–702.

Passos, D. O. et al. (2009). “Analysis of Dom34 and its function in no-go decay.” In: *Molecular Biology of the Cell* 20, pp. 3025–3032.

Pavlov, M. Y. et al. (2009). “Slow peptide bond formation by proline and other N-alkylamino acids in translation.” In: *Proceedings of the National Academy of Sciences of the United States of America* 106, pp. 50–54.

Pechmann, S. and J. Frydman (2013). “Evolutionary conservation of codon optimality reveals hidden signatures of cotranslational folding.” In: *Nature Structural & Molecular Biology* 20, pp. 237–243.

Pelechano, V. et al. (2015). “Widespread Co-translational RNA Decay Reveals Ribosome Dynamics”. In: *Cell* 161, pp. 1400–1412.

Peltz, S. W. et al. (1993). “mRNA destabilization triggered by premature translational termination depends on at least three cis-acting sequence elements and one trans-acting factor.” In: *Genes & Development* 7, pp. 1737–1754.

Peske, F. et al. (2005). “Sequence of Steps in Ribosome Recycling as Defined by Kinetic Analysis”. In: *Molecular Cell* 18, pp. 403–412.

Pettersen, E. F. et al. (2004). “UCSF Chimera–a visualization system for exploratory research and analysis”. In: *Journal of Computational Chemistry* 25, pp. 1605–1612.

Pickart, C. M. (2001). “Mechanisms Underlying Ubiquitination”. In: *Annual Review of Biochemistry* 70.1, pp. 503–533.

Pisarev, A. V. et al. (2007). “Recycling of eukaryotic posttermination ribosomal complexes”. In: *Cell* 131, pp. 286–299.

Pisareva, V. P. et al. (2011). “Dissociation by Pelota, Hbs1 and ABCE1 of mammalian vacant 80S ribosomes and stalled elongation complexes”. In: *The EMBO Journal*.

Polikanov, Y. S. et al. (2014). “A proton wire to couple aminoacyl-tRNA accommodation and peptide-bond formation on the ribosome.” In: *Nature Structural & Molecular Biology* 21, pp. 787–793.

Preis, A. et al. (2014). “Cryoelectron microscopic structures of eukaryotic translation termination complexes containing eRF1-eRF3 or eRF1-ABCE1”. In: *Cell Reports* 8, pp. 59–65.

Presnyak, V. et al. (2015). “Codon Optimality Is a Major Determinant of mRNA Stability”. In: *Cell* 160, pp. 1111–1124.

Qu, X et al. (1998). “The human DEVH-box protein Ski2w from the HLA is localized in nucleoli and ribosomes.” In: *Nucleic acids research* 26.17, pp. 4068–4077.

Rabl, J. et al. (2011). “Crystal Structure of the Eukaryotic 40S Ribosomal Subunit in Complex with Initiation Factor 1”. In: *Science* 331, pp. 730–736.

Radhakrishnan, A. et al. (2016). “The DEAD-Box Protein Dhh1p Couples mRNA Decay and Translation by Monitoring Codon Optimality”. In: *Cell* 167, pp. 122–128.

Rohou, A. and N. Grigorieff (2015). “CTFFIND4: Fast and accurate defocus estimation from electron micrographs.” In: *Journal of Structural Biology* 192, pp. 216–221.

Roy, B. and A. Jacobson (2013). “The intimate relationships of mRNA decay and translation.” In: *Trends in Genetics* 29, pp. 691–699.

Saini, P. et al. (2009). “Hypusine-containing protein eIF5A promotes translation elongation”. In: *Nature* 459, pp. 118–121.

Saito, S. et al. (2013). “The Hbs1-Dom34 protein complex functions in non-stop mRNA decay in mammalian cells.” In: *The Journal of Biological Chemistry* 288, pp. 17832–17843.

Scheres, S. H. (2012). “RELION: implementation of a Bayesian approach to cryo-EM structure determination”. eng. In: *Journal of Structural Biology* 180, pp. 519–530.

Scheres, S. H. (2014). “Beam-induced motion correction for sub-megadalton cryo-EM particles”. In: *eLife* 3, e03665.

Schluenzen, F et al. (2000). “Structure of functionally activated small ribosomal subunit at 3.3 angstroms resolution.” In: *Cell* 102, pp. 615–623.

Schmeing, T. M. and V Ramakrishnan (2009). “What recent ribosome structures have revealed about the mechanism of translation.” In: *Nature* 461, pp. 1234–1242.

Schmidt, C. et al. (2015). “Structure of the hypusinylated eukaryotic translation factor eIF-5A bound to the ribosome”. In: *Nucleic Acids Research* 44, pp. 1944–1951.

Schmidt, C. et al. (2016). “The cryo-EM structure of a ribosome–Ski2-Ski3-Ski8 helicase complex”. In: *Science* 354, pp. 1431–1433.

Schuller, A. P. et al. (2017). “eIF5A Functions Globally in Translation Elongation and Termination”. In: *Molecular Cell* 162, pp. 872–884.

Schulman, B. A. and J. Wade Harper (2009). “Ubiquitin-like protein activation by E1 enzymes: the apex for downstream signalling pathways”. In: *Nature Reviews Molecular Cell Biology* 10, pp. 319–331.

Schwartz, D. C. and R Parker (1999). “Mutations in translation initiation factors lead to increased rates of deadenylation and decapping of mRNAs in Saccharomyces cerevisiae.” In: *Molecular and Cellular Biology* 19, pp. 5247–5256.

Selmer, M. et al. (2006). “Structure of the 70S ribosome complexed with mRNA and tRNA.” In: *Science* 313, pp. 1935–1942.

Shao, S. and R. S. Hegde (2014). “Reconstitution of a Minimal Ribosome-Associated Ubiquitination Pathway with Purified Factors.” In: *Molecular Cell*, pp. 1–11.

Shao, S. et al. (2015). “Structure and Assembly Pathway of the Ribosome Quality Control Complex”. In: *Molecular Cell*.

Shao, S. et al. (2016). “Decoding Mammalian Ribosome-mRNA States by Translational GTPase Complexes”. In: *Cell* 167, pp. 1229–1240.

Shatkin, A. J. (1976). “Capping of eucaryotic mRNAs.” In: *Cell* 9, pp. 645–653.

Shen, P. S. et al. (2015). “Rqc2p and 60S ribosomal subunits mediate mRNA-independent elongation of nascent chains”. In: *Science* 347, pp. 75–78.

Sheth, U. et al. (2003). “Decapping and Decay of Messenger RNA Occur in Cytoplasmic Processing Bodies”. In: *Science* 805, pp. 805–808.

Shine, J and L Dalgarno (1974). “The 3’-terminal sequence of Escherichia coli 16S ribosomal RNA: complementarity to nonsense triplets and ribosome binding sites.”

In: *Proceedings of the National Academy of Sciences of the United States of America* 71, pp. 1342–1346.

Shoemaker, C. and R. Green (2011). “Kinetic analysis reveals the ordered coupling of translation termination and ribosome recycling in yeast”. In: *Proceedings of the National Academy of Sciences of the United States of America* 108.

Shoemaker, C. et al. (2010). “Dom34:Hbs1 promotes subunit dissociation and peptidyl-tRNA drop-off to initiate no-go decay.” In: *Science* 330, pp. 369–372.

Shoemaker, C. J. and R. Green (2012). “Translation drives mRNA quality control”. In: *Nature Structural & Molecular Biology* 19, pp. 594–601.

Sitron, C. S. et al. (2017). “Asc1 , Hel2 , and Slh1 couple translation arrest to nascent chain degradation”. In: *RNA*, rna.060897.117.

Soding, J et al. (2005). “The HHpred interactive server for protein homology detection and structure prediction”. In: *Nucleic Acids Research* 33, pp. 244–248.

Sonenberg, N. and A. G. Hinnebusch (2009). “Regulation of translation initiation in eukaryotes: mechanisms and biological targets.” In: *Cell* 136, pp. 731–745.

Song, H et al. (2000). “The crystal structure of human eukaryotic release factor eRF1–mechanism of stop codon recognition and peptidyl-tRNA hydrolysis”. In: *Cell* 100, pp. 311–321.

Spahn, C. M. et al. (2001). “Structure of the 80S ribosome from Saccharomyces cerevisiae–tRNA-ribosome and subunit-subunit interactions”. In: *Cell* 107, pp. 373–386.

Stansfield, I. et al. (1998). “Missense translation errors in Saccharomyces cerevisiae”. In: *Journal of Molecular Biology* 282, pp. 13–24.

Steitz, T. A. (2008). “A structural understanding of the dynamic ribosome machine”. In: *Nature Reviews Molecular Cell Biology* 9, pp. 242–253.

Sundaramoorthy, E. et al. (2017). “ZNF598 and RACK1 Regulate Mammalian Ribosome-Associated Quality Control Function by Mediating Regulatory 40S Ribosomal Ubiquitylation”. In: *Molecular Cell* 65, pp. 751–760.

Synowsky, S. a. et al. (2009). “Comparative multiplexed mass spectrometric analyses of endogenously expressed yeast nuclear and cytoplasmic exosomes.” In: *Journal of Molecular Biology* 385, pp. 1300–1313.

Takahashi, S. et al. (2003). “Interaction between Ski7p and Upf1p is required for nonsense-mediated 3’-to-5’ mRNA decay in yeast”. In: *The EMBO Journal* 22, pp. 3951–3959.

Teixeira, D. et al. (2005). “Processing bodies require RNA for assembly and contain nontranslating mRNAs.” In: *RNA* 11, pp. 371–382.

Tharun, S and R Parker (2001). “Targeting an mRNA for decapping: displacement of translation factors and association of the Lsm1p-7p complex on deadenylated yeast mRNAs.” In: *Molecular Cell* 8, pp. 1075–83.

Thoms, M. et al. (2015). “The Exosome Is Recruited to RNA Substrates through Specific Adaptor Proteins Article The Exosome Is Recruited to RNA Substrates through Specific Adaptor Proteins”. In: *Cell* 162, pp. 1029–1038.

Toh-E, A et al. (1978). “Chromosomal superkiller mutants of Saccharomyces cerevisiae.” In: *Journal of Bacteriology* 136, pp. 1002–7.

Tomko, R. J. and M. Hochstrasser (2013). “Molecular Architecture and Assembly of the Eukaryotic Proteasome”. In: *Annual Review of Biochemistry* 82.1, pp. 415–445.

Trapnell, C. et al. (2009). “TopHat: Discovering splice junctions with RNA-Seq”. In: *Bioinformatics* 25, pp. 1105–1111.

Tsuboi, T. et al. (2012). “Dom34:hbs1 plays a general role in quality-control systems by dissociation of a stalled ribosome at the 3’ end of aberrant mRNA.” In: *Molecular Cell* 46, pp. 518–529.

Tucker, M et al. (2001). “The transcription factor associated Ccr4 and Caf1 proteins are components of the major cytoplasmic mRNA deadenylase in Saccharomyces cerevisiae.” In: *Cell* 104, pp. 377–386.

Tucker, M. et al. (2002). “Ccr4p is the catalytic subunit of a Ccr4p/Pop2p/Notp mRNA deadenylase complex in Saccharomyces cerevisiae.” In: *The EMBO journal* 21, pp. 1427–1436.

Tuller, T. et al. (2010). “An evolutionarily conserved mechanism for controlling the efficiency of protein translation”. In: *Cell* 141, pp. 344–354.

Ude, S. et al. (2013). “Translation elongation factor EF-P alleviates ribosome stalling at polyproline stretches.” In: *Science* 339, pp. 82–85.

Unterholzner, L. and E. Izaurralde (2004). “SMG7 Acts as a Molecular Link between mRNA Surveillance and mRNA Decay”. In: *Molecular Cell* 16, pp. 587–596.

van Hoof, A et al. (2000). “Function of the ski4p (Csl4p) and Ski7p proteins in 3’-to-5’ degradation of mRNA.” In: *Molecular and Cellular Biology* 20.21, pp. 8230–43.

van Hoof, A. et al. (2002). “Exosome-mediated recognition and degradation of mRNAs lacking a termination codon.” eng. In: *Science* 295, pp. 2262–2264.

van Wijk, S. J. L. and H. T. M. Timmers (2010). “The family of ubiquitin-conjugating enzymes (E2s): deciding between life and death of proteins”. In: *The FASEB Journal* 24, pp. 981–993.

Vanacova, S. and R. Stef (2007). “The exosome and RNA quality control in the nucleus”. In: *EMBO Reports* 8, pp. 651–657.

Voorhees, R. M. and V. Ramakrishnan (2013). “Structural Basis of the Translational Elongation Cycle”. In: *Annual Review of Biochemistry* 82, pp. 203–236.

Wang, L. et al. (2005). “Domain interactions within the Ski2/3/8 complex and between the Ski complex and Ski7p.” In: *RNA* 11, pp. 1291–1302.

Weir, J. R. et al. (2010). “Structural analysis reveals the characteristic features of Mtr4, a DExH helicase involved in nuclear RNA processing and surveillance.” In: *Proceedings of the National Academy of Sciences of the United States of America* 107, pp. 12139–44.

Weixlbaumer, A. et al. (2008). “Insights into Translational Termination from the Structure of RF2 Bound to the Ribosome”. In: *Science* 322, pp. 953–956.

Weng, Y et al. (1996). “Genetic and biochemical characterization of mutations in the ATPase and helicase regions of the Upf1 protein.” In: *Molecular and Cellular Biology* 16, pp. 5477–90.

Wilson, D. N. and J. H. Cate (2012). “The Structure and Function of the Eukaryotic Ribosome”. In: *Cold Spring Harbor Perspectives in Biology* 4, a011536–a011536.

Wimberly, B. T. et al. (2000). “Structure of the 30S ribosomal subunit”. eng. In: *Nature* 407, pp. 327–339.

Wohlgemuth, I. et al. (2008). “Modulation of the rate of peptidyl transfer on the ribosome by the nature of substrates.” In: *The Journal of Biological Chemistry* 283, pp. 32229–32235.

Wolff, E. C. et al. (1990). “Cleavage of spermidine as the first step in deoxyhypusine synthesis: The role of NAD”. In: *Journal of Biological Chemistry* 265, pp. 4793–4799.

Woolstenhulme, C. J. et al. (2013). “Nascent peptides that block protein synthesis in bacteria”. In: *Proceedings of the National Academy of Sciences* 110, pp. 878–887.

Woolstenhulme, C. J. et al. (2015). “High-Precision Analysis of Translational Pausing by Ribosome Profiling in Bacteria Lacking EFP.” In: *Cell Reports* 11, pp. 13–21.

Wyers, F. et al. (2005). “Cryptic pol II transcripts are degraded by a nuclear quality control pathway involving a new poly(A) polymerase.” In: *Cell* 121, pp. 725–737.

Yonashiro, R. et al. (2016). “The Rqc2/Tae2 subunit of the ribosome-associated quality control (RQC) complex marks ribosome-stalled nascent polypeptide chains for aggregation”. In: *eLife* 5, e11794.

Zavialov, A. V. et al. (2002). “Release of peptide promoted by the GGQ motif of class 1 release factors regulates the GTPase activity of RF3.” In: *Molecular Cell* 10, pp. 789–98.

Zavialov, A. V. et al. (2005). “Splitting of the Posttermination Ribosome into Subunits by the Concerted Action of RRF and EF-G”. In: *Molecular Cell* 18, pp. 675–686.

Zhou, J. et al. (2012). “Crystal structures of 70S ribosomes bound to release factors RF1, RF2 and RF3”. In: *Current Opinion in Structural Biology* 22, pp. 733–742.

Zhou, T. et al. (2009). “Translationally Optimal Codons Associate with Structurally Sensitive Sites in Proteins”. In: *Molecular Biology and Evolution* 26, pp. 1571–1580.

# Acknowledgements

The PhD is a long (and sometimes rocky) road. During this time, I was lucky to meet many amazing people that made the entire trip really enjoyable. First, I want to thank Roland for all his support and mentoring. You took me under your wing way before I started my PhD in your lab. Thank you for not only being a boss that is super easy to work for, but also for promoting and teaching independence. This is one of the major things I learned during my time here, I will make sure to put it to good use in the future.

I would also like to thank Daniel Wilson for all his support and his effort in the eIF-5A project and being my second advisor. Especially since now, you had to come from Hamburg and are not longer within our neighbourhood. Without you, we probably would have never been able to publish this fast. I learned a lot from you, and I probably will always fear your evil top-spin curve balls on the tennis court.

Thank you to PD Dietmar Martin and Prof. Klaus Förstemann for being part of my thesis committee and their part in this defense, and Prof. Karl-Peter Hopfner and Franz Herzog as being my 5th and 6th advisor.

A thank you goes to Prof. Elena Conti, Prof. Alain Jacquier and Micheline Fromont-Racine for their big part in the Ski complex project. I enjoyed my time working and collaborating with you and I am grateful for all your inputs and ideas.

A special thanks goes to Quentin Defenouillère. We had a lot of fun during your visits here (some of it because of experiments, some of it because of the delicious Weißbier) and a lot of your work influenced me greatly and helped starting off a lot of experiments that were crucial for this project. I hope we have the time for more adventures in the future, mon ami!

I like to thank the Boehringer Ingelheim Foundation fellowship for all their funding, summer schools and seminars creating this truly amazing network and atmosphere.

One of the biggest parts of having a successful PhD is the people that are around you day in, day out, so here it goes:

Many thanks to our fearless microscopy team with Otto Berninghausen, Susi Rieder and Charlotte Ungewickell for all their work and efforts! And also to all of our lab technicians Andrea Gilmozzi and Joana Musial...I think I can safely assume that without you the entire lab would probably break down. I want to especially mention Heidi Sieber, we worked on a lot of things together and you were a tremendous help. Thank you for all that you did!

Thank you to Lukas Hangover for all your computational master skills and fearless dives into the dangerous CCP4 world with me.

Thank you to Clara and Anne for all the fun times, dancing nights, drinks, lunches and (sometimes really, really weird) discussion that we had! I will deeply miss all of it!

Thank you to Vivek and Markus for all your profiling work. I think we can say for 100% that it made the entire story that much better, keep it up!

Thank you to Sarah for being the best "Nebensitzer" (I checked, there is no English word for that) you can have. I'll miss our discussions and chats, but always remember: "Today is the day!".

Thank you to Kadda for being the best student/dancing partner/"Nebensitzer-on-the-other-side" you can have. I hope I could teach you one or two things and I also hope that for now you keep on the path of being "Mini-Me" until your project is done (did I hear a Science paper?)! The best tip I can give you for your future is to take it one salsa-step at a time...preferrably on two ;)

Thank you to André for being the best lab mate you can have. We hit it off in week 2 of my practical course during the master's and traveled through many digitial (12-3+5/17, power-small), virtual (did someone say ASU?) and real-life (we can cure hiccups with handstands!) adventures till then. You put the bro in bro-cessing. Thanks to your tremendous efforts you put into organizing group events, stay like you are. Know that I will be there for you if you ever fall back to M&M's and rum...oh, and I will make sure that you will still hear the word "BIF" at least once a week ;)

Thank you to all other members of the Beckmann and Wilson lab, the young and the old. You all are part of this amazing working atmosphere that we have! Keep it up and appreciate every moment of it!

And finally the one person I want to say the biggest thank you of them all: Thomas. To me, you personify mentor, supervisor, but most importantly friend and truly amazing guy. We worked for 5 years together, starting with you teaching me

about *in vitro* translations and ending with me teaching you how to do model building. We had so many deep discussion, fun trips (I want to go back to Japan!), late-night paper writing session, nail-biting tennis matches and more. I can safely say that I wouldn't be where I am today without your help. I hope we grew together and I could in the end pay you back by teaching you one or two things in return. Stay as you are and keep rocking (or in your case probably metalling)!

The last words of this thesis are fittingly for the two people with whom everything began: my amazing parents! I couldn't put into words what your support and love means to me. So I will keep it at a simple "Thank you from all my heart". I hope you know how much everything you do/did means to me.